Developing Novel Imaging Techniques for Analysis of Non-Fixed *Cryptosporidium parvum* Oocysts under Physiological Conditions

Tansy M.R. Vallintine

Supervisors: Dr Anastasios D. Tsaousis, Dr Wei-Feng Xue

School of Biosciences

University of Kent

A thesis submitted to the University of Kent, Faculty of Sciences for the degree of MSc in Microbiology

2018

Acknowledgements:

I would like to thank the members of the Tsaousis lab for their help throughout this project, and Dr Anastasious Tsaousis and Dr Wei-Feng Xue for their supervision of this project and guidance in writing this thesis. I would also like to thank the Kent Fungal Group for use of their fluorescence microscope. I would especially like to thank Dr Mark Price for his expertise in SEM and FESEM imaging, and for allowing me to use said machines, and Dr Lyne Josse for providing the cell lines used here, and providing training in cell culture, fluorescence staining, fluorescence imaging and infection procedure throughout the project. I would also like to thank Dr Ben Blakeman for his advice in the use of AFM in air.

Contents:

Abbreviations:

PBS: Phosphate buffered saline

FBS: Foetal bovine serum

GI: Gastrointestinal

SEM: Scanning electron microscopy

AFM: Atomic force microscopy

AAC C: accelerating voltage

Bp: base pairs

HPLC: high performance liquid chromatography

DAPI: 4', 6-diamidino-2-phenylindole

FITC: Fluorescein isothiocyanate

PCR: Polymerase chain reaction

r.t: Room temperature

b.f: bright field

Abstract:

Cryptosporidium is a waterborne apicomplexan parasite typically infecting the upper gastrointestinal tract of humans and animals. Infection in immunocompetent hosts can cause acute self-limiting diarrhoeal symptoms, although in infants and the immunocompromised, infection can be life threatening. The infective stage of the parasite survives in the environment as a hardy cyst/spore or 'oocyst'. These oocysts have high resistance to disinfectants, enabling them to survive for long periods in various environments whilst remaining infective. The nature and characteristics of these "spores" remain elusive, and further research into oocyst composition is necessary to enable the development of effective water treatment methods and medical prophylaxis, for which options are currently limited. This project describes a novel method for live imaging and peak force quantitative nanomechanical property mapping of *Cryptosporidium* spp. oocysts using atomic force microscopy (AFM). Applying this method, data on the surface topography and deformation characteristics of *Cryptosporidium parvum* oocysts has been acquired and analysed to identify physiological characteristics of live oocyst of the species *C. parvum*, both in air and in a near native liquid environment. Scanning electron microscopy (SEM), field emission scanning electron microscopy (FESEM), and fluorescence microscopy were used for comparison between imaging methods, and previous reports. This work will enable investigations into live *Cryptosporidium* spp. oocyst structure, composition, and mechanical properties in unprecedented depth. In turn these capacities can be used to inform and advance our understanding of host specificity and excystation control, and to develop new methods for treatment and eradication of the parasite, all areas of vital importance to progress research towards combating this significant disease.

Keywords: *Cryptosporidium parvum*, oocysts, AFM, SEM, fluorescence microscopy.

1.0 Introduction

1.1: General background

Cryptosporidium is a water borne apicomplexan parasite infecting the epithelial lining of the upper gastrointestinal (GI) and respiratory tracts of humans and other vertebrate species. Infection causes the disease cryptosporidiosis, a major international cause of diarrhoeal disease in humans and animals. In the immunocompetent, infection with *Cryptosporidium* causes mild to acute self-limiting diarrhoea and/or respiratory symptoms, however in infants and the immunocompromised, infection can be fatal. Cryptosporidiosis is primarily spread via the faecal-oral route, and can survive in the environment for prolonged periods as hardy cyst or 'oocysts'. Due to the mode of transition, the highest infection rates occur in developing countries where water sanitation systems can be inefficient or absent. It is responsible for 50.8% of all parasite induced waterborne infections (Putignani and Menichella, 2010), and 8-19% of diarrhoeal complaints in developing countries (Gatei et al., 2006).

There is currently no effective vaccine against cryptosporidiosis, and the only effective treatment is the broad spectrum antiparasitic drug nitazoxanide, which can only be used to treat otherwise healthy individuals (Ali et al., 2014; Sparks et al., 2015). Due to a lack of effective medications, there is an urgent need to develop new techniques to advance research into these parasites and aid the development of new and effective prophylaxis and treatments.

1.2 Cryptosporidiosis

Cryptosporidiosis is common and pervasive disease, with accounts in humans occurring in 95 countries and on all continents except for Antarctica (Feyer et al., 1997; Ryan, Fayer and Xiao, 2014). Cryptosporidiosis is understood to be responsible for up to 20 % of reports of childhood diarrhoea in less economically developed countries (Mosier and Oberst, 2000), with the proportion of affected individuals in a population ranging from 20 - 90 % (subject to region) (Dillingham, Lima and Guerrant, 2002). In a 2013 epidemiological study by Koltoff et al. reported that in a sample of over 22,000 children in Africa and Asia, *Cryptosporidium* was amongst the four pathogens causing the most acute diarrhoea, and as a cause of diarrhoea and death in children ranked second only to rotavirus (Scallan et al. 2011; Ryan, Fayer and Xiao, 2014). In the USA, the annual cost of hospitalisations from cryptosporidiosis can reach an estimated $485.8 million USD (Scallan et al., 2011). The total cost of the 1993 *C. hominis* outbreak in Milwaukee, Wisconsin (69 fatalities) (including medical treatment and decreased productivity) has been estimated at $96million USD (Corso et. al., 2003).

Although many cases of *Cryptosporidium* infection can be asymptomatic, infection more commonly causes symptoms such as diarrhoea, vomiting, and fever for a period of up to two weeks (Navin and Juranek, 1984, Sponseller, Griffiths and Tzipori, 2014). Infection is most commonly intestinal, although extraintestinal gastric, pancreatic, hepatobiliary, and pulmonary infection may also occur (Leitch, et al., 2012). Most *Cryptosporidium* cases occur in infants and the elderly, with research indicating that those under the age of two experience the most severe diarrhoeal symptoms (Jaggi et al., 1994; Neill et al., 1996), with malnutrition increasing duration of infection (Jaggi et al., 1994). In the immunodeficient, including HIV carriers, cancer and transplant patients (Gentile et al., 1991; Hong, Wong and Gutierrez, 2007), cryptosporidiosis can cause acute and persistent diarrhoea leading to wasting, malnutrition, electrolyte imbalance and potentially fatal dehydration (Centres for Disease Control (CDC), 1982). The diarrhoeal symptoms associated with cryptosporidiosis infections are thought to be a result of three factors: 1) malabsorption causing osmotic diarrhoea; 2) host secretagogues and inflammatory response triggered by the parasite; 3) parasite enterotoxin generated secretory diarrhoea (Leitch, et al., 2012). Symptomatic extraintestinal infections of the lung and pancreatic duct are more common in the immunocompromised (López-Vélez et al., 1995); a 1998 study by Rossi et al. reported that among a group to *Cryptosporidium* infected AIDS patients, the number having infection of the gastric mucosa was 98% (Rossi et al., 1998). Immunocompromised individuals can develop pulmonary *Cryptosporidium* as a complication from an intestinal infection, which can lead to respiratory failure and fatality (Kibbler te al., 1987; Meynard et al., 1996).

Cryptosporidium infection can be either anthroponotic or zoonotic, with livestock (principally calves) representing a significant reservoir of infection (Xiao, 2010; Ryan, Fayer and Xiao, 2014). Of the 26 confirmed species of *Cryptosporidium*, 20 species and genotypes have been reported to cause human infection, however the species accountable for the majority of outbreaks is *C. hominis*, closely followed by *C. parvum* (Xiao, 2010; Ryan, Fayer and Xiao, 2014). Recent contradictions include one outbreak cryptosporidiosis caused by *C. meleagridis* in a high school in Japan (Asano et al., 2006), and one of *C. cuniculus* due to contaminated drinking water in Northamptonshire, England (Chalmers et al., 2009; Puleston et al., 2014). With *Cryptosporidium spp.* oocysts ubiquitous in the environment, infection can occur via several routes (Xiao and Ryan, 2004). Anthroponotic transmission between humans can occur due to poor food hygiene in the home, or at institutions like nurseries and nursing facilities (Strausbaugh, 2001). Zoonotic infection commonly occurs directly in individuals living or working with animals, including pet owners, farm-workers, and veterinarians (Preiser, Preiser and Madeo, 2003). Food can also become contaminated at any point in the production and distribution process, from crop fertilisation with manure or contaminated

irrigation water, to the hands of food handlers or any other contaminated surfaces or equipment during preparation (Sischo et al., 2000; Xiao and Ryan, 2004; Smith et al., 2007).

The majority of outbreaks, however, have been ascribed to contamination of drinking water, either with *C. hominis* from human faecal matter, or due to water runoff from livestock with species such as *C. parvum* and *C. meleagridis* (Mac Kenzie et al., 1994, Pedraza-Díaz et al., 2001). In 1993 Milwaukee, Wisconsin experienced the largest confirmed outbreak of cryptosporidiosis in the USA. A population of 1.6 million individuals were potentially exposed, of these over 403,000 cases of related illness and 54 related mortalities were reported (mostly AIDS patients) (Mac Kenzie et al., 1994). This outbreak was primarily attributed to runoff from infected cattle entering the water supply and failing to be treated successfully due to a malfunction in the drinking water purification system. Genetic analysis showed that the primary species involved was *C. hominis*, suggesting that the outbreak was anthroponotic in origin (Zhou et al., 2004). Table 1 outlines selected recorded outbreaks, with outbreak location, source, type and *Cryptosporidium spp*. In addition to contamination of drinking water, oocyst resilience to chlorination has led to outbreaks of cryptosporidiosis as a result of contact with contaminated recreational water in swimming pools and water parks. Due to increased proximity to both wild and agricultural animals, children in rural areas are more likely to be infected with *C. parvum* and other zoonotic species than those living in urban areas (Tumwine et al., 2003), who are more likely to be infected anthroponotically with *C. hominis* (Llorente et al., 2007; Essid et al., 2008). *Cryptosporidium* is also a known cause of travellers' diarrhoea (Nair et al., 2008).

The pervasiveness of the *Cryptosporidium* parasite is the outcome of three factors; the substantial number of oocysts produced and excreted by the host, the environmentally hardy nature of the oocyst allowing long term survival of the parasite in the environment (several months in damp and temperate conditions), and the low dose of oocysts required for infection (Tolboom, 1996; Reinoso, Becares and Smith, 2008). The number of *C. parvum* oocysts required for infection in an otherwise healthy human host remains under debate, with research suggesting a median infective dose of between 132 oocysts (Chappell et al. 1996) to 82 oocysts (Okhuysen et al. 1999) with reports of infections occurring from doses of as low as 10 oocysts for both *C. parvum* and *C. hominis* (Okhuysen et al. 1999; Chappell et al. 2006). In calves, a lone shedding can release $6x10^7$ oocysts/gram of faeces (infected with *C. parvum*) (Uga et al., 2000), meaning that each shedding has a great capability of infection.

Table 1: Outbreaks of cryptosporidiosis listed with location, number of individuals infected, infection type, source and the species responsible.

Outbreak location and year	Individuals affected	Type	Source	Species	References
Carroll County, Georgia, USA. 1987	≈13,000	Waterborne	Public water supply	Unknown	(Hayes et al., 1989)
Milwaukee, USA. 1993	Est. 403,000 affected, 54 deaths	Waterborne	Contamination of drinking water from a sewage outlet	Unknown	(Mac Kenzie et al., 1994)
Minnesota, USA. 1995	15	Foodborne	Chicken salad at party	*C. parvum*	(From the Centres for Disease Control and Prevention. Foodborne outbreak of diarrheal illness associated with Cryptosporidium parvum-- Minnesota, 1995, 1996)
Stockholm Sweden, 2002	800-1000	Waterborne	Faecal accident in swimming pool	*C. parvum* genotype II	(Insulander et al., 2005)
Ohio, USA. 2003	12	Foodborne	Ozonated Apple Cider	*C parvum* subtype IIaA17G2R1	(Blackburn et al., 2006)
Östersund, Sweden. 2010.	≈27,000	Waterborne	Contamination of surface water by human sewage	*C. hominis* subtype IbA10G2	(Widerström et al., 2014)
Gipuzkoa, Spain. 2011.	26	Other	Day-care facility.	Unknown	(Artieda et al., 2012)
Indiana, Michigan, USA. 2011.	20	Other	Firefighting response-use of surface water contaminated with calf faeces.	*C. parvum*	(From the Centres for Disease Control and Prevention. Outbreak of cryptosporidiosis associated with a firefighting response — Indiana and Michigan, June 2011; 2012).
England and Scotland, 2012.	Over 300	Foodborne	Fresh pre-cut salad leaves.	*C. parvum gp60* subtype IIaA15G2R1	(McKerr et al., 2015)
Oregon, USA. 2013.	Est. 2780.	Waterborne	Municipal drinking water contaminated with cattle faeces.	*C. parvum*	(DeSilva et al., 2015)

At present 26 species of *Cryptosporidium* have been validated based on molecular, morphological, and biological information (Ryan, Fayer and Xiao, 2014). In addition to *C. hominis and C. pavum*, other species recorded to have caused cryptosporidiosis infection in humans include *C. meleagridis, C. cuniculus, C. ubiquitum, C. felis, C. canis, C. viatorum, C. muris, C. suis, C. fayeri, C. andersoni, C. bovis, C. scrofarum, C. tyzzeri, C. erinacei* (Leoni et al., 2006; Chalmers et al., 2009; Xiao, 2010; Feng et al., 2011b; Khan et al., 2010; Lucio-Forster et al., 2010; Chalmers et al., 2011; Waldron et al. 2011; Elwin et al. 2012a; Ng et al. 2012; Kváč et al. 2013a; Raskova et al. 2013; Adamu et al., 2014; Kvac et al., 2014a; Liu et al. 2014). Table 2 lists the 26 known *Cryptosporidium* species, with corresponding major hosts, and available information on human infection.

Variation in species infecting humans occurs based on geographical, seasonal and socioeconomic factors due to differences in infection source and transmission routes. Industrialised and developing nations also exhibiting variation in disease burden due to zoonotic vs. anthroponotic *Cryptosporidium* infection, with developed countries reporting mostly zoonotic infections, and anthroponotic infection being more common in developing countries (Xiao, 2010). In Middle Eastern countries anthroponotic *C. parvum* subtype transmission causes the majority of human infections, while *C. hominis* is the major species in many other less economically developed countries and industrialised nations, with low rates of c. parvum zoonotic transmission (Xiao and

Feng, 2008; Xiao, 2010; Nazemalhosseini-Mojarad et al., 2012). By comparison, *C. hominis* and *C. parvum* are both frequently identified as causing human infection in European countries and New Zealand (Ryan, Fayer and Xiao, 2014). Research indicates that countries with developing economies have a higher rate of infection with *C. felis* and *C. canis*, while C. ubiquitum is more commonly reported in industrialised nations (Ryan, Fayer and Xiao, 2014). Research conducted in Ireland, Canada, and the Netherlands found that *C. parvum* infections were predominant in spring, while *C. hominis* is was more common in autumn (Wielinga et al., 2008; Zintl et al., 2008; Budu-Amoako et al., 2012). Weilinga et al. (2008) reported age related variation in infection species in the Netherlands, with *C. parvum* more commonly infecting adults, and *C hominis* infection more frequently occurring in children.

Table 2: The 26 confirmed species of *Cryptosporidium* with their major host species. The authors of the initial accounts of each species are listed, with information on documented incidence of human infection.

Species name	Authors	Major host	Reports in humans
C. muris	Tyzzer (1907, 1910)	Rodents	Numerous reports (Feng et al. 2011b)
C.wrairi	Vetterling et al. (1971)	Guinea pigs	None reported
C.felis	Iseki (1979)		Many reports (Lucio-Forster et al. 2010)
C. serpentis	Levine (1980)	Snakes and lizards	None reported
C. melagridis	Slavin (1955)	Birds and humans	Commonly reported in humans
C. parvum	Re: Upton and Current (1985)	Ruminants	Commonly reported in humans
C. baileyi	Current et al. (1986)	Birds	None reported
C. varanii	Pavlásek et al. (1995)	Lizards	None reported
C. andersoni	Lindsay et al. (2000)	Cattle	Leoni et al. (2006); Morse et al. (2007); Waldron et al. (2011); Agholi et al. (2013); Liu et al. (2014)
C. canis	Fayeretal. (2001)	Dogs	Many reports (Lucio-Forster et al. 2010)
C. molnari	Alvarez-Pellitero and Sitja-Bobadilla (2002)	Fish	None reported
C. hominis	Morgan-Ryan et al. (2002)	Humans	Most common species in humans
C. galli	Re: Ryan et al. (2003c) Pavlásek (1999)[a]	Birds	None reported
C. suis	Ryan et al. (2004)	Pig	Xiao et al. (2002a); Leoni et al. (2006); Cama et al. (2007); Wang et al. (2013)
C. bovis	Fayer et al. 2005	Cattle	Khan et al. (2010); Ng et al. (2012); Helmy et al. (2013)
C. fayeri	Ryan et al. (2008)	Marsupials	Waldron et al. (2010)
C. fragile	Jirku et al. (2008)	Toads	None reported
C. macropodum	Power and Ryan (2008)	Marsupials	None reported
C. ryanae	Fayer et al. (2008)	Cattle	None reported
C. xiaoi	Fayer et al. (2010)	Sheep and goats	Adamu et al. (2014)
C. ubiquitum	Fayer et al. (2010)	Ruminants, rodents, primates	Commonly reported (Fayer et al. 2010; Elwin et al. 2012a)
C. cuniculus	Re: Robinson et al. (2010)	Rabbits	Chalmers et al. (2009); Anon (2010); Molloy et al. (2010); Chalmers et al. (2011)
C. tyzzeri	Re: Ren et al. (2012)	Rodents	Raskova et al. (2013)
C. viatorum	Elwin et al. (2012b)	Humans	Elwin et al. (2012b); Insulander et al. (2013)
C. scrofarum	Kváč et al. (2013b)	Pigs	Kváč et al. (2009a); Kváč et al. (2009b)
C. erinacei	Kváč et al. (2014b)	Hedgehogs and horses	Kváč et al. (2014a)

Re: re-description

[a]: initial description

1.3 Diagnosis and treatment:

The most frequently used diagnostic technique involves the detection of oocysts or antigens in the stool sample, in this case rate of shedding and stool consistency affects results, with more fluid stools giving better detection limits. If necessary samples can be distilled using a flotation technique such as a sucrose suspension (specific gravity 1.15-1.20), providing a concentrate oocysts product (Arrowood MJ., 1997). Bright-field staining of stool samples with techniques like the Auramine phenol method is the most affordable testing method, although analysis by a qualified technician is necessary (Arrowood MJ., 1997). The most efficient assays employ direct or indirect immunofluorescence, although these techniques are also the most expensive. Several commercial kits are obtainable for the detection of *Cryptosporidium* antigens in stool samples, these can be used in a clinical capacity to test either fixed or fresh samples. Epidemiological and genotyping studies more often employ molecular methods (Arrowood MJ., 1997; Cama et al., 2008; Jothikumar et al., 2008), of which recent studies include oocysts detection in faeces using PCR detection of the 18s rRNA gene (Jellison et al., 2004), and genotyping by PCR-RFLP analysis of the Hsp70 gene (Gobet, 2001).

Supportive or symptomatic treatment such as liquid and electrolyte replacements may be prescribed to immunocompetent patients to address severe diarrhoeal symptoms (Moroni et al., 1993; Blagburn and Soave, 2007). The only effective medication licenced by the US Food and Drug Administration for use in otherwise healthy and adults (Rossignol, 2010) against cryptosporidiosis is the broad spectrum antiparasitic drug nitazoxanide, which cannot be used to treat infants or the immunocompromised (Abubakar et al., 2007; Ali et al., 2014; Cabada et al., 2015; Sparks et al., 2015). The antibiotics paromomycin and azithromycin can be used in immunocompromised individuals but with limited efficacy (Cabada et al., 2015), and therefore tend to be used in combination with nitazoxanide, (Ali et al., 2014; Cabada et al., 2015). While treatments such as azithromycin, paromomycin and roxithromycin have been reported to cause reduced stool volume, frequency, and oocyst shedding, although eradication of the parasite is uncommon, and these treatments are yet to be FDA approved (Rossignol, 2010).

The most effective therapy for cryptosporidiosis in immunocompromised individuals involves improving the immune status with highly active anti-retroviral therapy (HAART) including an HIV aspartyl protease inhibitor (Abubakar et al., 2007; Cabada et al., 2015) in conjunction with nitazoxanide (Zardi, Picardi and Afeltra, 2005). AIDS patients may experience a relapse of infection previously believed to have been cleared by anti-retroviral therapy if their $CD4^+$ levels decline (Maggi et al., 2000). The diarrhoeal symptoms of cryptosporidiosis may also affect treatment efficacy through decreasing absorption of treatments, occasionally to sub-therapeutic levels as documented in AIDS patients by Brantley et al. (2003).

1.4 Life cycle:

Cryptosporidium spp. have a complex life cycle involving many stages (fig. 1), the infective stage of *Cryptosporidium* persists in the environment as an oocyst, hardy spore-like structures that can survive for several months under varying conditions (Reinoso, Becares and Smith, 2008). The sporulated thick walled oocysts are 4 - 6 µm in diameter (Fayer, Morgan and Upton, 2000).

Upon reaching the distal small intestine following ingestion by a host, the four sporozoites contained within the oocysts excyst and attach to the microvillous epithelial lining of the gastrointestinal tract (Borowski, Clode and Thompson, 2008). Infection can also occur in the upper GI tract or the respiratory tract, although respiratory infection is less common (Leitch and He, 2012). Receptors on the oocyst wall surface function to ensure cyst proximity to the lining of the host small intestine prior to excystation (Smith, Nichols and Grimason, 2005, Leitch and He, 2012). Excystation can be triggered *in vitro* using bile salts and incubation at 37 °C (Woodmansee, 1987). Acidic conditions will cause excystation in the 'gastric' species *C. muris* and *C. andersoni*, however species infecting the distal small intestine such as *C. hominis* and *C. parvum*, only excyst in the presence of taurochloric acid (Widmer, Klein and Bonilla, 2007)**.** The sporozoites released upon excystation are spindle shaped and roughly 4 x 0.6 µm in size (Leitch and He, 2012). The gliding motility employed by the sporozoite to reach and penetrate the outer surface of the host enterocyte is facilitated by an apical complex also found in other parasitic apicomplexan species (Borowski, Clode and Thompson, 2008), and powered by an actin-myosin motor (Arrowood, Sterling and Healey, 1991). Upon reaching the target cell movement through the mucus layer is enabled by enzymes produced by the sporozoite (Smith, Nichols and Grimason, 2005).

Upon attachment to the apical epithelial cell lining the sporozoite forms an extracellular parasitophorous vacuole, which enables the sporozoite to transform into a trophozoite and reproduces asexually via fission (schizogony- fig. 1 (a)) to produce type - 1 meronts. Following sporozoite attachment to the host enterocyte, a specialised secretory organelle or 'rhoptry' (a feature observed in the motile stages of parasitic apicomplexan protozoans) extends towards the host cell. The contents of the rhoptry pass through the neck to the host cell and establish the host cell/parasite interface (Bradley et al., 2005). The sporozoite is then engulfed by the host cell within a parasitophorous vacuole (Chen et al., 2005), a process which is facilitated by an expansion of the host cell due to increased levels of aquaporin 1 and sodium-glycose symporter SGLT1 at the interface between host and parasite (Chen et al., 2005). The parasitophorous vacuole consists of components originating from both the parasite and host cell (Borowski, Clode and Thompson, 2008). Amongst the components originating from the parasite is the feeder organelle (found in all intracellular stages of *Cryptosporidium*), a densely folded membranous structure formed during invagination of the parasite plasmanella over the terminal web (Fayer and Xiao, 2007). This

organelle is thought to enable parasite access to nutrients within the cytoplasm of the host enterocyte, an ability necessary for the survival of the parasite as genetic analysis of both *C. parvum* and *C. hominis* reveals compaction of the genome resulting strong host dependence due to in inadequate biosynthetic capacity (Abrahamsen, 2004, Xu et al., 2004). Located within the fully formed parasitophorous vacuole, the sporozoite undergoes dedifferentiation and subsequently differentiation to form the trophozoite (1.5 - 2.5 µm diameter) (Smith, Nichols and Grimason, 2005), accompanied by adjacent disorganisation and lengthening of the host cell microvilli (Leitch and He, 2012). Mitosis occurring inside the trophozoite triggers the development of a type - 1 meront, inside which the schizont residual body buds six or eight type - 1 merozoites. During this process the host cell microvilli flanking the type - 1 meront exhibit similar elongation and derangement as occurs in trophozoite formation (Mele et al., 2004). Following elongation of the type - 1 merozoites, the parasitophorous vacuole ruptures and the merozoites are released (Fayer and Xiao, 2007). The type - 1 merozoite is 0.4 x 1.0 µm in diameter, and rod-shaped in appearance with a narrowed tapering apical region (Borowski et al., 2009). Type - 1 merozoite motility, invasion of host enterocyte and initiation of asexual reproduction (formation of further type 1 meronts), are thought to occur as a result of similar mechanisms as described in sporozoite biology (Wanyiri et al., 2009). Upon release type - 1 merozoites can become type - 2 meronts (3 - 5 µm), or cause autoinfection by forming trophozoites. Type - 2 meronts release four type - 2 merozoites which form either male microgamonts, or female macrogamonts upon attachment to the host epithelial cell lining (Yang et al., 1996). These gamonts are the sexual stage in the life cycle of *Cryptosporidium*, named Gametogony (Borowski et al., 2009). Type - 2 merozoite shape varies in comparison to that of the type - 1 merozoite, are marginally larger, and exhibiting reduced motility (O'Hara and Chen, 2011).

The female macrogamont is 4 - 6 µm in diameter, roughly spherical in shape, and contains a large nucleus. Within the male microgamont, nuclei bud from the residual body to produce 16 microgametes (Yang et al., 1996). These non-flagellated microgametes are roughly 1.4 x 0.5 µm in diameter and rod-like in appearance. Upon exiting the microgamont, the microgametes fertilize neighbouring macrogamonts to produce a diploid zygote (Leitch and He, 2012).

Each zygote matures and differentiates into either a thin or thick-walled sporulated oocyst (sporogony) whilst remaining joined to the host cell. Once sporulation and differentiation are completed both thick and thin-walled oocysts disconnect from the host enterocyte. Thin-walled oocysts go on to excyst within the host and cause autoinfection (~20%), whereas hardy thick-walled oocysts exit the GI tract into the environment to be ingested by a new host, initiating a new cycle of infection (Fayer and Xiao, 2007).

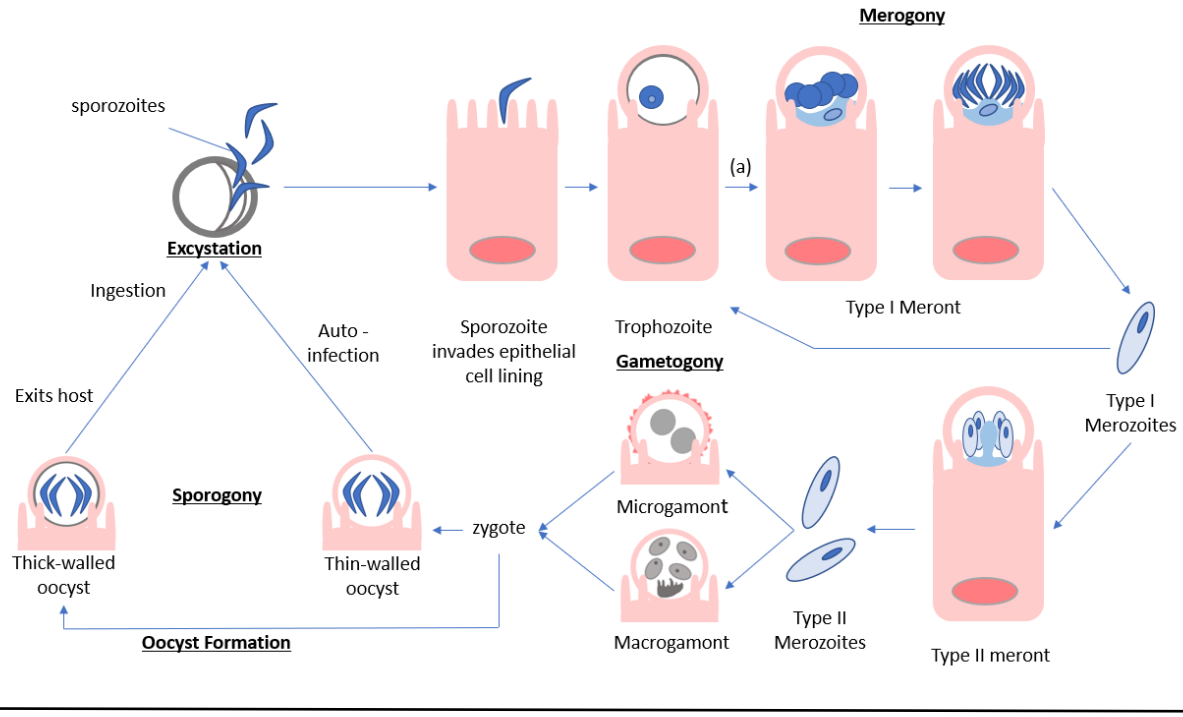

Figure 1: A schematic depicting the life stages and development of the *Cryptosporidium* parasite.

1.5 The oocyst:

Each *Cryptosporidium* oocyst contains four sporozoites and a residual body (Petry, 2004). The residual body comprises a lipid vacuole and amylopectin granules, and acts as a nutritional store for the sporozoites. Amylopectin levels can be used as an indicator of oocyst viability, as concentration diminishes over time due to sporozoite metabolism (Fayer et al., 1998; Petry, 2004). Unlike coccidian cysts, *Cryptosporidium* oocysts do not develop sporocysts (Petry, 2004; Jenkins et al., 2010), and have a unique complex zipper-like structure or 'suture' which extends across one third to a half of the wall. The suture structure is trypsin-bile sensitive and consists of a 50-nm groove which is flanked by two 165 nm wide bands (Jenkins et al., 2010). When exposed to excystation fluid the suture dissolves and the edges of the divide curl into the oocyst interior creating an opening through which the sporozoites can exit, leaving an empty spherical shell of oocyst wall (occasionally retaining a residual body) (Reduker et al., 1985b).

The oocyst wall acts to contain the sporozoites and shield them from harsh external influences both in the environment and the stomach of the potential host. This protective effect can impede embedding and dehydration of sporozoites in preparation for thin-section TEM analysis (Reduker et al., 1985a). Several studies have described the oocyst wall of *C. parvum* as being ~40 nm thick and consisting of three to four discreet layers when viewed under electron microscopy (Reduker et

al., 1985a, 1985b; Bouchet and Boulard, 1991; Pinckney et al., 1993; Fayer et al., 1997; Harris & Petry, 1999). These layers include an outer electron-dense layer, a translucent intermediate layer, and two inner electron-dense layers (Jenkins et al., 2010), the outermost layer is roughly 5 nm thick, exhibits variable electron density, and appears as a diffuse network in tangential sections, with areas of electron density followed by the electron transparent layer and a diffuse inner fibrillar array with marked linearity (Harris and Petry, 1999). As this outer layer can be partially eliminated using sodium hypochlorite, it is speculated to consist of acidic glycoprotein (Reduker et al., 1985a). The 10 nm electron dense central layer appears rigid and is believed to be composed of a complex lipid with a possible double unit membrane structure. It is this component that is thought to give *Cryptosporidium* oocysts their acid-fast red staining qualities (Harris and Petry, 1999). The innermost layer of the wall is comparatively thick measuring 20 nm across and is believed to comprise of filamentous glycoprotein with a potentially particulate structure (Bonnin et al.,1991; Jenkins et al., 2010). In perpendicular sections the suture structure appears to be located beneath the outer electron dense layer and central translucent layer (Jenkins et al., 2010). It is currently unknown which component of the wall lends the intact oocyst its rigidity and elasticity, however the information currently available suggests that the central glycolipid layer may be responsible for the oocysts mechanical resilience (Harris and Petry, 1999). The waxy hydrocarbon content of the electron-translucent layer may be involved in the temperature dependent permeability of the wall, while the presence of an the external glycocalyx provides a capacity for attachment and immunogenicity (Jenkins et al., 2010).

1.6 Phylogenetics:

Upon discovering *Cryptosporidium* in 1907, Edward Tyzzer classified the parasite as belonging to the coccidian family Asporocystidae due to comparative morphological features such as a lack of sporocysts and other apparently similar elements in the life-cycle (Tyzzer, 1907; Levine, 1988). More recently, suture complexes similar to those of *Cryptosporidium* oocysts have been described in the sporocyst walls of coccidians including *Toxoplasma* and *Sarcostysis,* which were thought to indicate a possible close phylogenetic relationship between *Cryptosporidium* spp. and the genus Sarcocystis and related genera (Thompson et al., 2016). Conversely, the location of the *Cryptosporidium* suture in the oocyst wall suggests that the similarities evolved independently (Speer, Fayer and Dubey, 2018). The coccidian classification was accepted until recent years despite *Cryptosporidium* possessing many features uncharacteristic of the coccidian family, including possession of an attachment organelle, the capacity for auto-infection through retention of thin-walled oocysts, and the epicellular developmental location of endogenous developmental stages in the parasitophorous vacuole (Barta and Thompson, 2006, Clode et al., 2015, Thompson et al., 2005,

Valigurová et al., 2007). Additionally, *Cryptosporidium* lack many significant coccidian features, including a micropyle and polar granules (Thompson, et al., 2016).

Many factors indicated that *Cryptosporidium* may be more closely related to the gregarines than coccidians. Recent observations have found that *Cryptosporidium* is not obligate intracellular, but instead can multiply epicelularly and extracellularly in the nutrient rich environment of biofilms (Hijjawi et al., 2004; Rosales et al., 2005; Karanis et al., 2008; Koh et al., 2013; Koh et al., 2014), a trait shared with the gregarines which can multiply similarly (Leander and Ramey, 2006; Clode et al., 2015). The gregarines and *Cryptosporidium* have many biological features in common, including the development of the myczocytosis-like feeder organelle, epicellular developmental location, gliding motility of motile life-stages, and diversity of trophozoite appearance (Sibley, 2004; Barta and Thompson, 2006; Valigurová et al., 2007; Borowski et al., 2008; Valigurová et al.; 2008 Borowski et al., 2010; Valigurová et al., 2013; Clode et al., 2015; Aldeyarbi and Karanis, 2016).

Cryptosporidium taxonomy has undergone numerous alterations over the years, and species number has increased considerably as modern molecular tools allow species recognition to be based on genetic analysis in combination with host occurrence and morphological characteristics (Thompson et al., 2016).

In addition to morphological similarities, Bull et al., (1998) reported a critical similarity in serological activity with *Monocystis* (a gregarine), and in 1999 Carreno et al. reported that SSU-rDNA sequencing supported that *Cryptoaporidium* is more closely related to gregarines than to coccidia. Similarly, a 2014 review of gregarine classification using gregarine site-heterogenous SSU-rDNA trees located *Cryptosporidium* within the gregarines, with close relation to all 'neogregaries' and many 'eugregarines' (Cavalier-Smith, 2014). The subclass Orthogregarina was established based upon these findings, containing Cryptosporidium and other closely related gregarines, as was *Cryptosporidium* own subclass, Cryptogregaria (Cavalier-Smith, 2014; Thompson et al., 2016). The Cryptogregaria subclass is classified/characterised as containing epicellular parasites of vertebrates that lack an apicoplast but do possess a feeder-organelle.

Modern imaging techniques contributed considerably both to the understanding of the shared physiological traits between *Cryptosporidium spp.* and the gregarines, and also the marked parallels in host-parasite relationship (Koh et al., 2014; Clode et al., 2015). As *Cryptosporidium* is most commonly a waterborne parasite, which can remain infectious in the environment for prolonged periods of time, recognition of *Cryptosporidium* as a gregarine and their related ability to reproduce in biofilms has implications for detection, transmission, survival in the environment and subsequent infection dynamics. The presence of additional life-stages in the environment may complicate surveillance and detection, while collection and prolonged survival in biofilms, which

can then enter the water supply in large numbers via biofilm sloughing, has implication for cryptosporidiosis transmission (Searcy et al., 2006; Angles et al., 2007; Thompson et al., 2016). These recent revelations reinforce the value of imaging studies and the development of new techniques to fundamental matters such as species taxonomy.

1.7: Microscopy

For the purpose of this thesis, several microscopic techniques have been utilised, some of which are described below.

1.7.1 Scanning Electron Microscopy

The scanning electron microscope generates images of a sample through scanning the surface with a focused electron beam, a sensor then gathers the signals (most commonly secondary electrons or SE) which are produced at various depths within the sample upon electron interaction with the atoms comprising the sample, and these signals are interpreted to generate an image of sample topography and/or chemical composition. Other signals produced upon electron excitation include back-scatter electrons (BSE), and characteristic x-rays. BSE are reflected from various depths within the sample by elastic scattering and interpreted to analyse sample density and composition. Characteristic X-rays are most commonly used in composition analysis and to measure the abundance of elements within a sample. SE are generated at the sample surface and are commonly used in generating high resolution images for topographical analysis, capable of revealing features less than 1 nm in scale (Stokes, 2008). Samples must be prepared to withstand the vacuum conditions and high energy electron beam to which they are exposed during imaging. Specimens which are non-conductive, as most biological specimens are, collect charge during scanning resulting in image defects and artefacts. For this reason, samples must be rendered electrically conductive at the surface and similarly grounded to prevent electrostatic charge accumulation, this usually involves either low vacuum sputter coating or high-vacuum evaporation deposition with a conductive material such as gold, platinum, tungsten or osmium (Brunk, Collins and Arro, 1981; Suzuki, 2002; Hawkes, 2012). Prior to coating, biological samples are typically fixed using agents such as glutaraldehyde and osmium tetroxide, and must be processed to dryness, commonly using chemical dehydration followed by critical point drying. As biological specimens tend to be fragile, non-conductive and thermally sensitive, SEM imaging often causes damage and artifacts, however preparation using the methods described above precludes live imaging, and the possibility of feature destruction or alteration under harsh preparation conditions, and/or obscuration of fine features during coating cannot be dismissed (Stokes, 2008). The recently developed technique Cryo-electron microscopy employs cooling of the sample to cryogenic temperatures to enable imaging of samples in their fully hydrated state, thus avoiding much of the specimen damage caused during sample dehydration, however cryo-freezing does not eliminate the need to render

biological samples electrically conductive, and very few facilities have the equipment necessary to practice the technique (Nogales, 2016).

In 2009, Borowski et al. used SEM to describe the full life-cycle of *C. parvum* produced in vitro (HCT-8 cell line culture). SEM has also been used to describe *Cryptosporidium* developmental stages produced within biofilms and compare these to stages generated in cell culture, and to confirm host cell independent formation of a parasitophorous vacuole structure, illustrating a possible mode of host free life cycle completion (Koh et al., 2014). SEM has been used to investigate *C parvum* oocyst wall ultrastructure of both intact and excysting oocysts (Reduker, Speer and Blixt, 1985), and to determine the efficacy of batch solar disinfection in inactivation of *Cryptosporidium parvum* oocyst and giardia cysts (McGuigan et al., 2006).

1.7.2 Transmission electron microscopy

Transmission electron microscopy (TEM) allows imaging of cell ultrastructure. Like other EM techniques, TEM imaging also requires fixing and dehydration of biological samples using an ethanol acetone series, in addition samples are then passaged through a transition solvent like propylene oxide, followed by infiltration and embedding in an epoxy resin. This resin block is then thin sectioned (50 – 100 nm thick), assembled on mesh grids, and stained using electron dense stains such as osmium tetroxide. Transmission of an electron beam through the thin section allows electron interaction with the sample forming a high-resolution image, this image is then focused onto an imaging mechanism such as a fluorescent screen or sensor (Griffin, 1990; Reimer and Kohl, 2010)). Whilst this technique allows imaging of internal structures, it cannot be used to gain topographical information. In relation to oocyst imaging, the resilience of the *Cryptosporidium* oocyst can interfere with fixing, staining and embedding of internal structures, causing shrinkage and deformation of interior components.

Borowski et al., (2009) used both SEM and TEM to characterise morphological features of *Cryptosporidium* life cycle features in an *in vitro* system. In 1999 Harris et al. used TEM to determine structural components of the oocyst wall, Aldeyarbi and Karanis (2016) used TEM to image stages of *Cryptosporidium* asexual multiplication *in vitro*.

1.7.3 Atomic Force Microscopy:

Atomic force microscopy (AFM) is a powerful multifunctional imaging platform, which utilises a high-resolution scanning probe microscopy (SPM) technique to image and manipulate a range of biological samples, from arrays of living cells to single molecules (Dufrene et al., 2017). A three-dimensional topographical map is obtained through physical interaction between a probe and the sample surface. The AFM uses a cantilever which has a sharp tip or 'probe' at the end. The probe is usually 2.8 - 8 µm tall with a radius of ≈2 nm. The deflections of the cantilever are measured when

the probe is bought close to the sample surface and used to generate a three-dimensional topographical map of the sample (Cappella and Dietler, 1999). Vertical resolution can reach to 0.1 nm (fractions of a nm), while due to convolution horizonal resolution is slightly lower, at around 1 – 5 nm (Gan, 2009).

As research progressively moves into the fields of genomics and proteomics, there will be an increasing requirement for techniques capable of elucidating how and where gene products interact to establish regulatory and metabolic pathways. High powered and versatile imaging techniques capable of describing and/or localising molecular interactions within the live oocyst under a close to natural environment will enable functional delegation of gene products. The extremely streamlined genome of *C. parvum* (Abrahamsen et al., 2004), in combination with their clinical importance, renders this parasite a prime candidate for functional analysis by imaging. The techniques necessary for appropriate live imaging remain to be developed.

A significant advantage of AFM imaging is that use of a fluid cell can enable imaging in liquid, with control over temperature, buffer composition and flow, allowing imaging of biological samples and live cells in a close to native environment (Drake, 1989; Radmacher et al., 1992). AFM can be used to measure surface forces, including van der Walls, steric, hydrophobic, and electric double layer (Cappella and Dietler, 1999; Considine et al., 2002). Using PeakForce QNM mode, it is also possible to map nano-mechanical measurements, including sample deformation, elasticity, dissipation and adhesion of the sample (Hoh et al., 1992; Lee, Chrisey and Colton, 1994; Boland and Ratner, 1995; Hinterdorfer et al., 1996; Muller, Baumeister and Engel, 1999; Allison, Hinterdorfer and Han, 2002; Benoit et al., 2000; Doktycz et al., 2003).

In addition to imaging and force measurement, AFM can also be used to manipulate biological samples mechanically through alteration of the force applied by the tip, or chemically through tip supplementation with chemical groups for manipulation of specific sites. In this way AFM has been used to manipulate and section a range of biological samples, from whole cells (microbial or animal) (Henderson, Haydon and Sakaguchi, 1992; Sokolov, Firtel and Henderson, 1996; Le Grimellec et al., 1998; Ong et al., 1999; Bolshakova et al., 2001; Doktycz et al., 2003), to chromosomes, viruses, membranes, and single proteins (Gerber and Lang, 2006; Müller and Dufrêne, 2008; Novak et al., 2009). The ability of AFM to image, probe surfaces, and manipulate samples makes this one of the most versatile imaging techniques currently available.

For liquid imaging of live cells, the method of immobilisation must be chosen with care to avoid compromising cell physiology whilst ensuring attachment is robust enough to withstand drag or detachment upon sample-probe contact. Competition between sample binding sites, substrate, and buffer constituents can impede attachment (Müller, Amrein and Engel, 1997), therefore

immobilisation techniques must be methodically developed for individual cell types and organisms. Commonly utilised techniques employ two major mechanisms; chemical immobilisation, and physical entrapment. Chemical attachment techniques commonly exploit the net negative charge of many bacterial and other cell types, utilising cationic substrate alteration to encourage steric interaction with the sample and adsorption to the surface (Doktycz et al., 2003; Beckmann et al., 2006; Plomp et al., 2007; Sullivan et al., 2007; Suo et al., 2008; Shu et al., 2008; Kuznetsov, Gershon and McPherson, 2008; Arce et al., 2009; Mortensen et al., 2009). Commonly used agents in steric chemical attachment include substrate coating with poly-L-lysine solution (Razatos et al., 1998; Robichon et al., 1999; Bolshakova et al., 2004; Micic et al., 2004), amino containing saline reagents such as 3-aminopropyltriethoxy silane (APTES) (Dorobantu et al., 2008; Cerf et al., 2009), and porcine gelatine (Doktycz et al., 2003; Venkataraman et al., 2006). Using glutaraldehayde, covalent attachment can be achieved by substrate cross-linking with amino groups attached to the substrate surface (Sullivan et al., 2007), however repulsion forces must be addressed to enable cell-surface contact and many buffers have been used for this purpose (van der Mei et al., 2000; Touhami, Jericho and Beveridge, 2004; Beckmann et al., 2006; Francius et al., 2008). Physical entrapment can be achieved through use of a substrate surface containing pores of similar diameter to the sample cell, or embedding within a matrix (Dufrene et al., 2011). A common immobilisation technique in imaging bacterial cells is drying of the sample to the substrate (Canetta et al., 2006; Plomp et al., 2007; Sahu et al., 2009), however dehydration of the sample often occurs, with cell flattening, collapse, and dehydration related deformities including marked folding and irregularity of the surface (Doktycz et al., 2003; Bolshakova et al., 2004). Further, this method does not ensure stability or viability in liquid imaging, the required method for live-cell studies. Typically, imaging in liquid shows bacterial cells to have a greater vertical height and a smoother surface than those imaged in air. Imaging in air can provide superior resolution of delicate features (Müller and Dufrêne, 2011; Dufrene et al., 2017), although as previously described, dehydration can produce multiple deformities.

As oocyst association with particles in solution can influence their sedimentation and movement in aquatic systems, chemical modification of AFM tips has been used to measure interaction forces between individual oocysts and particles found in soil in varying liquid environments (Considine at al., 2002; Searcy et al., 2005; Tufenkji et al., 2006). This data can be used to make predictions about oocyst migration in aquatic environments and to aid removal of *Cryptosporidium* oocysts in natural subsurface environments and filtering systems in water treatment facilities (Searcy et al., 2005). Table 3 provides information on the four major high-powered microscopy techniques.

Table 3: The advantages, requirements and limitations of the four major high-powered microscopy techniques.

Procedure/Attribute	Atomic Force Microscopy (AFM)	Super-Resolution Microscopy *	Transmission Electron Microscopy (TEM)	Scanning Electron Microscopy (TEM)
Resolution	≤1nm-50 nm	20-50 nm	0.2-10 nm	2-10 nm
Sample preparation and environment	Sample attachment to substrate or support, physiological conditions (buffer, temperature, CO_2)	Fluorescence labelling, physiological conditions (buffer, temperature, CO_2)	Deposition of sample on grid, fixing, dehydration (negative stain), vitrification (cryo-electron microscopy)	Freezing, fixing, critical point drying, metal plasma deposition
Artefacts	Tip, force, scanning	Bleaching, toxicity	Dehydration, crystal formation, beam damage	Dehydration, metal shadowing, beam damage.
Advantages	Imaging under native conditions possible, labelling and staining not necessary, high signal to noise ratio, measurement of many parameters (biological, physical and chemical)	3-D cellular structures, high spatiotemporal resolution, monitoring biomolecular processes in live cells	Solves protein atomic structures, provides conformational images of proteins and complexes, images intracellular structures with molecular-resolution	Surfaces of tissues, cells, and interfaces at nm scale resolution
Limitations	Limited to surfaces	Limited to fluorescence labels	No life processes	No life processes

**Photoactivated localisation microscopy (PALM), stochastic optical reconstruction microscopy (STORM), stimulated emission depletion (STED).*
Adapted from Dufrene et al., (2017)

1.8: Research Aims:

Given the critical need for new techniques for use in research into *Cryptosporidium* species, this project aimed to develop a set of imaging tools for investigating the surface characteristics and mechanical properties of infectious non-fixed *Cryptosporidium parvum* oocysts in a close to physiological environment. SEM and AFM imaging methods were investigated.

For successful AFM analysis under fluid, sample ability to withstand probe contact requires a sufficient method of sample immobilisation to the substrate surface to prevent sample detachment and/or drift. To develop such a method, multiple oocyst immobilisation techniques were assessed, including differing substrate, immobilisation method and suspension buffer. For FESEM analysis *C. parvum* oocyst samples were imaged using the Hitachi S3400 series SEM. Here a backscatter electron sensor was used to measure density. The Hitachi S4700 (cold) field emission SEM, with Bruker "XFlash" quad-element EDX detector was used to gain high definition of oocyst surface morphology and chemical composition analysis. For fluorescence microscopy oocysts were analysed using the Olympus 1 x 81, and images were captured using the Andor Zyla 4.2 plus sCMOS camera. For AFM analysis, oocyst samples were imaged using the Bruker Multimode 8 SPM in peak-force tapping ScanAssyst QNM in air and in liquid modes and analysed using NanoScope Analysis v1.40r1. Experiments were set up to test the ability of the developed AFM technique to image live infectious oocysts by means of infection of cell cultures with imaged oocysts and detection of subsequent de novo produced oocysts using fluorescence microscopy. Optimisations were performed; however, the final experiments could not be completed due to time constraints.

2.0 Methods:

2.1 Sample Preparation:

C. parvum oocyst source and filter purification:

C. parvum oocyst stock (IOWA isolate) was obtained from Bunch Grass Farm, Deary, Idaho and stored at 4°C. To ensure maximum sample purity, oocyst stock suspension was filter sterilised prior to slide deposition. 500 µl/slide of 2 x 10^7 oocysts/ml stock solution (approximately 1 x 10^7 oocysts/slide) stock was filtered using a syringe filter with 0.45 µm pore size (Sartorius Minisart® syringe filter) and rinsed through with 50 ml HPLC water (Thermo Fisher Scientific). For oocyst retrieval from the filter membrane, fluid flow was reversed for a volume of 15 ml and deposited into a fresh 15 ml falcon tube. The filtered oocysts were pelleted by centrifugation at 2,000 x g for 18 minutes, the supernatant removed, and the pellet re-suspended in 50 µl/slide HPLC water.

Glass Slide preparation and oocyst filter sterilisation:

15 mm spherical glass coverslips (Agar Scientific) were pre-washed with 70 % EtOH (Thermo Fischer Scientific) and detergent to remove surface contaminants and fatty deposits and rinsed in HPLC water. Cover slips were then attached to metal AFM specimen discs (Agar Scientific) using double sided adhesive, and 50 µl 0.01 % (imaging in air) or 0.05 % (imaging in liquid) poly-l-lysine solution (Sigma Aldrich) was applied to the centre of each coverslip. Slides were then placed in a warming oven at 60 °C for approximately 30 minutes until dry.

50 µl filter sterilised sample solution was deposited to the dried poly-l-lysine coated surface of each previously prepared slide and allowed to sediment in a humid environment at room temperature (r.t.) overnight. At no point were the samples allowed to dry. Following overnight sedimentation, slides were rinsed of excess oocysts using 2 ml HPLC water/slide and covered with a fluid droplet to ensure oocysts remained fully hydrated. For AFM imaging in air to ensure minimal sample dehydration whilst achieving sufficient dryness to allow imaging, samples were drained of the hydration droplet, air dried and subjected to a gentle nitrogen stream for four seconds directly prior to imaging.

Preparation of mica slides:

12mm mica slides (Agar Scientific) were prepared for sample deposition by attachment to metal AFM discs using double sided adhesive tape. To provide a sterile smooth substrate, the mica layers were split at the edges of the disc using a sharp implement, and the intact apical layer was removed using rubberized adhesive tape.

2.2 Substrate and immobilisation optimisations:

Buffer optimisation - DDh20 v 1x PBS v 10x PBS

For liquid AFM imaging, the effects of buffer salt concentration on oocyst appearance and levels/numbers of attachment was assessed using confocal light microscopy. 0.01 % poly-l-lysine treated slides with attached oocysts were prepared as previously described (see sample preparation) until the point of oocyst pellet resuspension, at which point oocyst pellets were re-suspended and deposited to slides in 20 µl aliquots of either ddH_2O, 1x PBS, or 10x PBS (PBS-Dulbecco A, OXOID). Slides were allowed to sediment for 40 minutes before rinsing and viewing under a ddH_2O droplet using confocal light microscopy.

Immobilisation - Gelatine v Poly-l-lysine

All slides were cleaved as previously described to provide a sterile smooth substrate (see Preparation of Mica Slides). Gelatine solution was prepared by aliquoting 100 ml HPLC water to a sterile bottle and microwave heating to boiling point. 0.5 g of gelatine (Sigma Aldrich, gelatine from porcine skin, type A strength 300, Lot SLBUS185) was added to the heated water and vortexed gently to dissolve, and the mixture was allowed to cool to 60 - 70 °C. A portion of the cooled gelatine solution was transferred to a sterile beaker, and mica discs were briefly lowered into the solution and removed, before being allowed to dry on edge at room temperatures overnight. Poly-l-lysine coated slides were prepared by aliquoting 50 µl of freshly prepared 0.01 % poly-L-lysine solution to the centre of each slide and drying in a 60 °C drying oven for 30 minutes.

Residual contaminants were removed from oocyst stock solution using filter sterilisation as previously described. The filtered oocysts were pelleted by centrifugation at 200 x g for 18 minutes, the supernatant removed, and the pellet re-suspended in 50 µl/slide HPLC water.

50 µl of oocyst suspension was aliquoted to the centre of each of the gelatine and poly-l-lysine treated slides and allowed to sediment for 20 minutes before rinsing with 2 ml HPLC water. All slides were imaged using confocal light microscopy at 40x magnification, and images captured using a hand-held camera.

Buffer optimisation for poly-l-lysine: Water v PBS over time

For AFM imaging in fluid, the effects of 1x PBS sodium chloride and sodium phosphate diluents on oocyst adherence over time were assessed using confocal light microscopy. Glass and mica sample slides with *C. parvum* oocysts immobilised using 0.01 % poly-l-lysine were prepared as previously described (see sample preparation). Following washing, sample deposition sites were covered in droplet of 1x PBS or HPLC water and imaged using fluorescence light microscopy. At intervals of 20 minutes slides were rinsed using 2 ml of 1x PBS or HPLC water as appropriate, immediately re-

covered with a droplet of the same liquid, and imaged at areas of high oocyst adherence density using confocal light microscopy.

Glass versus Mica

As oocysts were observed to adhere to glass slides, light microscopy was used to evaluate oocyst deposition numbers on glass vs mica slides prepared both with and without 0.01 % poly-L-lysine prepared as previously described.

Poly-l-lysine concentration with sedimentation time on glass:

The effects of poly-l-lysine concentration in combination with sedimentation time (over a period of 1 hour) on oocyst adherence numbers were assessed using light microscopy. Glass slides were prepared with 0.01 %, 0.03 %, and 0.05 % poly-l-lysine and *C. parvum* oocyst samples as previously described. Slides of each ply-l-lysine concentration were imaged after sedimentation periods of 15 minutes, 30 minutes, and one hour using confocal light microscopy.

Atomic force microscopy in liquid poly-l-lysine optimisation:

To test the effect of poly-L-lysine concentration on oocyst resistance to probe contact during liquid AFM, glass slides with attached oocysts were prepared with poly-L-lysine at concentrations of 0.01 %, 0.02 %, 0.03 %, 0.04 %, 0.05 %, 0.06 % and 0.07 % as previously described and imaged using AFM in liquid. Slides were not allowed to dry at any point prior to imaging.

2.3 Atomic force microscopy

Imaging:

AFM analysis was performed using the Bruker Multimode 8 SPM, and the resulting data was analysed using NanoScope Analysis v1.40r1. Images in air were attained using Bruker ScanAsyst-AIR probes, while ScanAsyst-FLUID or ScanAsyst-FLUID+ probes were used for imaging in liquid.

Oocysts were imaged using ScanAsyst® in air and liquid modes. Peak force quantitative nanomechanical mapping (PeakForce QNM®) mode in air and in liquid was used for mechanical property measurement. For optimal measurements using PeakForce QNM® mode, probe spring constant was calibrated prior to each session and on introduction of each new probe. For scanning large areas in air to locate oocysts, parameters were set at a view window of 100 µm, with relatively high scan-rate of between 0.558 - 0.988 Hz, a low number of samples per line and lines per view (between 256 and 512), and a peak force setpoint of between 10 - 20 nN. For scanning of large areas in liquid, scan rate and peak force setpoint were decreased to between 0.1 and 0.2 Hz, and 1 and 5 nN respectively. For high-resolution imaging of smaller areas and individual oocysts, the

number of samples per line and scan lines/view were increased to between 512 and 1024, and scan rate was decreased to 0.1 Hz.

In instances where deposition or drag were apparent during liquid imaging, scan rate and peak force setpoint can be decreased to between 1 - 5 nN. Whilst decreasing the peak force setpoint can result in softer, less defined images, it can enable imaging of less firmly immobilised samples that could otherwise become displaced upon tip-sample contact, and results in decrease noise. Difficulties arising during imaging in air, such as probe 'sticking' due to residual surface moisture, can be addressed by decreasing scan rate to the minimum (0.100 Hz) and/or additional nitrogen drying for a further 2 - 3 seconds, although oocysts hydration may be compromised.

Data analysis:

AFM images were analysed using NanoScope Analysis V. 1.5 particle analysis, slice and bearing analysis functions. Prior to analysis images were first order flattened and plane fit applied where applicable. For statistical analysis of oocyst measurements between imaging conditions mean values, sample variance, sample standard deviation and standard error were calculated for height, volume, area and diameter measurements. The significance of the difference between the measurement means for each condition was calculated using a 2-sample t-test assuming unequal variance.

2.4 Scanning electron microscopy and field emission scanning electron microscopy:

For SEM analysis *C. parvum* oocyst samples were imaged using the Hitachi S3400 series SEM. Here a backscatter electron sensor was used to measure density. The Hitachi S4700 (cold) field emission SEM (FESEM), with Bruker "XFlash" quad-element EDX detector was used to gain high definition of oocyst surface morphology and chemical composition analysis.

Initial scanning electron microscopy of fixed oocyst:

250 µl of 2 x 10^7 oocyst/ml stock per sample (5 x 10^6 oocysts/sample) was filtered as previously described and resuspended in 25 ul HPLC water/sample were deposited to adhesive electrically conductive carbon discs ('Leit' tabs) (Sigma-Aldrich) mounted on metal specimen stubs (Sigma-Aldrich) and allowed to air dry. Samples were then fixed overnight in 2.5 % glutaraldehyde. Prior to imaging using the Hitachi S3400 series SEM, samples were rinsed with HPLC water and allowed to air dry.

Samples were imaged under standard parameters, at accelerating voltages of between 10 and 0.5 kV.

Non-fixed FESEM imaging and EDX chemical analysis parameters:

Oocysts were imaged with the aperture in, acceleration voltage set at 0.5-0.7 kV, and beam current set to 2 µA. To image at varying depths within the sample, acceleration voltage was increased incrementally from 5 kV (surface imaging) to 30 kV (through the sample to the underlying substrate). The facility to image at varying depths within the sample aids determination of feature location, i.e. whether situated on/within the oocyst wall or below it, internal to the oocyst.

For composition analysis the EDX detector was used to analyse oocysts using the parameters described in imaging, chemical analysis was performed at varying depths within the sample through incrementally increasing the accelerating voltage.

2.5 Fluorescence Microscopy:

To assess the infectivity of AFM imaged oocysts (both in liquid and in air), cell culture infections were performed, and de novo produced oocysts were detected using the Olympus 1x81 fluorescence microscope, and images captures using an Andor Zyla 4.2 plus SCMOS camera at 1,000x magnification. For oocyst detection, samples were stained with both Crypt-a-Glo™ (Waterborne Inc.), a fluorescein labelled antibody specific to *C. parvum* oocyst stages, and 4',6-diamidino-2-phenylindole (DAPI) for DNA staining. In addition, fluorescence microscopy of stock oocysts and non-imaged oocysts produced by infection of cultured cells were performed as a positive control. Images were edited using ImajeJ.

Staining protocol:

Glass coverslips were treated with pol-l-lysine, and 9 ml oocyst stock solution (1 x 10^7 oocysts/slide) was filtered, resuspended, and applied to dried coverslips as previously described. Once dried down, the samples were fixed using 45 µl methanol/slide to enhance DAPI staining. Once the fixative had fully dried (≈30 minutes), as pertinent, ≈45 µl Crypt-a-Glo™ antibody solution (Waterborne Inc) was applied to the fixed sample spot at the centre of each coverslip, and samples were left to stain at r.t. in a humid chamber for a minimum of one hour (overnight staining can be adopted if sampled are stored in at 4 °C). Slides were then rinsed of Crypt-a-Glo™ using 1 ml HPLC water. Once dry, 45µl Fluoroshield™ with DAPI (Sigma Aldrich) or Fluoromount™ Aqueous Mounting Medium (Sigma Aldrich) as appropriate was applied to each slide prior to cover-slip application. Cover-slips were then sealed with nail varnish (Boots) and stored in aluminium foil (Wilko Retail LTD) until viewing.

Fluorescence imaging of stock oocysts:

For fluorescence imaging of stock oocysts, samples were separated into two immobilisation conditions, one group of oocysts were immobilised to coverslips using 0.01 % poly-l-lysine (as in

AFM imaging in air), and one group immobilised using 0.05 % poly-l-lysine (as in liquid AFM imaging) Each of these groups was then divided into three conditions (each repeated in triplicate), including oocysts stained with *Cryptosporidium* oocyst specific Crypt-a-Glo™ fluorescent stain, oocysts stained only with DAPI stain for imaging of genetic material, and oocysts stained with both DAPI and Crypt-a-Glo™. Immobilisation conditions were compared for analysis of oocyst attachment numbers and patterning.

2.6 Cell Culture:

Cell revival:

For cryopreservation, cells were frozen in the standard growth medium + 5% DMSO. Fresh COLO-680N or HCT-8 cells were removed from storage at -80 °C and placed on dry ice before thawing in a water bath at 37 °C. Freshly made RPMI-1640 media (Sigma-Aldrich. Lot no. RNBF8560) containing 10 % heat inactivated foetal bovine serum (h.i FBS- Sigma -Aldrich. Lot no. BCBR0289V), penicillin (100 U/ml), and streptomycin (100µg/ml) per ml was similarly heated to the same temperature.

In the class ll biosafety cabinet, 10 ml fresh warmed media was aliquoted to a fresh 15 ml falcon tube, followed by addition of 1ml thawed cell suspension. This suspension was homogenised, and cells washed of dimethyl sulfoxide (DMSO - cryoprotectant) (Sigma-Aldrich) by pelleting at 300 x g for three minutes. The supernatant was removed and the pellet re-suspended in 10 ml fresh warmed media. The resulting cell suspension was transferred to a T25 flask and incubated at 37 °C with 5% CO_2.

Culture Splitting and Bulk Up:

Once the revived cells reached a confluency of roughly 70 - 80 % (1 - 2 days), they were split to continue culture in 2 x new T75 flasks. Fresh RPMI media with 10 % h.i FBS, and penicillin and streptomycin per ml, 1x f.s. PBS and 0.25 % trypsin EDTA were heated in a water bath to 37°C to avoid cell shock due to cooling (roughly 40 minutes). In the biosafety cabinet media supernatant was removed, and the T25 flasks rinsed with 10 ml warmed PBS (for removal of excess media, as FBS can inactivate trypsin). 2 ml 0.25 % trypsin was added the flask, ensuring full coverage of the base and attached cells, and incubated for roughly two minutes until the cells became turbid (as with confluency, turbidity can be verified using confocal light microscopy). Once turbid, 10 ml media was added to deactivate the trypsin prevent cell damage due to prolonged exposure. 10 ml of the cell suspension was transferred to a fresh 15 ml falcon tube and pelleted by centrifugation at 300 x g for 3 minutes. Following careful removal of the supernatant the pellet was re-suspended in 10 ml

fresh warmed media. 10 ml of fresh media was added to each of two T75 flasks, followed by addition of 2.5 ml of the new cell suspension. This process was repeated when the cells reached confluency (roughly every 3 days). The first splitting is cell passage 1, the cultures can only be passaged 16 times before cell integrity become compromised and fresh cells must be revived. For further culture bulking, 6 ml of the washed cell suspension from the T75 flasks was added to 24 ml fresh media in fresh T175 flasks and maintained in future passages by detachment with 5 ml 0.25 % trypsin, and passage of 2.5 ml of final washed suspension into 27.5 ml fresh media.

2.7 Infection experimental procedures:

Excystation composition experiment:

In addition to imaging at sections through the sample, globular cluster feature location was further investigated through parallel imaging and chemical analysis of whole oocysts, excysted filter isolated oocysts walls, excysted internal components isolated from oocyst walls and excysted non-filtered oocysts (see figure 2), in each of the above conditions cluster feature presence and location/patterning were analysed.

Excystation procedure:

≈1 x 10^7 oocysts/excystation condition (0.5 ml f.s stock) were pelleted at 2,000 x g for 8 minutes. The pellet was resuspended in 500 µl excystation solution (100 µl 0.01 % trypsin + 400 µl 0.5 % sodium hypochlorite) in 1 ml microfuge tubes, and incubation at 37 °C for 3 - 4 hours or until sporozoites exceed 80 % of the theoretical maximum (4x the number of oocysts-monitor excystation progression using a haemocytometer). Oocyst material was then pelleted at 2,000 x g for 8 minutes and washed in 1x f.s PBS.

Excystation solution filtering and sample preparation:

Excystation solution was filtered and isolated oocyst walls retrieved as previously described for oocyst stock sterilisation, isolated excysted oocyst contents were retrieved by pelleting filtered solution at 2,000 x g for 8 minutes. For all samples, supernatant was removed, and pellets were re-suspended in 20 µl HPLC water. Each sample was then deposited to carbon leit tabs as previously described. Samples were imaged the Hitachi S4700 FESEM as previously described.

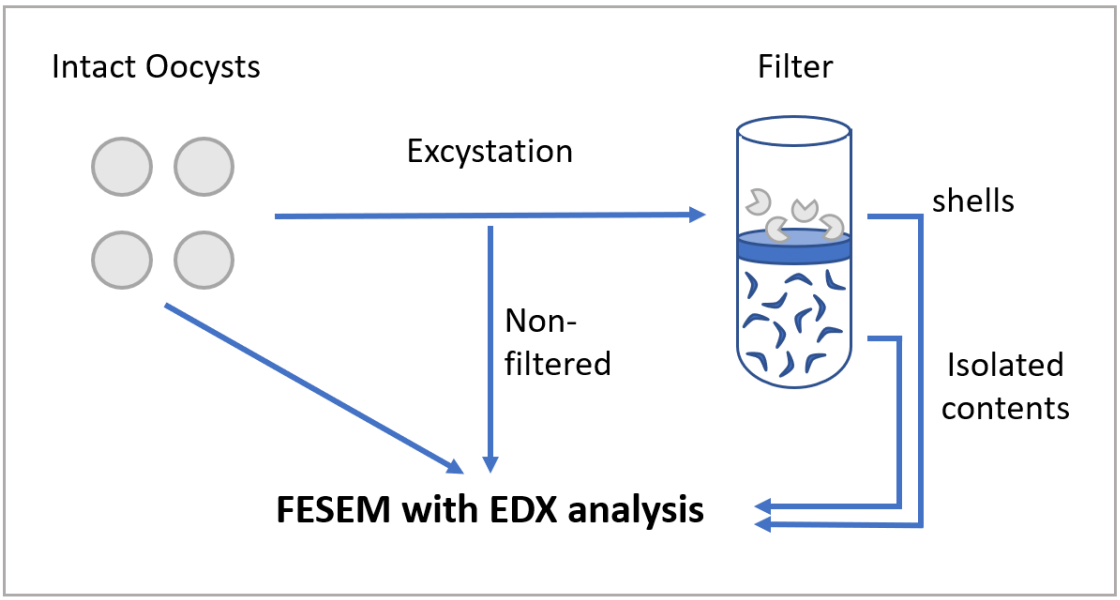

Figure 2: Schematic illustrating FESEM imaging and EDX compositional analysis experimental design.

Initial infection for fluorescence imaging: non-AFM imaged control and determination of optimal cell type for short-term oocyst production:

For determination of the optimal cell line for infection and production on *de novo* oocysts in the short-term COLO-680N (as described Miller et al., 2018) or HCT-8 cell lines (Sifuentes and Di Giovanni, 2007). Cell cultures of both cell lines and oocyst excystation were performed as previously described (see 'excystation procedure' and 'cell culture'). For infection, old media was removed from T75 flasks containing cultured cells at 70 % confluency (one flask with HCT-8, one with COLO-680N) and replaced with fresh media (warmed to 37 °C). Each flask was then inoculated with 52 µl excystation fluid and stored at 37 °C.

As these cell lines are known to begin producing oocysts at differing days post infection (Sifuentes and Di Giovanni, 2007; Koloren and Dinçer, 2008; Miller et al., 2018) the supernatant from HCT-8 cell lines was removed and stored for analysis at day seven and COLO-680N cultures were similarly processed on day thirteen.

To establish success of failure of infection, cell culture supernatant was removed, aliquoted to fresh 15 ml falcon tubes, and larger cell debris removed by pelleting at 300 x g for 3 minutes, followed by removal of the supernatant. The supernatant was spun again at 5,000 x g for eight minutes, the resulting supernatant removed, and the pellet re-suspended in 100 µl 1 x f.s. PBS (repeated twice as wash step). Fluorescence staining and slide preparation were performed as previously described (see 'staining protocol').

Infection with imaged oocysts and fluorescence microscopy:

For infections using AFM imaged oocysts, multiple parallel infections and conditions were enabled by cell growth and infection on coverslips in 24 - well plates. There were three conditions per infection: the infection condition (both cells and excysted sporozoites), wells containing cells only, and wells containing excysted sporozoites only (as negative controls). These conditions were repeated twice to give a total of 8 slides per condition across the 24 wells, allowing imaging of slides at different dates post infection (see figure 3).

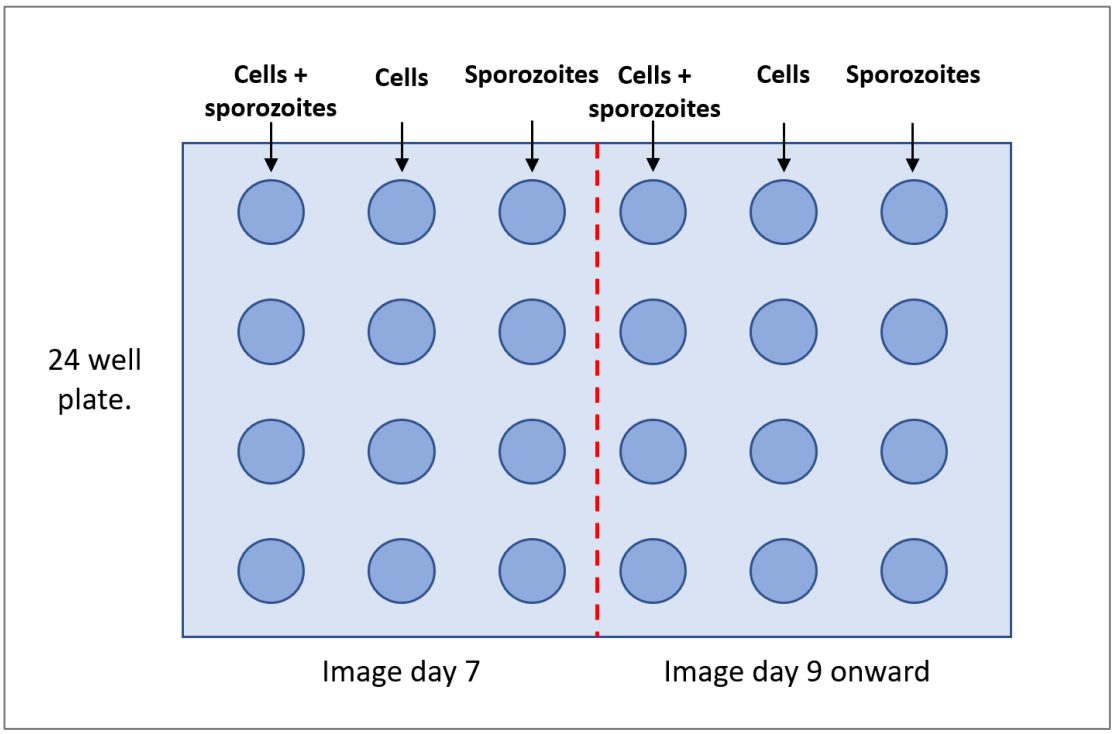

Figure 3: Schematic representation of cell culture infections and control sample preparation design.

Well plates containing circular glass coverslips were UV sterilised for one hour. Cells of one T75 culture flask were detached, washed and re-suspended as previously described. 1 ml fresh media was added to each well, and 100 µl cell suspension was added to 16 of the 24 wells, leaving 8 wells as cell-free controls. Well plates were incubated at 37°C until cell confluency reached roughly 70 % (2 - 3 days), at which point infection protocol can proceed.

For infection, AFM imaging was conducted as previously described. Glass slides with attached imaged oocysts were halved, submerged in microfuge tubes containing 500 µl excystation solution (see excystation procedure), and incubated for 3 - 4 hours (due to variability in oocyst-slide attachment, theoretical maximum sporozoite yield could not be calculated). Glass slide shards were

removed, rinsed of excess excystation solution with 1x f.s. PBS (retained), and imaged using confocal light microscopy to ensure absence of retained oocysts and/or sporozoites. Excystation mixtures were pelleted at 2,000 x g for 8 minutes, the supernatant removed, and the pellet re-suspended in 500 µl 1x f.s PBS (repeated twice to wash). The media in the well plates was replenished with fresh media (1 ml/well, warmed to 37 °C), and 16 of the 24 wells were inoculated with 100 µl of oocyst excystation product (see figure 3). Well plates were incubated at 37 °C for seven days prior to initial fluorescence staining and imaging, and a further 2-3 days for delayed fluorescence imaging.

2.8 Analysis of non-oocyst globular features:

Atomic force microscopy: *E. coli*, stock treated with antibiotics

For clarification of rod-like and globular feature origin, stock solution was tested for bacterial contamination pre and post filtering, samples were treated with broad-spectrum antibiotics and imaged using AFM in air, and *Escherichia coli* was imaged using AFM in air for comparison with features in untreated samples.

DH5α strain *E. coli* cultures were obtained, colonies immobilised and imaged using 0.01 % poly-l-lysine for AFM in air as previously described for immobilisation and imaging of *C. parvum* oocysts. Images were analysed and features present compared to those in non-treated samples.

For antibiotic treatment of stock solution, 2 ml fractions of stock solution were treated with 2 µl 100 mg/ml ampicillin, and 2 µl 50mg/ml chloramphenicol (1:1000). After two days, samples were filtered and prepared for imaging using AFM in air as previously described.

PCR

Four PCR reactions were performed using the 27F and 1292R primer set to test for bacterial DNA in oocyst stock solution by targeting the V6 region of the 16S SSU rRNA gene. Alongside filtered and non-filtered oocyst stock solution, DH5α strain *E. coli* DNA was used as a positive control, and a DNA free solution was used as a negative control. The 27F and 1292R primer set produces a fragment roughly 1,484 bp in length. Forward primer sequence: 5'- AGA GTT TGA TCN TGG CTC AG- 3', reverse primer sequence: 5'- GG TTA CCT TGT TAC GAC TT- 3'.

For PCR analysis of stock solution, 50 µl of filtered stock solution was prepared and pelleted as previously described for AFM analysis of oocysts. For maximum content retention, 50 µl of non-filtered oocyst stock was pelleted at 14,000 x g for 5 minutes. Both pellets were re-suspended in 2 µl HPLC water.

Reactions were completed at 50 µl total volume per reaction. Individual reactions consisted of: 25 µl PCR buffer, 4 µl forward primer (5 pmol/µl), 4 µl reverse primer (5 pmol/µl), 2 µl sample for analysis/DNA, and 15 µl HPLC water.

Reactions had a preliminary denaturation interval of 94°C for 2 minutes, followed by 30 cycles of 1 minute at 91 °C, a 1-minute annealing period at 55 °C, followed by an extension period of 72 °C for 2 minutes. The incubation cycle was completed with a final 2-minute period at 72 °C. Reactions were stored on ice pending gel analysis.

Gel analysis:

1 % agarose gel was prepared containing 4 µl ethidium bromide per 50 ml gel. 50 µl samples were mixed with 10 µl loading buffer. 20 µl of sample was loaded per well, against 10 µl 1Kb ladder (Invitrogen cat: 10787018). The gel was separated at 70v. The gel was imaged using the G:BOX gel imaging system (Syngene).

3.0 Results:

3.1 Scanning electron microscopy and field emission scanning electron microscopy:

Scanning electron microscopy analysis of fixed oocysts:

In order to determine the capabilities of the scanning electron microscopy in imaging non-sputter-coated *Cryptosporidium* oocysts, initially *C. parvum* oocysts were fixed using 2.5% glutaraldehyde and imaged using the Hitachi S3400 series SEM.

SEM analysis of fixed oocysts resulted in desiccation and concave collapse of oocysts, with very few oocysts retaining their spherical hydrated shape. SE imaging resulted in some charging of the sample, causing 'glow' effects with decreased surface resolution. SE analysis also revealed some variation in the pattern of oocyst collapse, with most in areas of confluent attachment taking on a concave 'bowl-like' shape, where single oocysts assumed a convex form with flattened edges. BSE density analysis and SE surface topography revealed distinctive 'globular cluster features' within the raised borders of the concave collapsed oocysts (fig 4).

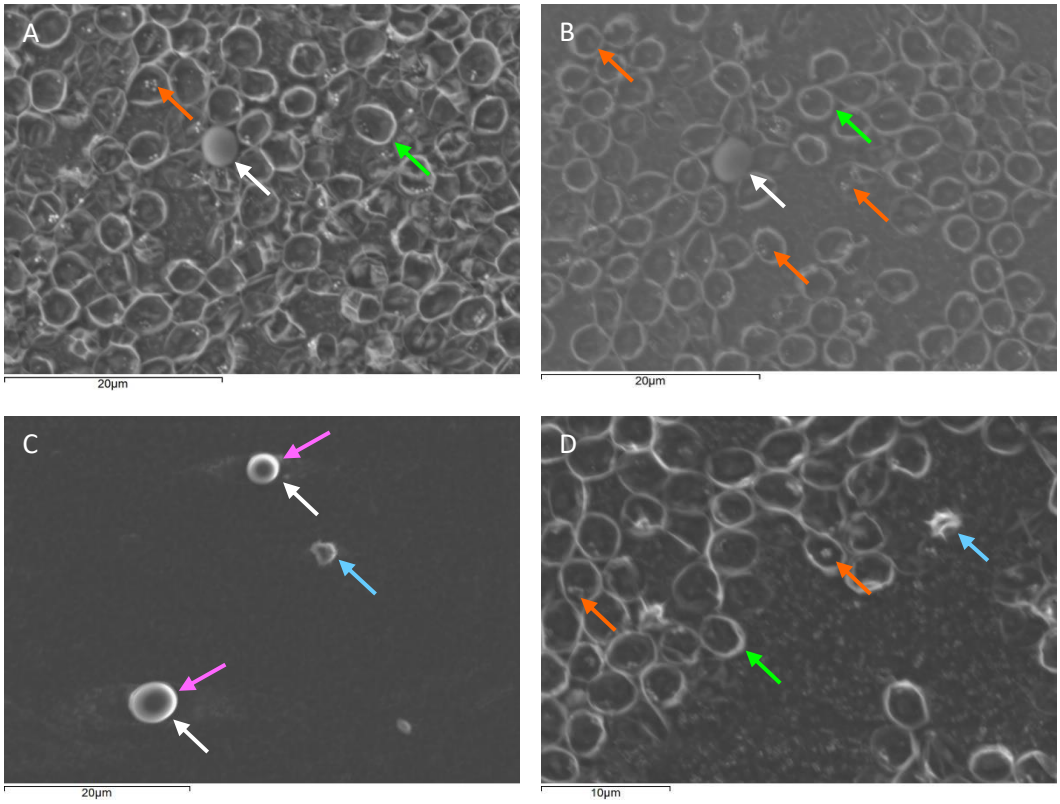

Fig. 4: SEM analysis of fixed oocysts.
BSE imaging at 2710 and 2700 x magnification (A and B respectively) reveals desiccation and concave collapse of oocysts (green arrows). Few oocysts retain a spherical appearance (white arrows). SE imaging (C and D) shows charge 'glow' effects (pink arrows), and variation in oocyst collapse patterning (convex collapse - blue arrows). BSE (A and B), and SE analysis (C and D) reveal 'globular features' within the concave oocysts (red arrows).

Field emission scanning electron microscopy analysis of unfixed oocysts

As sample fixing conferred no apparent benefit and potentially removed oocysts further from their natural state it was determined that the purposes of this study would be best met by continuing SEM analysis using non-fixed oocysts. The capabilities of FESEM to provide greater image resolution were also assessed using non-fixed oocysts.

FESEM analysis of non-fixed oocysts allowed higher resolution imaging of individual oocysts than SEM analysis. Imaging at low accelerating voltages (ACC V) in combination with exposing the sample to vacuum conditions whilst still covered in a thin water droplet allowed imaging of large numbers of oocysts at around 600 x magnification prior to the widespread appearance of dehydration effects and oocyst collapse (fig 5).

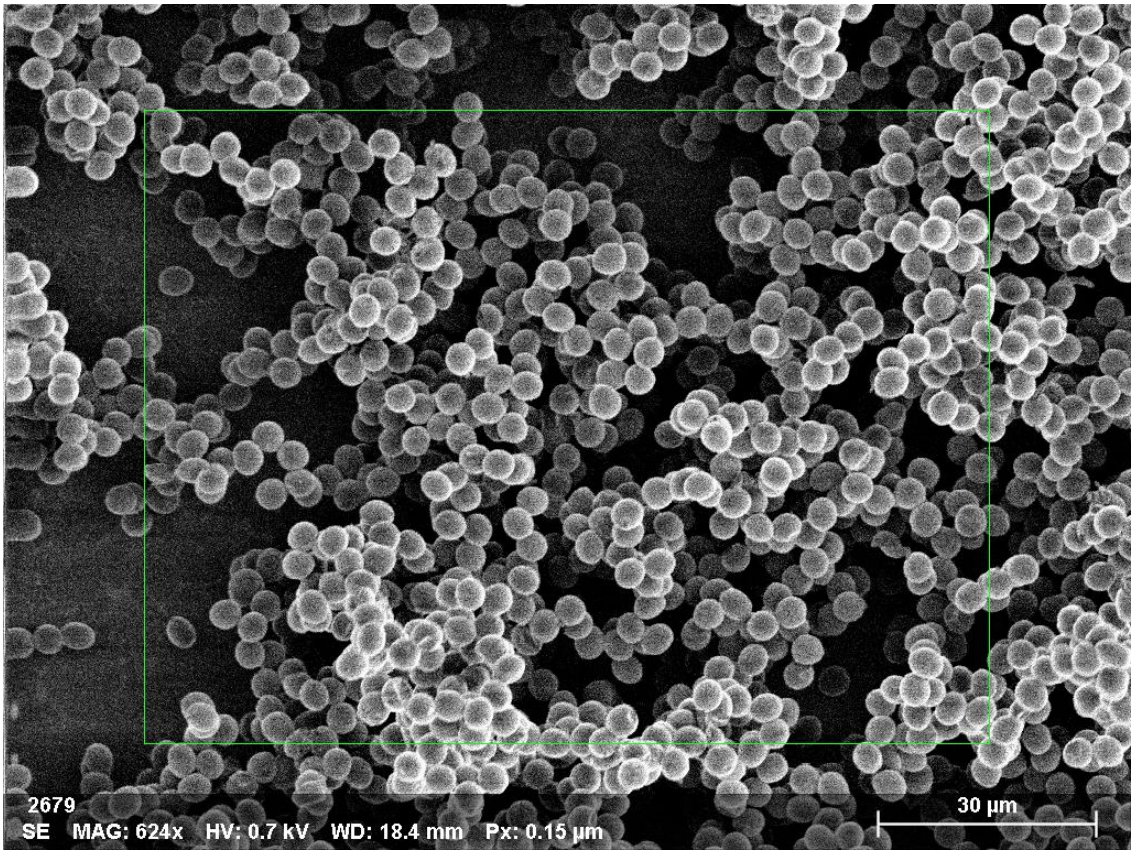

Fig 5: FESEM imaging
FESEM image of non-fixed oocysts at low magnification and ACC V allows imaging of large numbers of oocysts that did not collapse. (The green square shows the area over which the SEM would provide an EDX map).

Imaging with an accelerating voltage of 1.5 allowed high resolution images of the oocyst surface at higher magnifications with a decreasing rate of oocyst collapse, revealing what appeared to be a 'dimple' like feature on the oocyst surface (fig 6), which to our knowledge has not been documented in previous research. Increasing the ACC V to 5 kV and above caused charge effects and decreased resolution of surface topography as electrons passed deeper into the sample, whilst imaging at lower accelerating voltages resulted in decreased resolution due to a low resulting signal (fig 6 and 8). Imaging collapsed oocysts revealed unknown 'globular cluster' features within the raised boarders of the oocyst walls (figure 7).

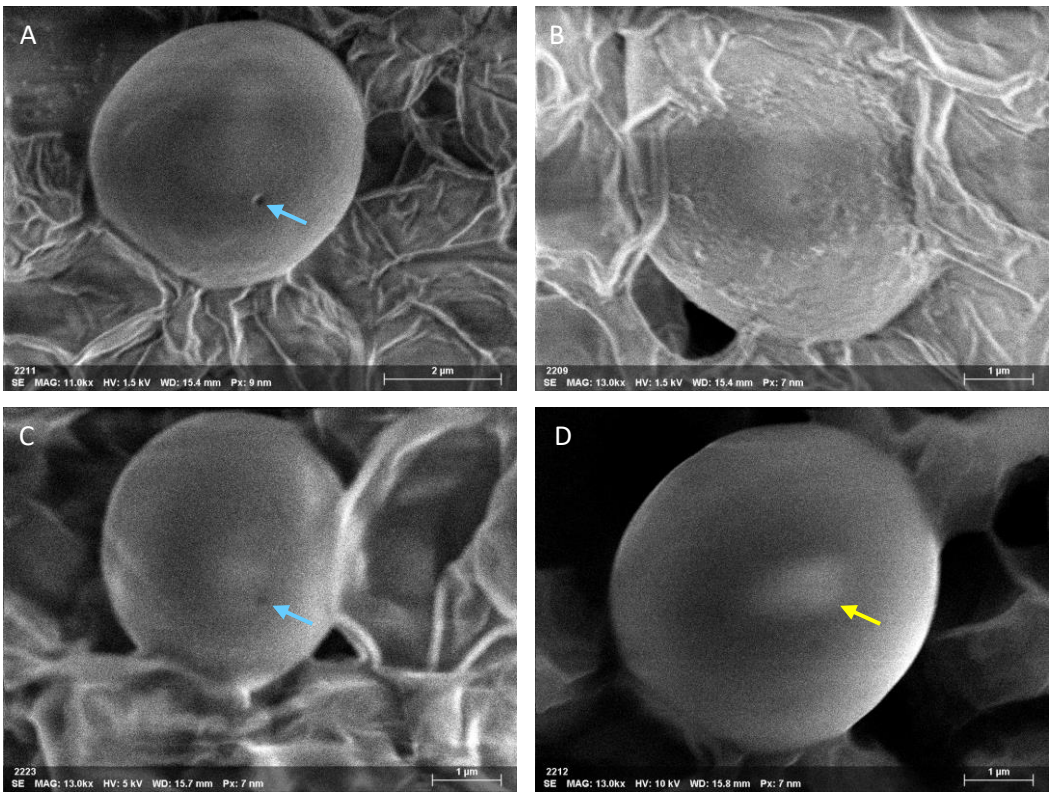

Figure 6: FESEM imaging of unfixed oocysts.
Few oocysts remain intact without fixing and can be imaged without collapsing at up to 13,000 x magnification. Accelerating voltages of 1.5 Kv allow high resolution imaging of oocyst surfaces (A and B), where higher accelerating voltages of 5-10 kV result in increasingly low resolution (C and D) and charge effects (yellow arrow). Images A and C show a dimple-like feature located on the oocyst surface (blue arrow).

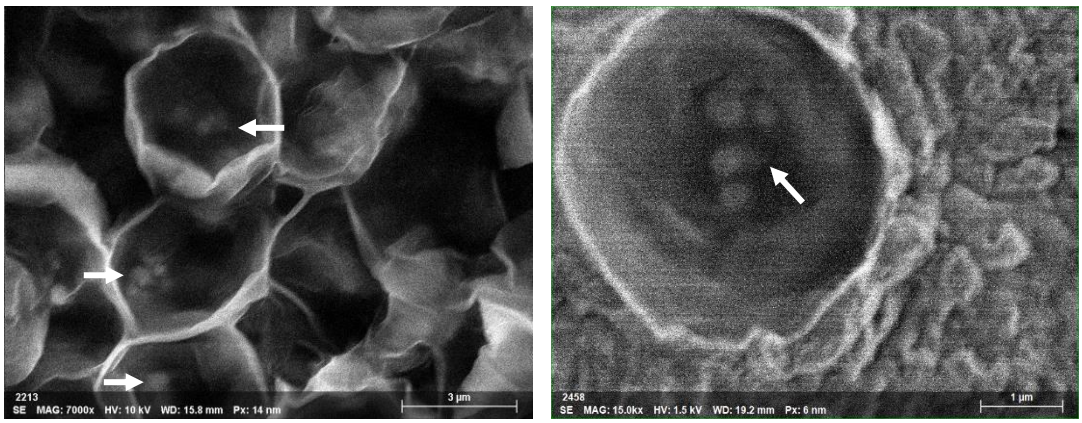

Fig. 7: FESEM analysis of collapsed oocysts.
FESEM analysis revealed the presence of 'globular cluster' features internal to the raised edges of the collapsed oocyst walls (white arrows).

Sample exposure to vacuum conditions and electron beam damage causes dehydration and collapse of oocysts, beginning with creasing and indentation of the outer shell, as shown in figure 8.

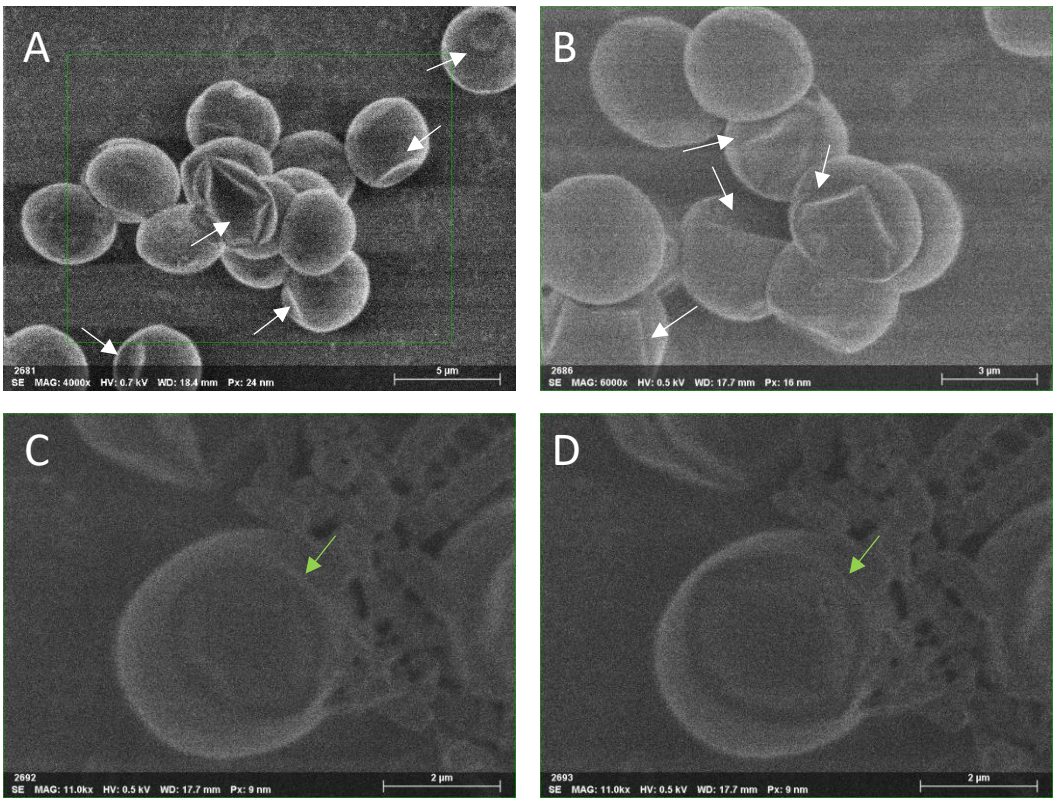

Fig 8: Effects of imaging conditions upon non-fixed oocyst structural integrity.
Increasing magnification leads to rapid collapse of oocyst structure, as shown in images A and B (white arrows).
Addressing cavitation speed by lowering ACC V led to a corresponding decrease in signal, and therefore image resolution. Image A was attained at 0.7 Kv, and image B at 0.5 Kv.
Progression of cavitation can occur over a period of a few seconds (C and D-green arrows), here image D was captures within a 5 second interval of image C.

Analysis of 'globular cluster' feature location by imaging at varying accelerating voltages:

Use of SE analysis with progressively increasing acceleration voltage revealed that previously identified 'globular cluster' features were most clearly visible at accelerating voltages of between 10 and 20 Kv, suggesting that they are situated beneath the oocyst wall (Fig. 9).

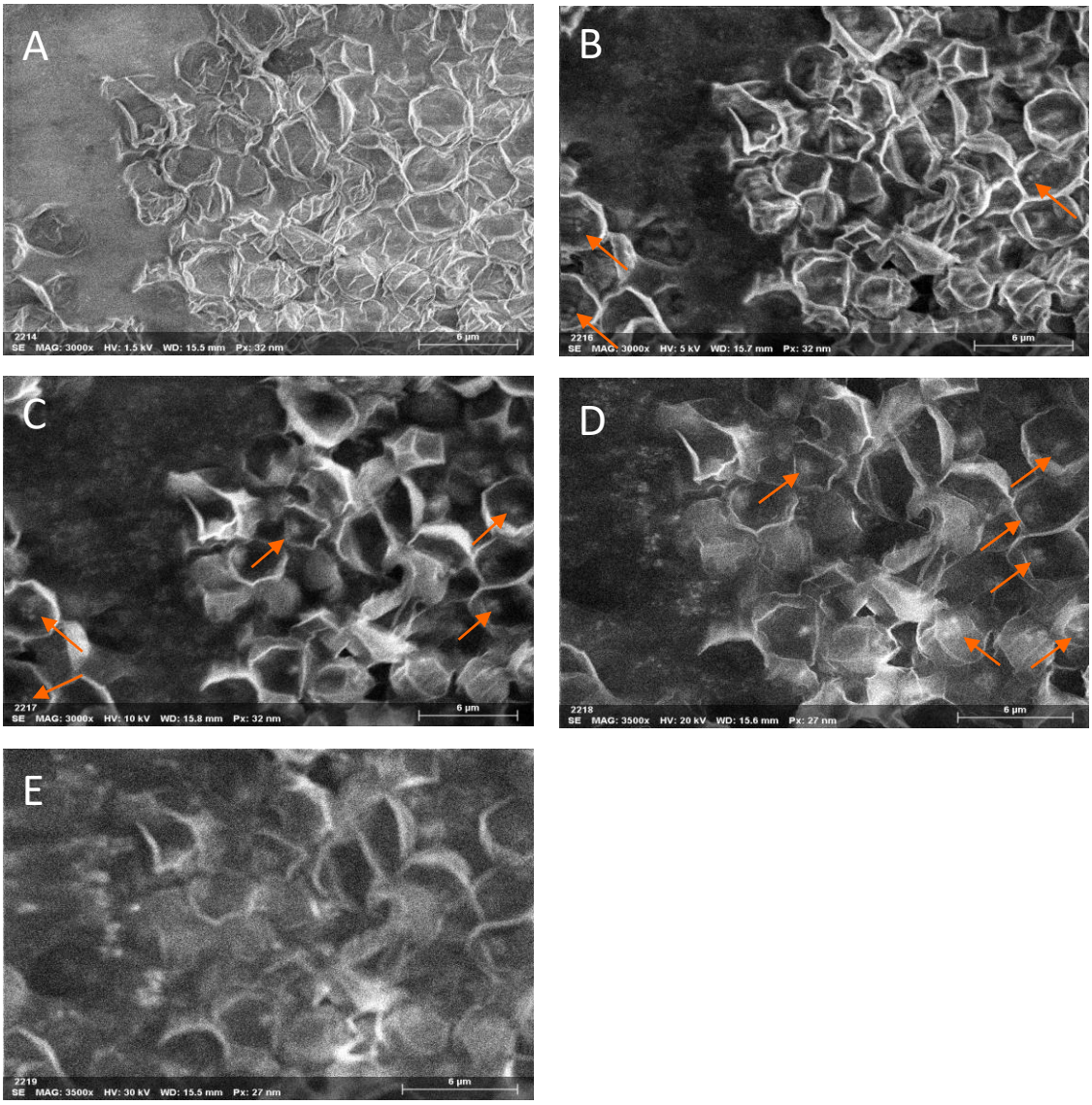

Figure 9: Use of SE analysis with increasing acceleration voltage to image at progressive depths through the sample for 'globular cluster' feature analysis.
Low accelerating voltage of 1.5 Kv provides high resolution imaging of the sample surface (A), whereas increased ACC V of between 5 Kv and 20 Kv provides data from beneath the outer oocyst surface (B-D). Increasing the ACC V to 30 Kv images the underlying substrate (E). Cluster feature location is indicated with red arrows.

EDX analysis of 'globular cluster' features:

EDX analysis was applied to help investigate the nature of the 'globular cluster' features through providing maps of sample chemical composition which can be directly compared to SE generated images.

EDX analysis revealed that areas of 'globular cluster' location revealed by SE analysis co-localised with areas of high phosphate and magnesium, appearing in similar 'cluster' patterning and form.

This data suggests that these features are high in phosphate and magnesium content (fig. 10). Many areas of co-localisation between phosphate and magnesium content were not paralleled in SE analysis.

EDX analysis of whole vs. excysted oocysts revealed that the cluster patterning observed in whole oocysts was not present in any condition in which excystation had occurred. Excysted and excysted filtered samples displaying very low levels of phosphorus and magnesium content overall with disperse and approximately even distribution (fig. 11). Filter isolated oocyst contents did not reveal significant signal levels or patterning for any chemical element.

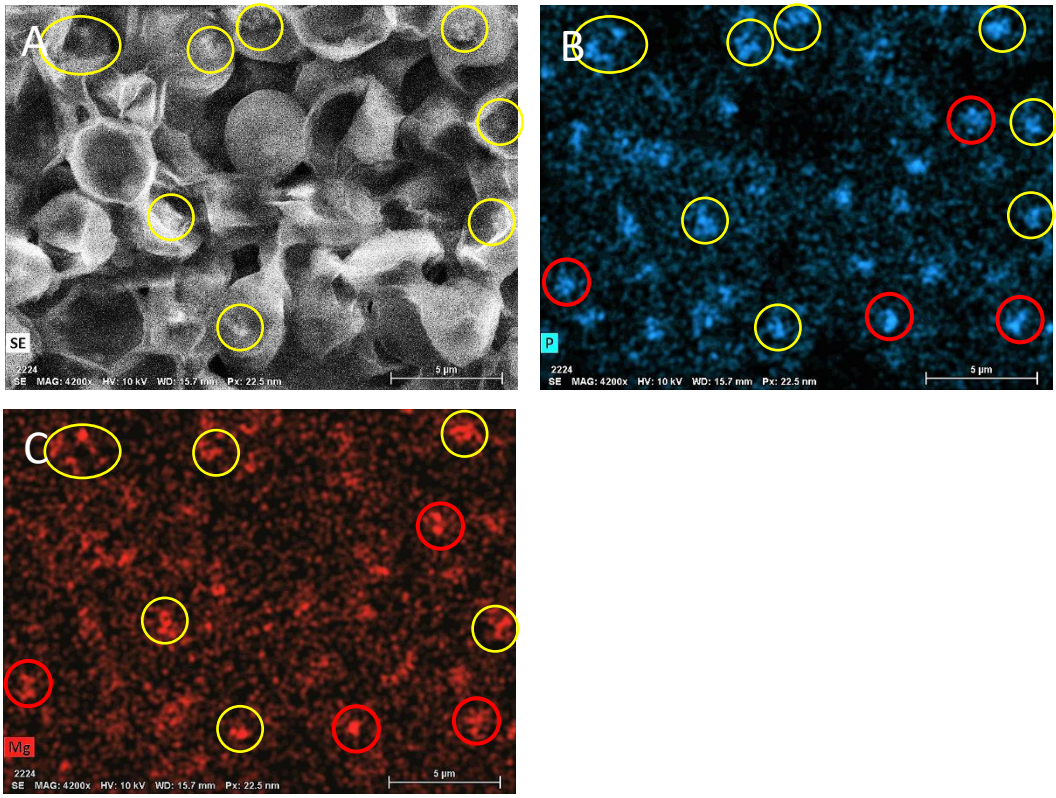

Fig. 10: EDX analysis of 'globular cluster' features.
EDX analysis reveals areas of phosphate and magnesium co-localisation (A and B respectively) with 'globular clusters' shown by SE analysis (A). Analysis reveals areas of co-localisation between all three views (yellow bands). Red bands indicate areas high in Mg and P not visible in SE analysis (A).

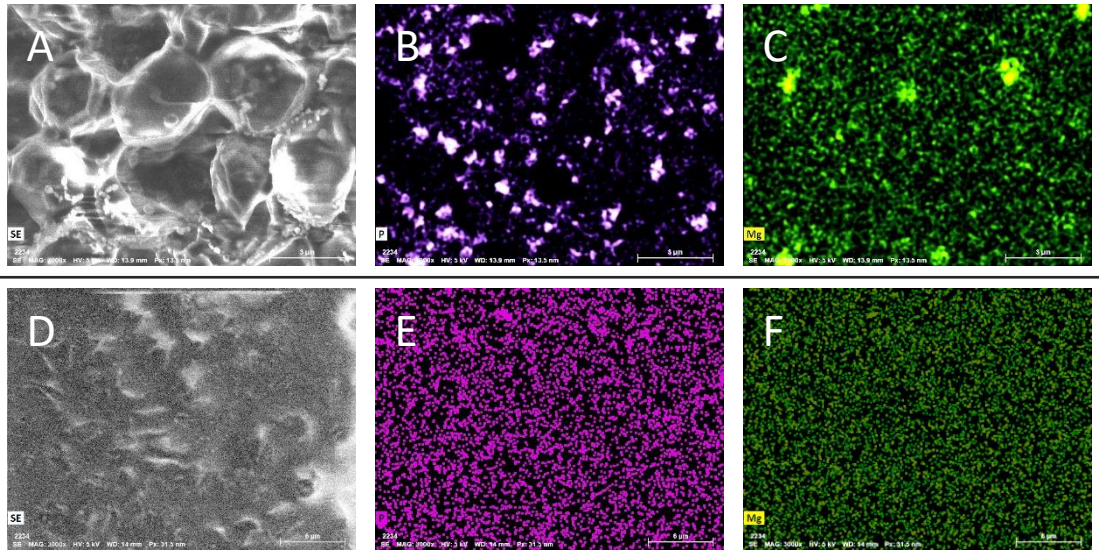

Fig. 11: EDX analysis of whole and excysted oocysts.
Whole oocyst surfaces (A-C) are analysed using SE imaging (A) and EDX analysis (B and C). EDX analysis reveals 'clusters' of co-localisation in phosphorus and magnesium. SEM imaging of excysted samples (D-F) reveals flattened oocyst shells (D). EDX analysis shows no clustering of magnesium or phosphorus localisation (E and F).

3.2 Immobilisation optimisation for atomic force microscopy:

To determine the optimal substrate, immobilisation treatment and buffer/imaging solution for immobilisation of oocysts for AFM imaging, light microscopy was used to compare oocyst adherence frequencies between mica slides treated with poly-L-lysine vs. gelatine, non-treated glass and mica surfaces, glass slides treated with varying concentrations poly-L-lysine, and 1xPBS vs HPLC water as buffer/imaging solution.

Glass vs. mica:

Glass surfaces were found to provide superior attachment numbers and strength to mica surfaces.

Gelatine vs. poly-l-lysine:

Optimisations established that gelatine does immobilise *C. parvum* oocysts, but that poly-l-lysine provides superior oocyst attachment numbers (fig. 12).

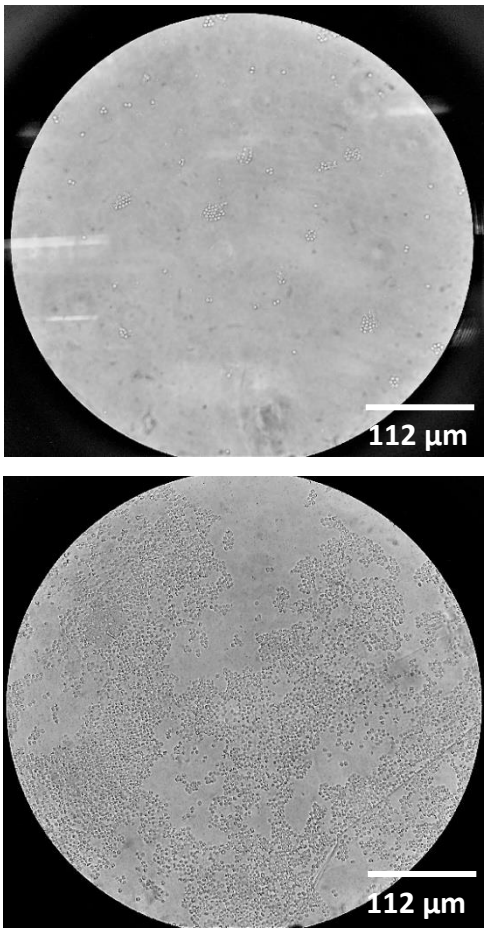

Fig. 12: Gelatine vs. poly-l-lysine immobilisation
Representative image samples of oocyst immobilisation using porcine gelatine vs. poly-l-lysine, imaged using a compound light microscope at 400 x mag.

Poly-l-lysine concentration:

Poly-L-lysine optimisations using confocal light microscopy in conjunction with AFM imaging revealed an inverse relationship between the effects of poly-l-lysine concentration on attachment number and strength of attachment.

Buffer optimisation:

Buffer optimisations determined that use of 1x PBS as a buffer solution for oocysts immobilised using poly-l-lysine results in progressive oocyst detachment over time (Fig. 13). During the 80-minute time frame over which slides were imaged, samples covered in a droplet of HPLC water showed no noticeable decrease in oocyst numbers between washes, samples covered in PBS

showed decreasing numbers from the first wash after 20 minutes. Results were consistent between glass and mica slides.

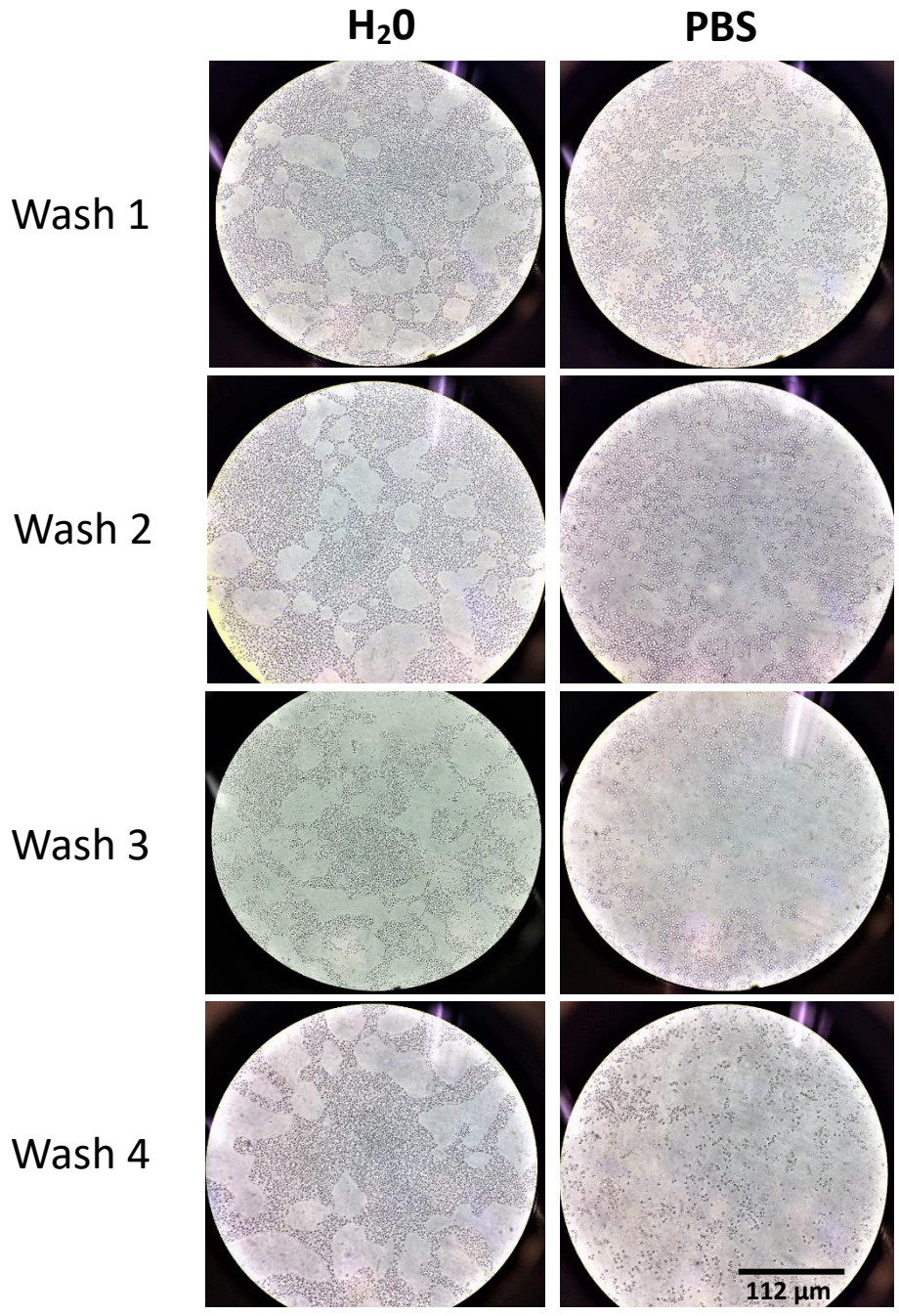

Fig. 13: Buffer optimisation for oocyst immobilisation using poly-l-lysine on glass. Buffer optimisations revealed that hydration in PBS causes progressive detachment of oocysts over time. Optimisations were imaged using a compound light microscope at 400 x mag.

3.3 Atomic force microscopy:

In AFM imaging of *C. parvum* oocysts, both imaging conditions (imaging in air or liquid) and age of oocyst resulted in varying oocyst appearance and attachment characteristics. Initial AFM images of *C. parvum* oocysts under liquid were of oocysts shed three to five months prior to analysis. These images were compared to those of fresher oocyst stock, which was imaged within 1 month of shedding. In all cases, oocysts images under liquid maintained a hydrated appearance, with no collapse of the oocyst wall (Fig. 14). Older oocysts displayed increased attachment strength, decreased numbers, and more disperse attachment than exhibited by freshly produced oocysts, which exhibited comparatively closer packing with a lower overall attachment stability despite an increased substrate and oocyst-oocyst contact area (Fig. 15).

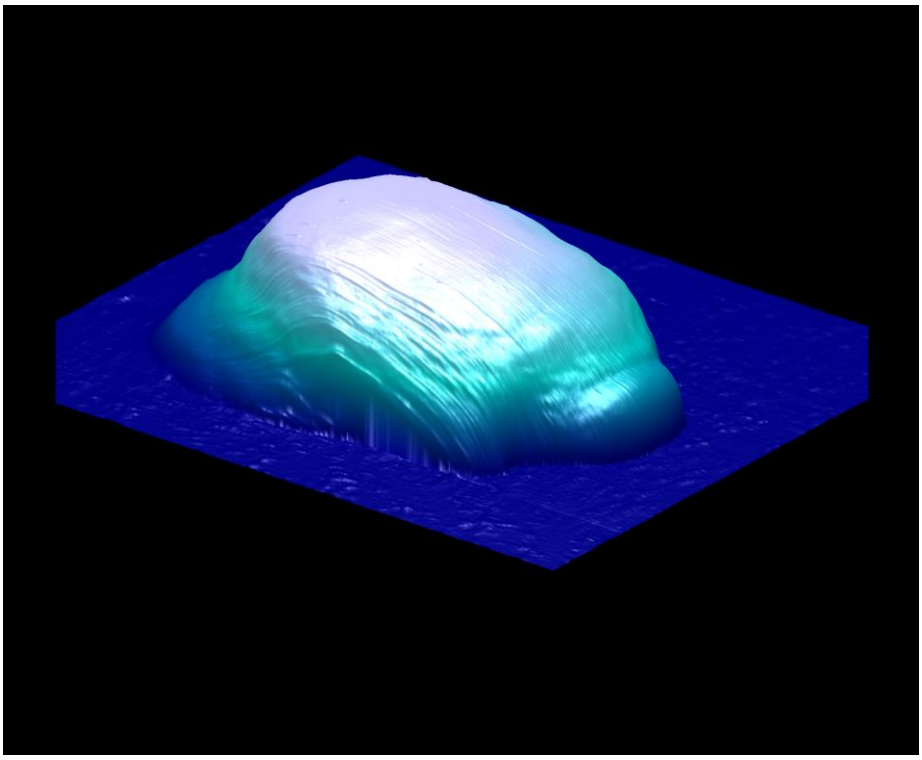

Fig. 14: Liquid AFM
Three-dimensional AFM image of a single oocyst imaged under fluid within 1 month of shedding. Scan size: 6 µm.

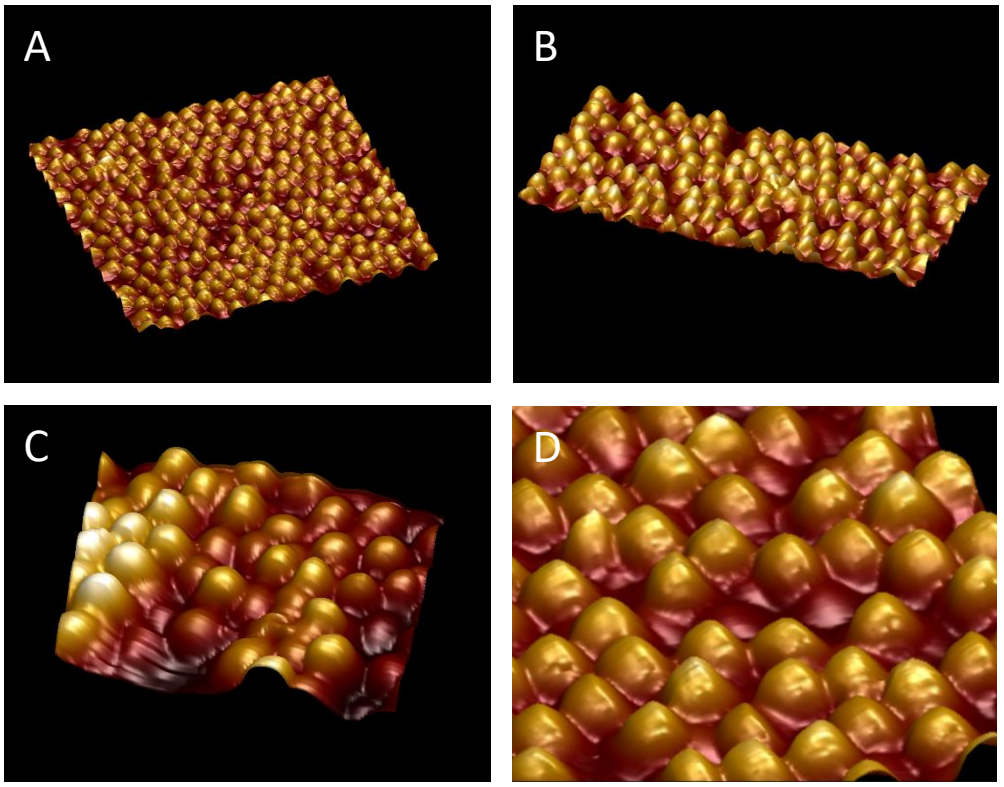

Figure 15: AFM images of C. parvum oocysts under liquid.
Oocysts imaged within 1 month of shedding exhibit confluent attachment with oocysts appearing roughly spherical at scan diameter 100 µm (A and B). Decreasing scan size to focus on individual oocysts (C – scan diameter 48.4 µm) results in the appearance of scan lines, whereas using the zoom function results in greater magnification with fewer scan artifacts (D – 6 µm).

Images under liquid show freshly produced oocysts (imaged within 1 month of shedding) to be roughly spherical with smooth surfaces lacking any ultrastructural features. In comparison, oocysts imaged three to five months post shedding displayed increasingly irregular, lumpy form (Fig. 16).

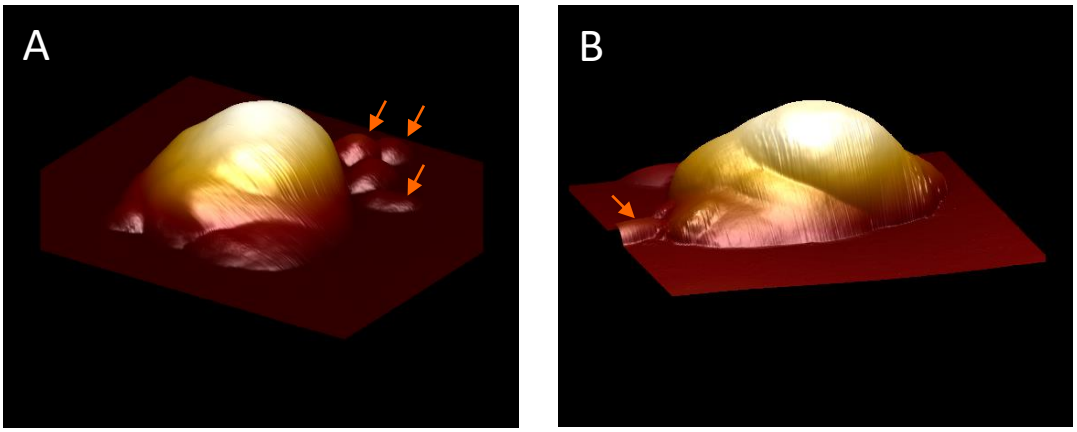

Fig 16: AFM images of oocysts imaged under liquid 4 months post shedding.
Three-dimensional topographical display reveals that oocysts stored for between three to five months prior to imaging develop an irregular 'bumpy' appearance. The presence of unknown globular features increases as oocyst stock ages (red arrows). Scan size: 12.6 µm (A), 10 µm (B).

In addition to changes in oocyst appearance with age, rod-shaped features were present in stock solution which had been stored for three months (Fig. 17). These features were roughly 6 - 7 µm in length and 1.5 – 2 µm across. As stock solution aged further, rod-shaped features were replaced with increasing numbers of small globular features (Fig. 18). These unidentified features were between 1 – 2 µm in diameter and roughly spherical in shape.

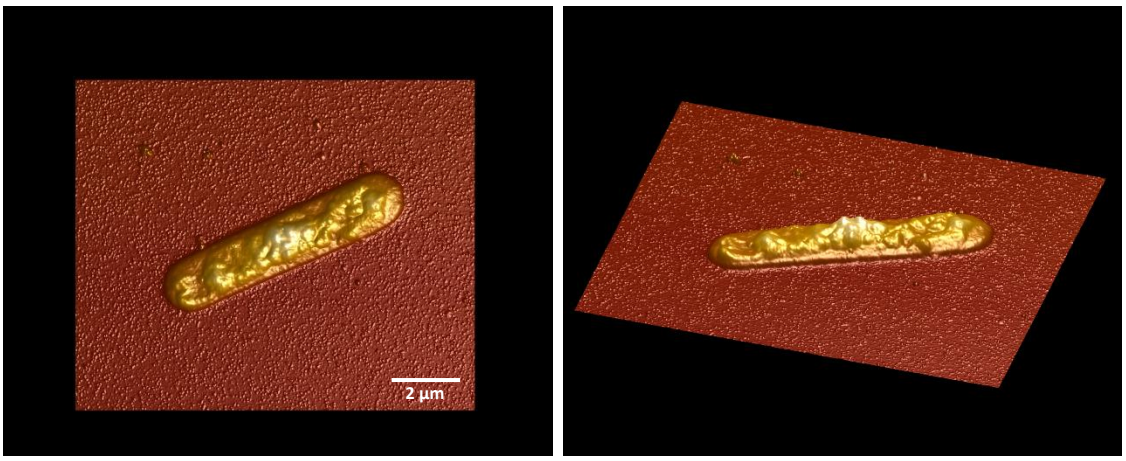

Fig. 17: AFM in air imaging of non-oocyst features
Oocyst stock imaged three months after shedding contained multiple rod-like features, each roughly 7µm in length, and 1.5 µm in diameter. Scan size 11 µm.

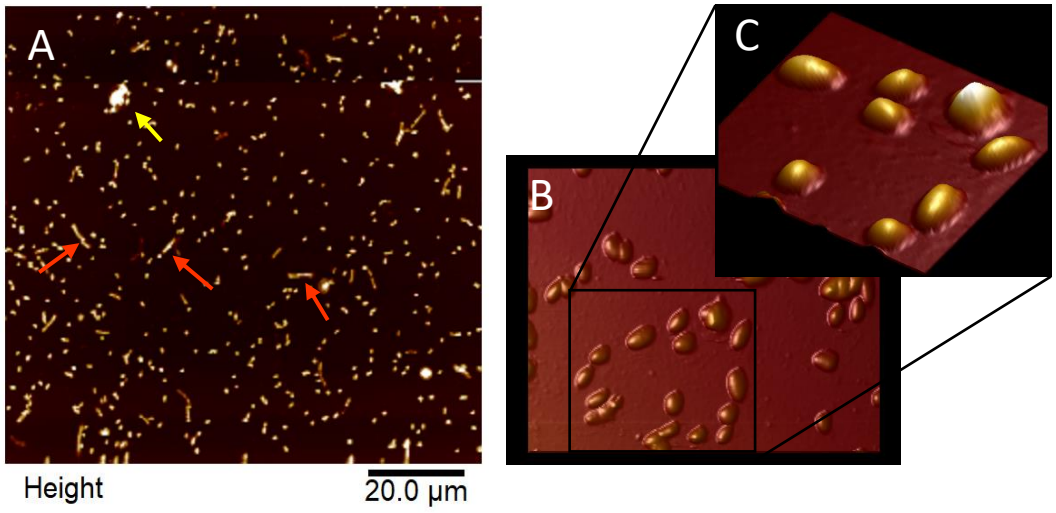

Fig. 18: AFM images of non-oocyst globular features
Images were captured in air at scan size 100 µm (A), 33.2 µm (B), and 18.2 µm (C). Image A: red arrows indicate where stretch effect has resulted in drag, yellow arrow indicates an oocyst.

Both fresh and older oocysts imaged in air displayed higher attachment stability and numbers than seen in liquid conditions, with oocyst exhibiting cluster attachment patterning (Fig. 19). When imaged in air, oocyst appeared flattened, with some variation in collapse patterning. Individual oocysts displayed a tendency to fall flat, with the topographical profile of the oocyst contents visible (convex appearance in section) and folding and irregularity of the surface (Fig.20), while oocysts situated within clusters always displayed raised edges with a deflated central region (concave appearance in section), giving the appearance of a honeycomb like structure (Fig. 19).

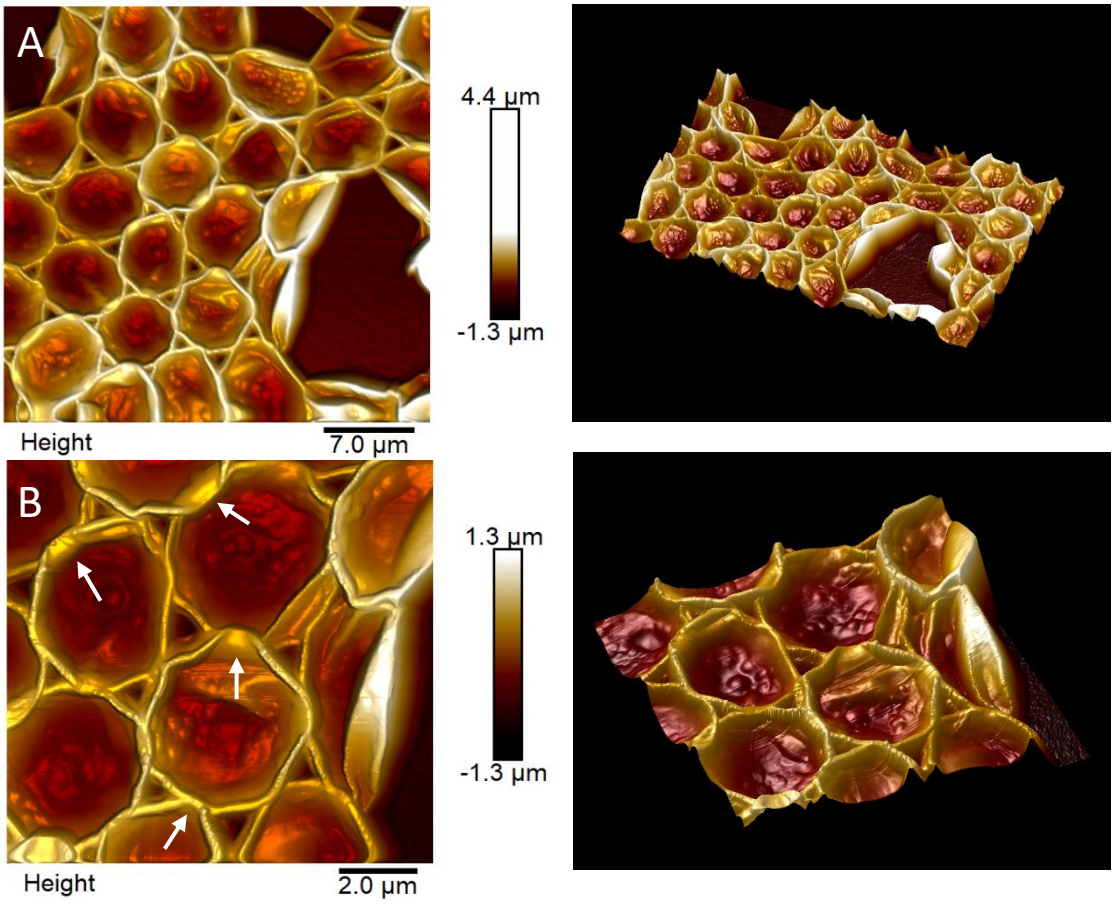

Fig. 19: AFM imaging of oocysts in air.
When imaging in air, confluent attachment resulted in concave dehydration patterning. Decreasing scan size from 33.2 µm (A) to 11 µm (B) revealed areas of adhesion at points of contact between oocyst walls (white arrows). 'Globular cluster' features previously identified in FESEM analysis are visible internal to the raided borders of the oocyst walls. Oocysts imaged within 1 month of shedding.

In all cases, imaging in air provided enhanced resolution of oocyst surfaces over oocysts imaged in liquid, enabling imaging of features such as the opened suture structure of an excysting oocyst (Fig. 21). In some instances, imaging in air revealed angular repetitive patterning resembling scoring of the oocyst surface, with parallel features running angles distinctive from the scanning angle. Further analysis found that the nature and direction of the patterning remained unchanged upon alteration of the scan angle, suggesting that these features are not scan line artifacts (figures 21 and 22).

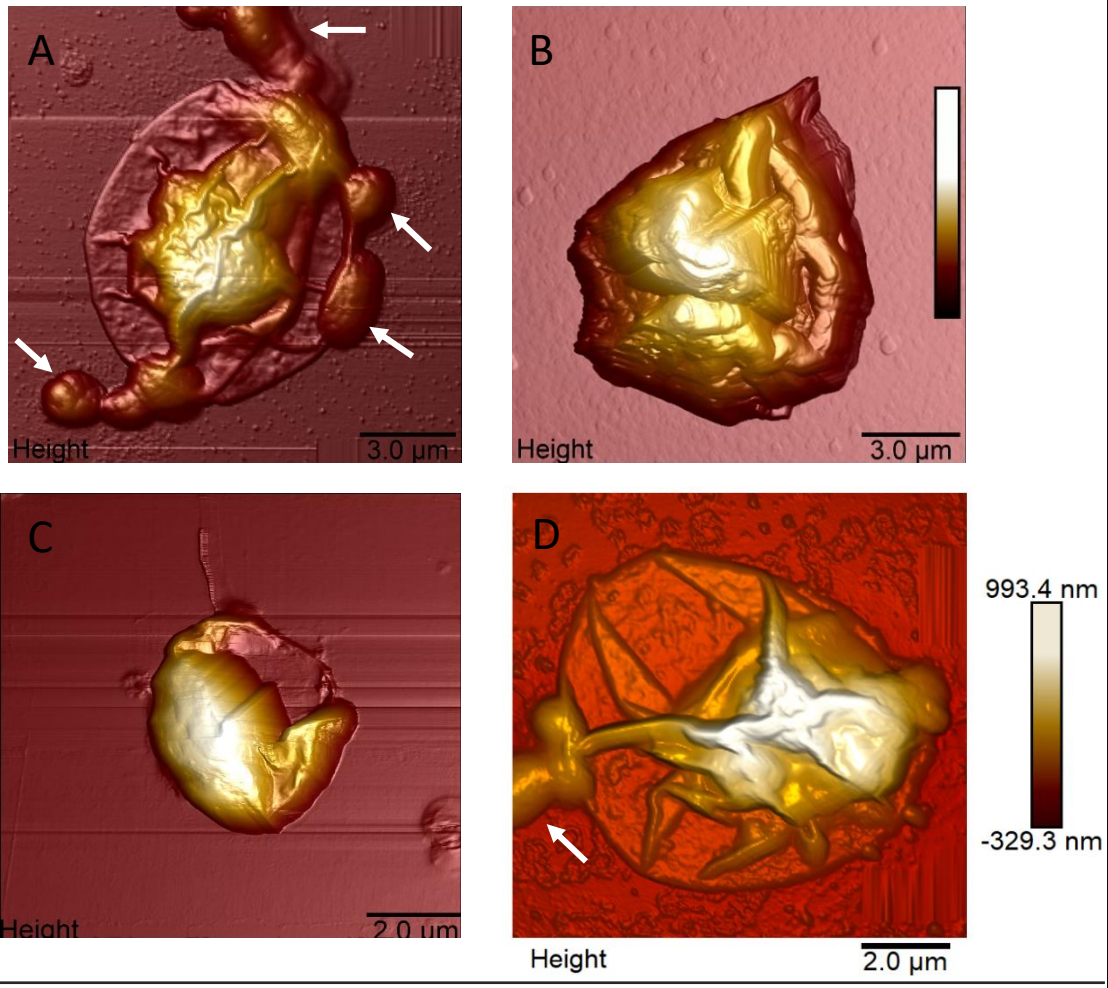

Fig. 20: High resolution AFM images of oocysts imaged in air
Single oocysts exhibiting stages of 'convex' dehydration form. Some globular features are visible (white arrows - A and D).

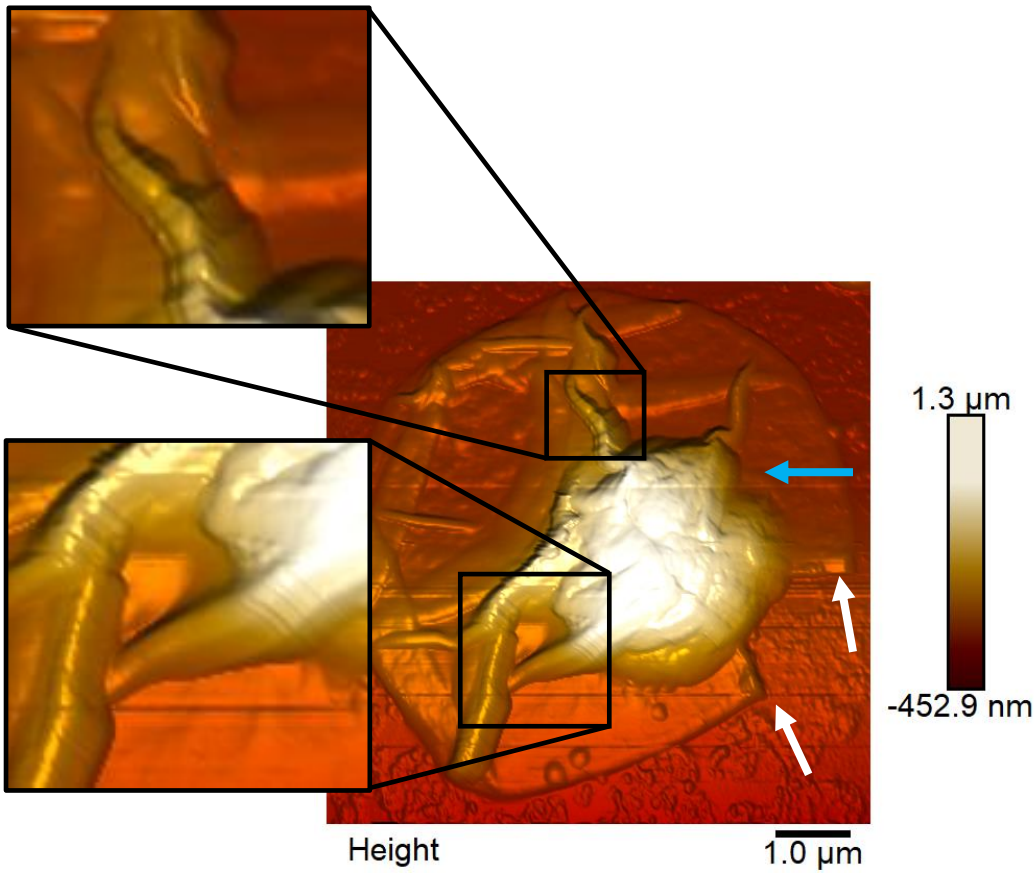

Fig. 21: AFM in air, identification of fine features.
A C. parvum oocyst imaged in air, showing an open suture structure (edges indicated with white arrows). Parallel repetitive angular features are visible (within black boxes).
Scan line direction is indicated (blue arrow).

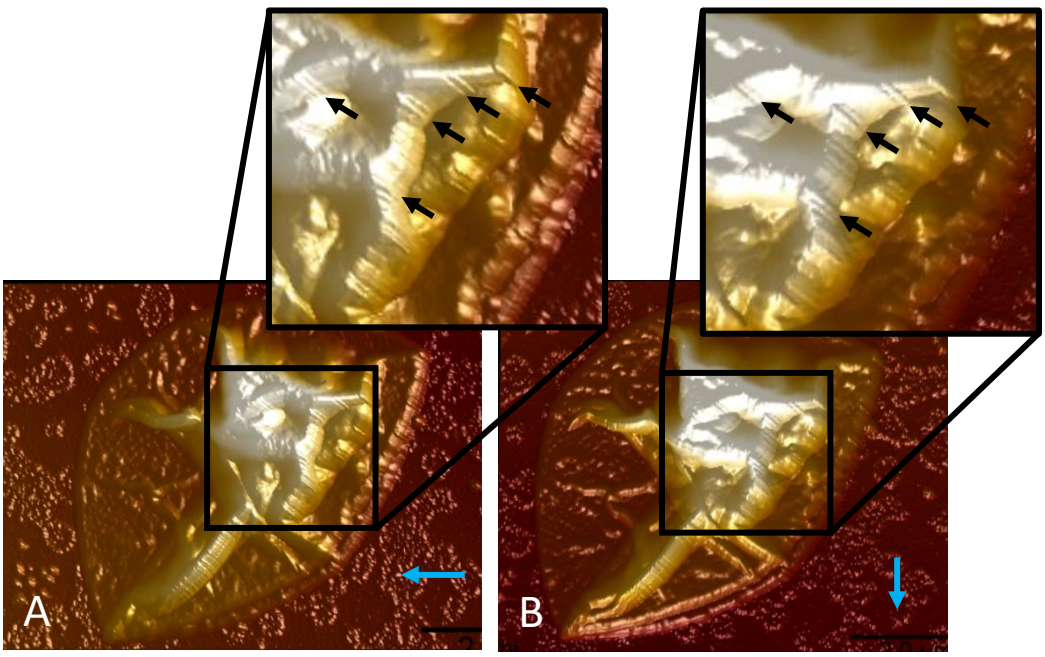

Fig. 22: Single oocysts imaged at different scan angles.
Parallel angular features remain unchanged when scan angle is altered from 0° (A), to 90° (B). Blue arrows indicate scan direction, black arrows indicate the location of prominent features.
Scan size 8 µm.

AFM imaging in air revealed smaller features adhering to surfaces of oocysts imaged over 4 months post shedding (Fig. 23).

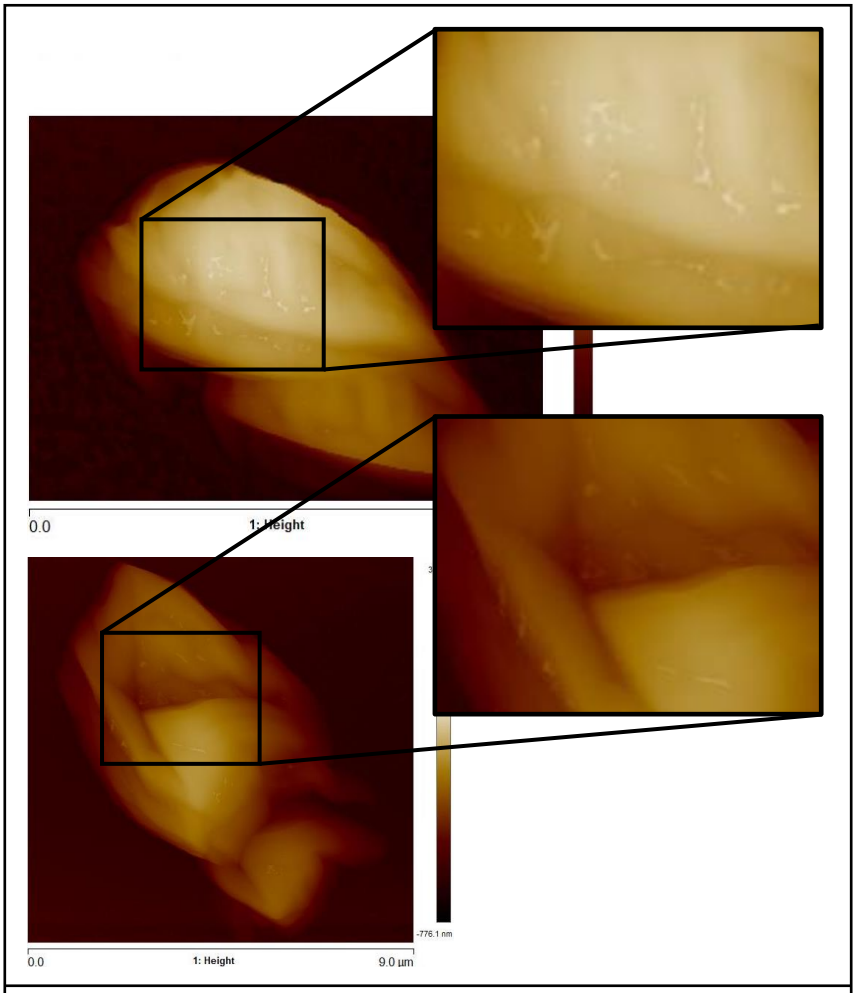

Fig 23: AFM height representation. Detection of small surface features. AFM imaging in air of oocysts imaged 5 months post shedding revealed widespread small surface features.

QNM analysis of oocysts imaged within one month of shedding revealed ripple-like patterning in deformation and adhesion forces (Fig. 24).

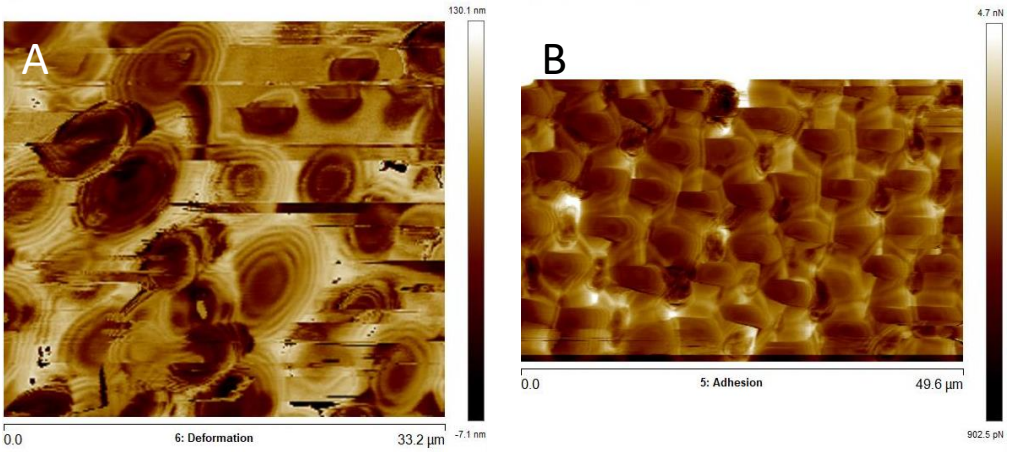

Figure 24: Deformation and adhesion readings for oocysts imaged within 1 month of shedding.
QNM analysis of oocysts imaged within one month of shedding revealed ripple-like patterning in deformation and adhesion forces (A and B respectively).

3.4 Data analysis:

Using the NanoScope Analysis 'slice' function, the mean height of oocysts imaged in liquid was founds to be 2.07 µm, where the mean height (measured at the highest point) of oocysts imaged in air was 1.51 µm. The 'particle analysis' function was used to determine both the area and diameter of individual oocysts. Oocysts imaged in liquid had a mean area and diameter of 24.82µm^2 and 5.5 µm respectively, where oocysts images in air had a mean area of 22.8 µm^2 and a 5.17µm mean diameter. The 'bearing analysis' function was used to determine oocyst volume, oocysts in liquid had a mean volume of 33.57 µm^3, where those imaged in air had a mean volume of 17.91 µm^3. Table 4 displays the complete set of statistical values calculated from oocyst measurements.

	Height		Area		Volume	
	Air	Fluid	Air	Fluid	Air	Fluid
Mean	1.509	2.064	22.788	24.815	17.907	33.565
Variance	0.397	0.457	111.707	116.838	2223.858	455.852
St. dev.	0.63	0.676	10.569	10.809	14.962	21.351
St. err.	0.168	0.195	2.93	3.12	3.999	6.163
n	14	12	13	12	14	12
t-value	0.042		0.641		0.046	

Table 4: AFM statistical values
The mean, variance, standard deviation, standard error t-value and n (sample number) for the height, area and volume of C. parvum oocysts imaged under AFM in both air and fluid.

To determine if there was a significant difference between the means of each measurement (height, area or volume) between each condition (images in air or in fluid) a two-sample t-test assuming unequal variance was performed for each measurement, where p>0.05 = not significant (ns), p ≤ 0.05 = significant (*). Bar graphs displaying mean measurement under each condition with standard error and t-test significance results are displayed in figure 24.

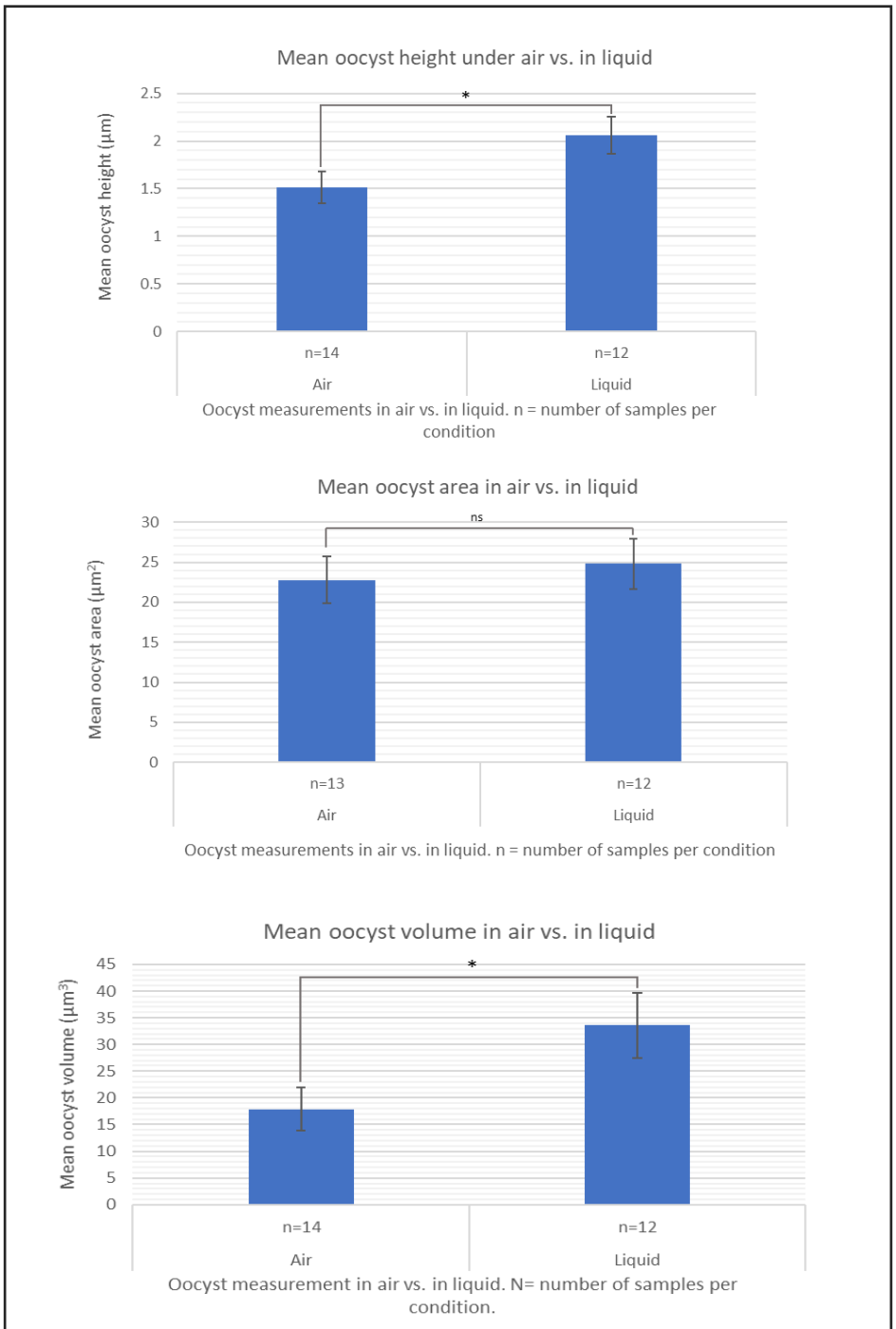

Fig 24: Bar graphs displaying the mean values for each measurement under the two imaging conditions.
Bars represent the mean values for each measurement. Asterisks and 'ns' annotation denote t-test significance results, where ns = not significant, * = significant, where p = 0.05. Error bars represent calculated standard error.

Statistical analysis revealed a significant difference between the mean values of volume and height of oocysts imaged in air and in fluid, with both height and volume of oocysts imaged in liquid being significantly greater than those imaged in air. There was no significant difference in oocyst area between the two conditions.

3.5 Analysis of non-oocyst globular features

To help determine the nature of non-oocyst globular features, samples of stock solution were treated with penicillin and chloramphenicol prior to AFM imaging to assess the effect of antibiotic treatment on globular feature appearance and frequency. Additionally, due to the faecal shedding of stock oocysts, AFM imaging and analysis of *E. coli* was carried out to allow visual comparison with unknown globular features. PCR analysis of oocyst stock and *E. coli* samples were completed to detect potential bacterial presence in the oocyst supply.

Imaging of oocyst stock treated with penicillin and chloramphenicol:

Antibiotic treatment had no effect on the appearance of rod-shaped or non-oocyst globular features.

E. coli AFM analysis:

AFM analysis in air was used to establish *E. coli* morphology and appearance under conditions corresponding to those used during imaging of the unknown features present in oocyst stock solution (Fig. 26). The *E. coli* cells exhibited a subtly different appearance to the unknown features, being more elongated in shape. The NanoScope Analysis particle analysis function was used to measure mean area and volume of *E. coli* cells, found to be 1.91µm^2 and 1.55µm respectively.

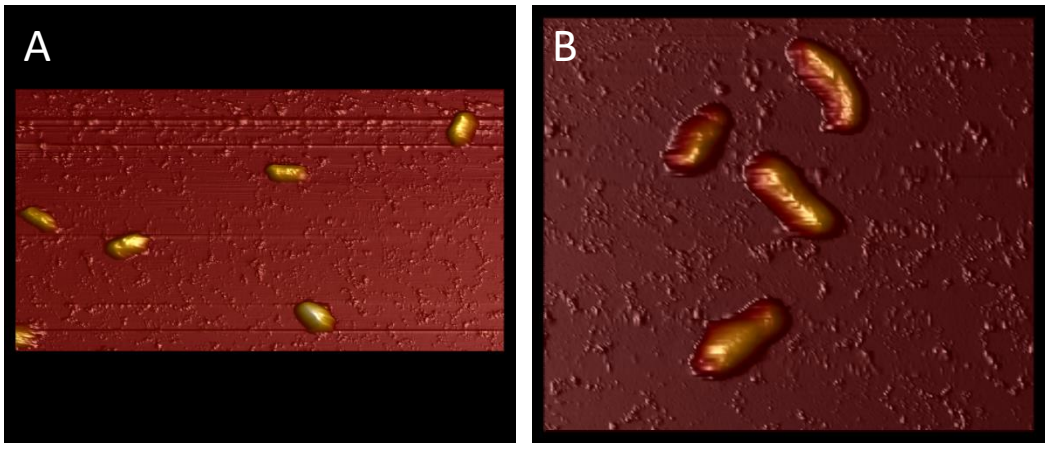

Fig. 26: AFM images of *E. coli* in air.
Image A: 22µm scale view. B: 11.9 µm scale view.

PCR gel analysis of oocyst stock bacterial content:

PCR gel analysis identified a strong band corresponding in size to the primer target fragment (1,484 bp) for both the *E. coli* positive control sample and non-filtered oocyst stock. For both *E. coli* and non-filtered oocyst stock samples, a faint band is visible at around 740 bp (see Fig. 27), this is likely a result of non-specific primer binding and could be a result of too many cycle numbers being used, or the annealing temperature being too low (Viljoen, Nel and Crowther, 2005; Biolabs, 2018). These results indicate that bacterial contamination is present within the oocyst stock, and that this contamination is at least partially addressed by filter sterilisation. However, it cannot be determined whether filter sterilisation reduces bacterial numbers sufficiently to preclude bacterial contamination as the source of the unknown features imaged using AFM.

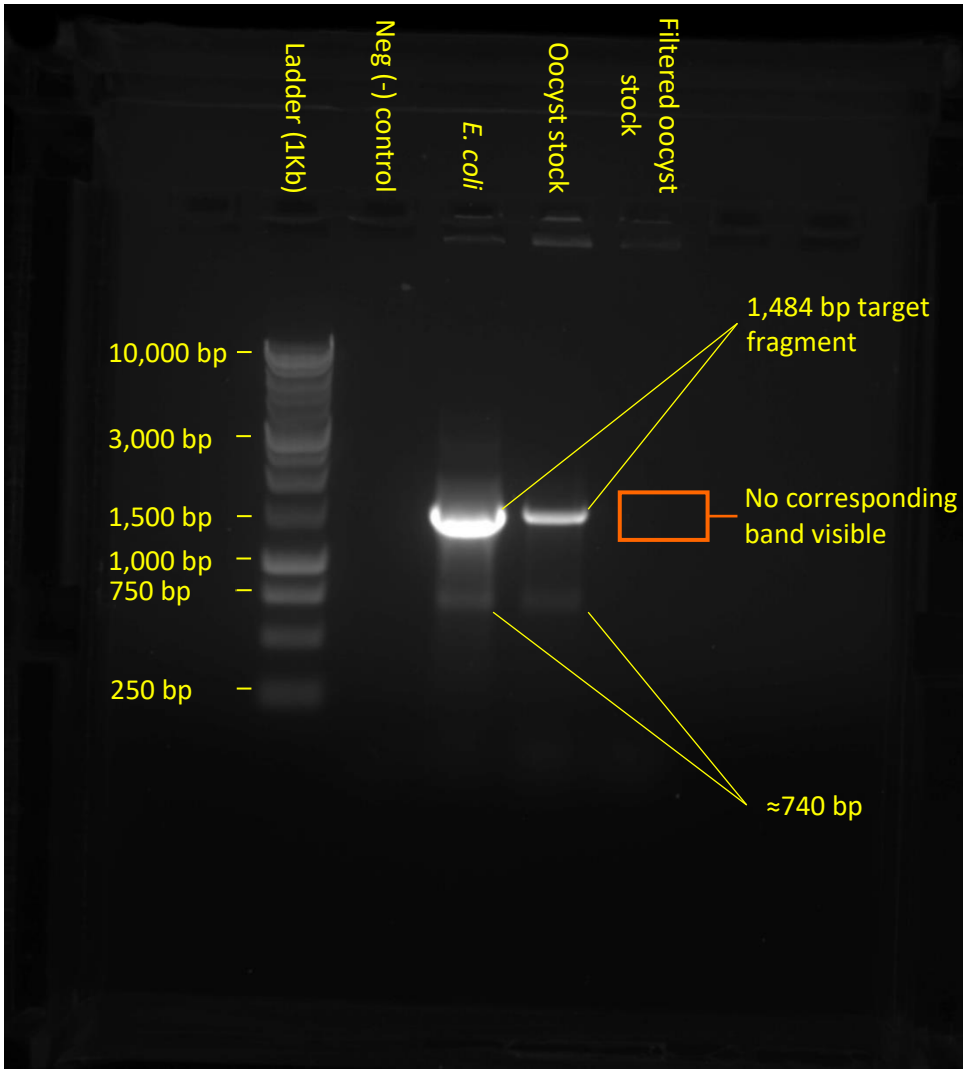

Fig. 27: PCR gel analysis.
Both the *E. coli* positive control sample and non-filtered oocyst stock produced a strong band corresponding in size to the primer target fragment (≈1,484 bp). These samples also produced faint bands at ≈740 bp, likely a result of non-specific binding. No bands of any size were visible in the sample containing filtered stock.

3.6 Fluorescence microscopy

Fluorescence imaging of stock oocysts:

Fluorescence imaging of stock oocysts was carried out to provide a standard for comparison with potential infection products. Oocysts stained with Crypt-a-Glo™ appeared roughly spherical and fluoresced evenly when imaged under FITC. DAPI staining enabled imaging of sporozoite genetic material, resulting in clusters of bright fluorescence from within each individual oocyst (Fig. 28). DAPI staining in conjunction with Crypt-a-Glo ™ enables verification of intact oocysts by confirmation of sporozoite content, and thus supports de novo oocyst production as opposed to residual shells from excystation solution. Samples prepared with 0.01% poly-l-lysine displayed increased numbers of oocyst attachment in comparison to those prepared with 0.05% poly-l-lysine as previously described.

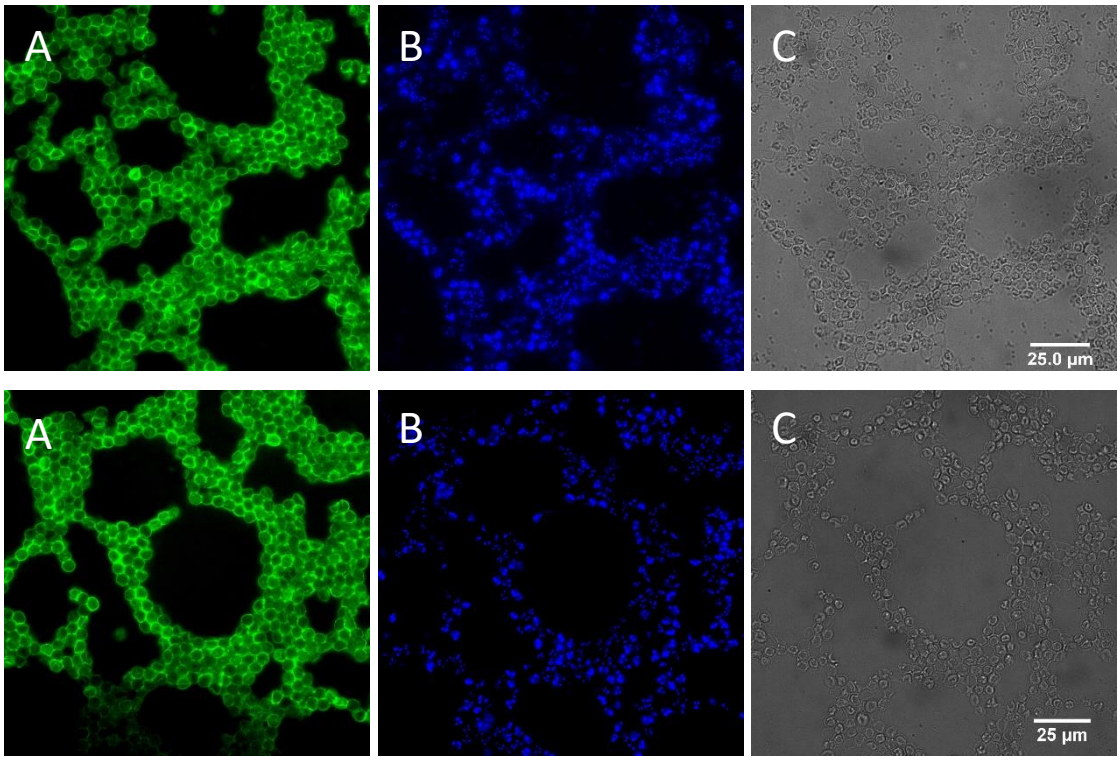

Fig. 28: Fluorescence imaging of stock oocysts.
Crypt-a-Glo™ fluorescence under FITC(A), DAPI staining of sporozoite DNA (B) and corresponding bright-field images (C).

ImageJ merge function was used to overlap FITC and DAPI channels. In comparing BF and merged images reveal that flat smooth oocysts (visible in BF) contain no genetic material (no DAPI fluorescence in corresponding merged image). These flattened oocysts are empty shells, having excysted in solution. Areas of DAPI fluorescence external to any oocyst walls (BF and FITC), are also visible, suggesting some oocyst damage or excystation occurred at some point after sample deposition (Fig. 29).

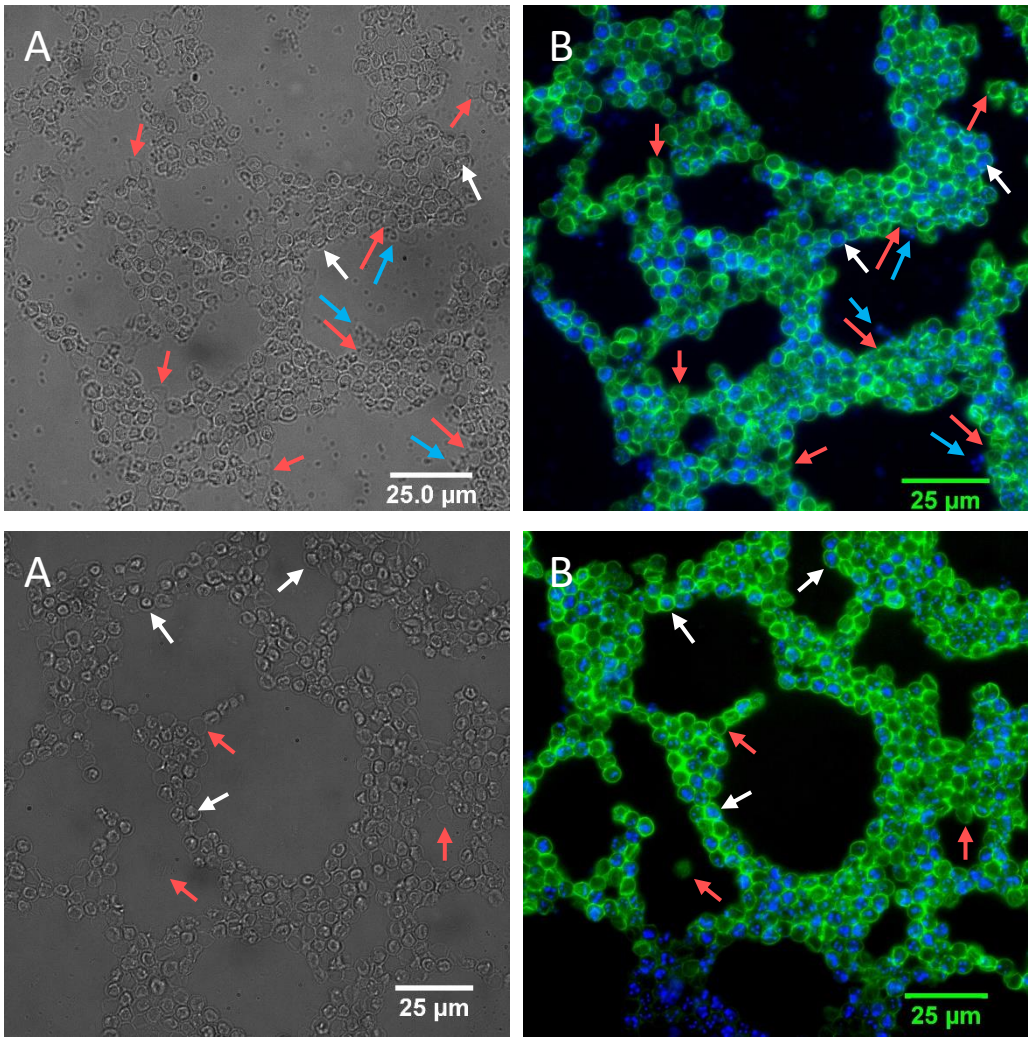

Fig. 29: Merge function facilitates identification of whole vs. excysted oocysts.
Comparison of BF (A) and FITC-DAPI merged images (B) revealed that oocysts that appear flat and smooth under BF have no DNA content (DAPI stain) (red arrows). These are likely excysted oocysts. Oocysts which appear raised and uneven were more likely to contain genetic material, suggesting that these oocysts were non-excysted (white arrows). Blue arrows indicate genetic material external to oocysts (excysted oocyst contents), found in proximity to excysted shells.

3.7 Infection cell line optimisation and fluorescence imaging:

To determine the optimal cell line for *C. parvum* infection experiments, HCT8 and COLO-680N cultures were inoculated with excysted *C. parvum* sporozoites, and the resulting production of de-novo produced oocysts was assessed using fluorescent microscopy.

HCT8:

Supernatants removed from HCT8 cell line cultures showed no visible signs of successful infection and resulting oocyst production (Fig. 30).

COLO-680N:

Supernatants removed from COLO-680N cultures contained intact extracellular oocyst stages (Fig. 31), indicating that these cultures were successfully infected and supported the complete life cycle of the parasite.

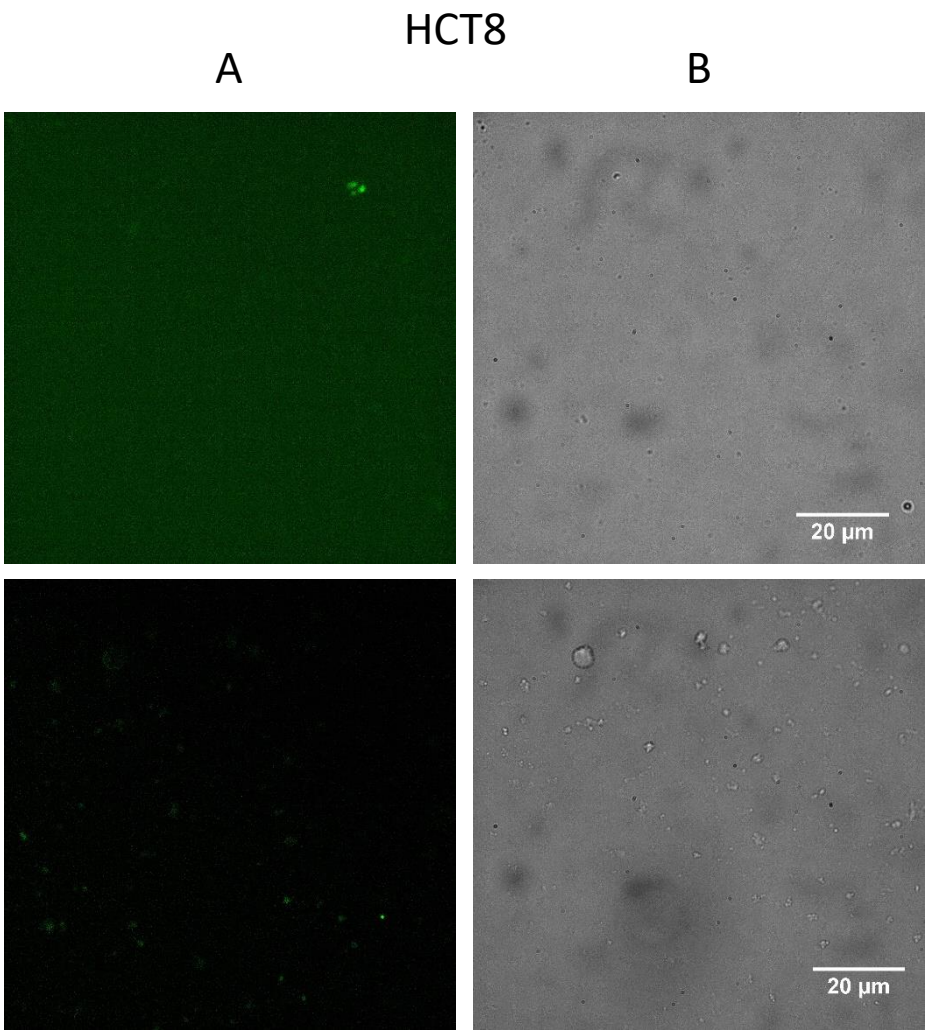

Fig 30: Fluorescence imaging of HCT8 culture supernatants.
Fluorescence imaging did not detect any oocyst-like fluorescent features under FITC (column A). Column B: corresponding bright-field images.

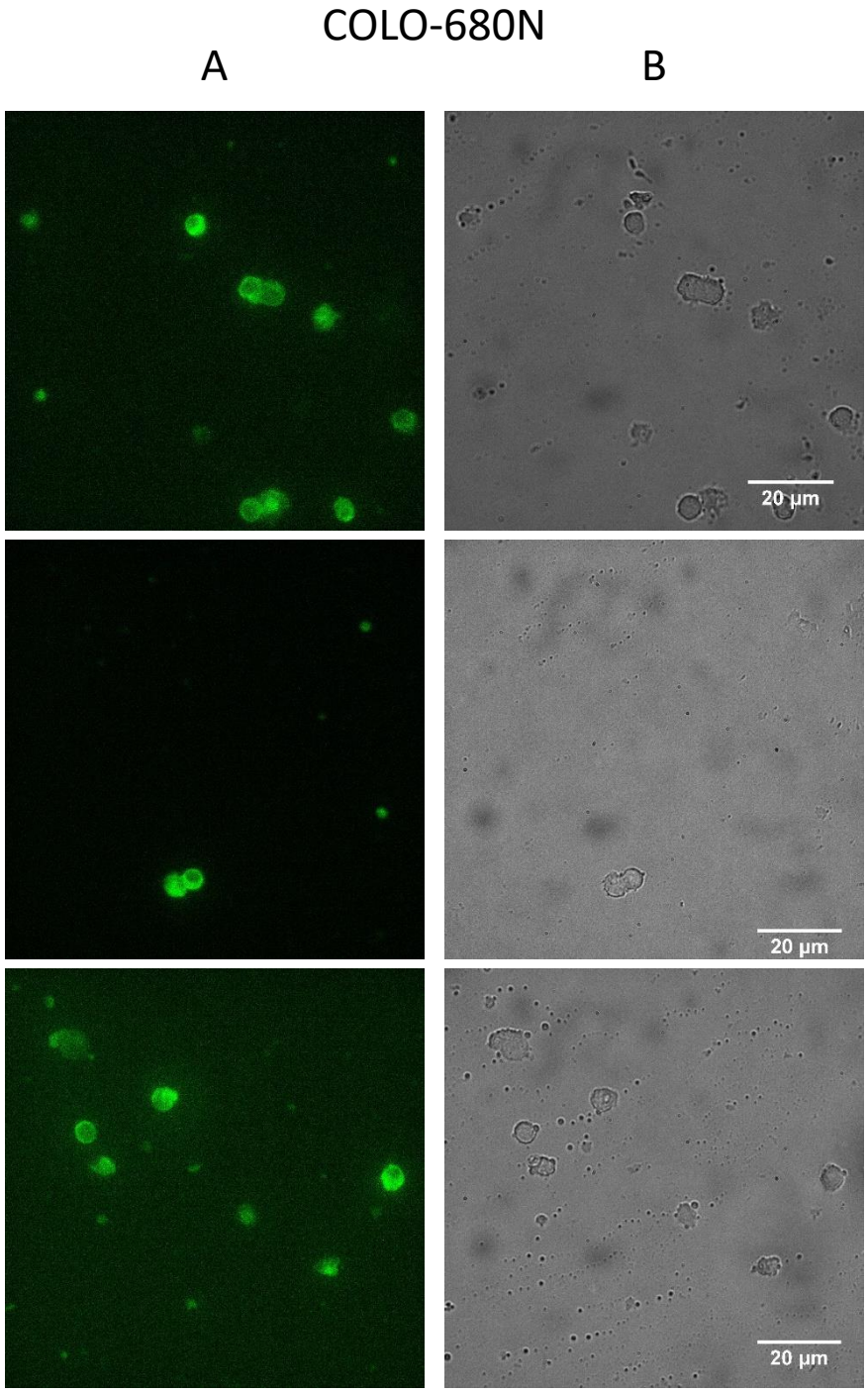

Fig. 31: Fluorescence imaging of Colo-680N culture supernatants.
Fluorescence imaging of Colo-680N supernatants revealed oocyst-like fluorescent features under FITC (column A). Column B shows corresponding BF images.

4.0 Discussion:

Until now, high resolution imaging of *C. parvum* has been limited to imaging of fixed (for AFM) and fixed and sputter coated (for FESEM) samples. Any information gathered by such studies has the potential to be flawed, as fixing involves killing samples and alteration of their protein structure and mechanical properties, for example by cross-linking between proteins (using formalin) or precipitation/denaturing (using methanol). FESEM analysis requires that biological samples are moved further from their natural state, as previously fixed samples must be critical point dried (which involved exposure to high pressure and temperature) (Chandler and Roberson, 2009), and coating of features in an ultrathin layer of conductive material (e.g. gold/palladium alloy) (Suzuki, 2002). The described AFM technique will allow researchers to reliably attain biologically accurate high-resolution imaging and nano-mechanical data of *C. parvum* oocysts for the first time.

4.1 Field emission scanning electron microscopy:

FESEM analysis revealed what appeared to be a small 'dimple' feature on the surface of selected oocysts, spatially located on the apical side of spherical non-fixed oocysts. Further, analysis of collapsed oocysts showed that each oocyst contains a small cluster of globular features, which exhibit higher density than other oocyst contents (SE analysis), and higher Mg/P content than any other sample constituent (EDX analysis). SE imaging at varying accelerating voltages in combination with EDX analysis of excysted vs. whole oocysts indicated that these features were contained within the oocyst and exit upon excystation.

By imaging at maximum hydration and using relatively gentle parameters (low to minimum accelerating voltage), it was possible to image unfixed oocysts for a short period before structural collapse under FESEM. Speed of collapse increased with increasing magnification and ACC V, therefore resolution remained poor as low accelerating voltage causes low resulting signal.

Cold field emission SEM microscopy uses a more focused electron beam than standard SEM, and therefore provides higher resolution imaging, however vacuum conditions must be much higher, placing samples which charge (such as oocysts) under much harsher conditions. Due to the relationship between accelerating voltage and signal strength, imaging of oocysts required a similar compromise between imaging resolution and rate of oocyst collapse. The progressive collapse of oocysts observed under both SEM and FESEM are likely a result of sample dehydration due to vacuum and electron beam exposure. Desiccation of oocysts causes difficulty in distinguishing between possible oocyst features and dehydration effects. At 40 minutes, damage due to vacuum exposure is extensive.

Dimple feature:

The infrequent appearance of the dimple feature observed in combination with its similar relative positioning on each oocyst suggests that this may be an imaging artefact, or an element which is only detectible when the feature is directly facing the electron beam on the surface of a fully hydrated oocyst. In this instance it is possible that this feature is not visible using other imaging techniques as it is not located to the outermost layer of the oocyst wall and is therefore only detectible by SEM which allows imaging at depths within a sample in addition to surface analysis. Further investigation would be required to determine its origin, potentially using TEM in combination with proteomics.

Globular cluster analysis:

Imaging at sections through the sample revealed that the globular cluster features were most visible at ACC V of between 5 - 20 kV. This suggests that the features in question were not located to the outer surface of the oocyst wall, but instead were internal to the oocyst. EDX analysis of excysted vs. whole oocysts further supports this theory, as no cluster patterning of phosphorus and magnesium or any other elements was seen in any of the excysted samples, suggesting that these features leave the oocyst upon excystation and are likely destroyed by electron beam exposure. The location, cluster appearance and composition of these features suggests that they could be oocyst residual bodies (R.B), which are suggested to act as an energy store to support sporozoite metabolism within the oocyst. Past studies have demonstrated that like the cluster features, the r.b typically exits the oocyst upon excystation (Harris, Adrian and Petry, 2004; Kar et al., 2011). As DNA has a high phosphate ion content (Griffiths et al., 1999), and magnesium cations have been demonstrated to have a role in DNA stabilisation (Anastassopoulou and Theophanides, 2002; Guéroult et al., 2012) it was also considered that the globular cluster features could be sporozoite genetic material, although the granular nature, close clustering, and topographical imaging of similar features using AFM in air suggest this explanation is improbable.

Due to the harsh non-physiological imaging conditions of FESEM imaging, in combination with the inability to image at high resolution whilst maintaining oocyst integrity, FESEM was not pursued as a method of high resolution imaging of oocyst surface features.

4.2 Atomic force microscopy:

Immobilisation:

Substrate optimisations revealed that glass surfaces were found to provide superior attachment numbers and strength to mica surfaces. Immobilisation assessment established that gelatine does

immobilise *C. parvum* oocysts, but that attachment numbers are much lower than those provided by poly-l-lysine. Further, buffer optimisations revealed that application of 1x PBS to sample slides using poly-l-lysine for sample immobilisation results in progressive oocyst detachment over time. Continued poly-l-lysine optimisations revealed that with increasing concentration of poly-l-lysine, the number of oocysts attaching to the substrate decreased, however the strength of the attachment formed increases. For oocysts shed within one to two months of imaging, a glass substrate with poly-l-lysine concentration of between 0.07 and 0.08 % provided sufficient attachment strength for AFM imaging in liquid whilst maximising oocyst attachment numbers. For oocysts imaged between three and five months post shedding, a glass substrate with 0.05 % poly-l-lysine provided similar results.

Establishing a reliable sample-substrate attachment technique is an essential first step in any scanning-probe based imaging technique. For accurate measurement of many biological samples (including oocysts) it is desirable to avoid drying and to maintain biologically relevant conditions, necessitating sufficient immobilisation strength to withstand probe interaction forces under fluid.

Previous research into bacterial immobilisation for AFM imaging has revealed that bacteria containing a glycocalyx (like the glycocalyx layer found at the outer layer of the *Cryptosporidium parvum* oocyst wall (Jenkins et al., 2010) can be successfully immobilised by slide coating with porcine gelatine (Allison et al., 2011). Due to the possible similarity in oocyst wall surface chemistry, oocyst adherence numbers were compared between slides treated with poly-l-lysine and slides treated with porcine gelatine, and poly-l-lysine was found to provide superior attachment numbers.

Traditionally, 0.01% poly-l-lysine has been used for oocyst immobilisation (Koh et al., 2013; Koh et al., 2014). Under aqueous conditions *C. parvum* oocysts have a net negative surface charge (Drozd and Schwartzbord, 1996; Ongerth and Pecoraro, 1996; Considine, Dixon and Drummond, 2002; Hsu and Huang, 2002). As poly-l-lysine is a cationic polymer (Farrell et al., 2007) the oocyst negative zeta potential enables steric interaction and thus immobilisation to the substrate. 0.01% poly-l-lysine proved to provide sufficient immobilisation for oocyst immobilisation in air, enabling reliable, repeated high-resolution imaging of individual oocysts. It is possible that drying down increases attachment strength through increasing oocyst surface contact with the substrate, or alteration electrostatic and steric interactions, as hair-like proteins extending from the oocyst surface into solution collapse (Considine, Dixon and Drummond, 2002; Kuznar and Elimelech, 2005; Searcy et al., 2006). For oocyst imaging in fluid, increased concentration of poly-l-lysine and therefore increased electrostatic interaction was necessary for sufficient sample immobilisation. The inverse relationship between oocyst attachment numbers and the strength of attachment suggests multiple interactions are involved in oocyst-surface adhesion. Given this relationship gelatine

immobilisation should not be discluded as a possible immobilisation technique in future AFM research. Glass surfaces were found to provide superior attachment to mica surfaces, which are commonly used for immobilisation of cells and oocysts in AFM imaging in air (Uchihashi, Watanabe and Kodera, 2018). As the two surfaces have very similar composition and surface chemistry, this may be a result of the increased roughness of glass in comparison to mica.

Increasing detachment of oocysts over time under PBS was likely a result of ionic interference with poly-l-lysine – oocyst electrostatic interaction. For this reason, deionised HPLC water served as a superior liquid imaging medium for use with this immobilisation method.

Appearance:

AFM analysis in fluid revealed that *C. parvum* oocysts are roughly spherical and smooth in appearance, with irregularity and 'lumpiness' increasing as oocysts age. Imaging in air, however revealed varying sedimentation patterns between oocysts imaged in air and in liquid, in addition to different collapse patterning in air dependent upon oocyst-oocyst proximity with evidence of oocyst wall interaction at contact points. Imaging in air also revealed unusual surface topography in collapsed oocysts and provided increased resolution in comparison to liquid imaging. Data analysis revealed significant differences between the mean values of height and volume of oocysts between the two imaging conditions (imaged in air vs. in fluid).

For imaging in air, sample collapse was a result of dehydration as previously observed in FESEM analysis. This partial dehydration was unavoidable, as imaging of humid samples resulted in 'sticking', a phenomenon caused by probe tip adhesion to minuscule water droplets on the substrate and sample surfaces (Schroder, Benton and Rai-Choudhury, 1996). The variation in dehydration profile observed between lone and confluent oocysts may be a result of the oocyst-oocyst wall interaction indicated in figure 4 resulting in adherence between adjacent oocyst walls.

It is possible that the decreased image resolution when imaging under fluid could be a result of increased frequency noise in fluid imaging (Rode et al., 2011), or due to interaction between the tip and oocyst surface structures (Amro et al., 2000; Bolshakova et al., 2001; Doktycz et al., 2003). Use of contact over non-contact mode can increase resolution, however in soft biological samples as in this study this method is not recommended as tip contact can alter the sample (Keyvani et al., 2017).

The difference in poly-l-lysine concentration required for immobilisation of oocysts imaged within one month of shedding compared to those imaged after four to five months could be due to a decrease in oocyst wall rigidity (increased elasticity) with age leading to a decrease in force translated through the oocyst body, causing less stress to be applied to the poly-l-lysine-oocyst steric interaction upon probe contact. It is also possible that a decrease in surface proteins extending into solution over time could result in increased oocyst-poly-l-lysine contact. Data

analysis revealed that there was no significant difference in oocyst area between the two imaging conditions, discluding increased surface area as a possible cause. Comparison of nano-mechanical measurements between oocysts of different ages could be used to investigate this theory further, although due to the decreased peak force required to image oocysts shed within one month of imaging resulting in inadequate nanomechanical feedback, a stronger immobilisation method may be required. The uneven 'lumpy' appearance of oocysts imaged between three to five months post-shedding could be a result of decreased oocyst wall integrity with corresponding changes in rigidity. The relatively smooth appearance of oocysts imaged in fluid compared to the collapsed flattened appearance with heightened resolution of those imaged in air is congruent with results of other investigations imaging other cell types, including bacterial cells (Doktycz et al., 2003).

4.3 Data analysis:

Data analysis of oocyst measurements acquired through AFM imaging revealed that oocysts imaged in fluid have significantly greater height and volume than those imaged in air. Volume measurements exhibited the greatest mean difference, as oocysts volume decreases as internal fluid evaporates during desiccation. This effect is likely also responsible for the decrease in height observed. No significant difference was detected in the surface area covered by individual oocysts imaged in air and in fluid, as oocysts flatten upon dehydration whilst the oocyst wall surface area remains unchanged.

The accuracy of the estimated mean values for each measurement could be improved by increasing the number of samples (n) analysed. In this study relatively few samples were analysed due to time constraints.

4.4 Oocyst features:

As imaging at different scan angles did not alter the appearance of the repetitive groove-like features, these are not likely to be tip effects, and may be previously undocumented features only visible under certain conditions, and dependent upon partial oocyst dehydration. These features could be a collapse patterning caused by arrangement of structural components in the oocyst wall, such as the ordered linear protein matrix described by Harris and Petry (1999).

The small features observed on the surface of oocysts imaged after five months in storage were likely debris from excysted oocysts contents degrading in solution.

4.5 Non-oocyst globular features present in stock solution:

The results of the PCR indicated the presence of bacterial DNA within the sample, however the failure of antibiotic treatment to remove the globular features present within the stock solution suggests that these are not bacterial in nature.

Although the majority of the literature describes sporozoites as being 4 x 0.6 µm in size (Borowski et al., 20009; Leitch and He, 2012), a 2004 paper by Franz Petry provides light microscopy images of freshly excysted sporozoites, the majority being banana shaped and roughly 7 µm in length and 2 µm in diameter, similar in size to the rod-like features. This paper also documents sporozoite shrinkage and rounding following a 24-hour period stored in solution post excystation. It is possible that the rod-shaped features seen in oocyst stock imaged 3 months post shedding were recently excysted sporozoites, possibly 'flattened' from their natural curved banana like shape by the effects of drying and poly-l-lysine interaction. In this case the replacement of these features with increasing numbers of smaller globular features could be a result of sporozoite shrinkage and rounding due to increased time in solution. The large size of the rod-shaped objects suggests that they are unlikely to be bacterial contaminants.

4.6 Future research:

Imaging of harvested cell line supernatants could not be completed due to time constraints, therefore an essential next step in this research will be to confirm that the developed AFM technique enables imaging of live infectious oocysts through completion of the described cell culture infection experiments. It may be necessary to scale up experiments in order to image enough oocysts to cause infection and repeat the experiment for oocysts imaged both in liquid and in air.

The study could be expanded to analyse and compare physiology of oocysts of different *Cryptosporidium* species. Further, as previously discussed relating to phylogenetic classification of *Cryptosporidium*, the enhanced capacities of this method could be used to review and compare the morphology of Cryptosporidium oocysts to cysts of other parasitic genera such as *Giardia*. In this instance modification of immobilisation method may be required due to differing cyst surface chemistry. Similarly, this technique may be used to compare topographical and nano-mechanical measurements between oocysts shed from animal infections and thick and thin-walled oocysts produced through cell line infection.

Future research could utilise the described method of AFM imaging in air for three-dimensional and nano-mechanical analysis of non-fixed oocyst walls at a sub nm scale. This method has the potential to identify structures located to the oocyst wall and in combination with proteomic analysis shed light on oocyst host recognition and excystation initiation.

5.0 Conclusion

In summary, a new method has been developed for reliable AFM imaging and analysis of non-fixed *C. parvum* oocysts in fluid and in air where previously analysis of *Cryptosporidium spp*. oocysts using high-powered microscopy techniques have required a minimum of sample fixing prior to imaging. This will allow researchers to attain dependably biologically accurate imaging and mechanical data on *C. parvum* oocysts for the first time. With modification, this technique can be expanded to provide similar information on other cryptosporidium species, and cysts of other parasitic Genera. Research into the oocysts of these parasites is of vital importance, as this is the environmentally hardy, highly infectious stage which has allowed cryptosporidiosis to become a disease of such global significance. Due to the versatile nature of AFM analysis, the described method will enable imaging, measurement of nano-mechanical forces, and sample chemical and physiological manipulation of the oocyst surface down to individual proteins located to the oocyst wall. These capabilities will open new avenues for research into oocyst proteomics in non-fixed samples. The information offered by such studies has the potential for use in the development of new treatments for eradication or de-activation of oocysts within the water supply, and the technique will add to the tools available for this vital research into the biology of the *Cryptosporidium* parasite.

6.0 Bibliography

Abrahamsen, M. (2004). Complete Genome Sequence of the Apicomplexan, *Cryptosporidium parvum*. *Science*, 304(5669), pp.441-445.

Abubakar, I., Aliyu, S., Arumugam, C., Hunter, P. and Usman, N. (2007). Prevention and treatment of cryptosporidiosis in immunocompromised patients. *Cochrane Database of Systematic Reviews*.

Adamu,H.,Petros, B.,Zhang,G.,Kassa,H.,Amer,S.,Ye,J.,Feng,Y. and Xiao, L. (2014). Distribution and clinical manifestations of *Cryptosporidium* species and subtypes in HIV/AIDS patients in Ethiopia. PLOS Neglected Tropical Diseases 8, e2831.

Agholi, M., Hatam, G.R. and Motazedian, M.H. (2013). HIV/AIDSassociated opportunistic protozoal diarrhea. AIDS Research and Human Retroviruses 29, 35 –41.

Aldeyarbi, H. and Karanis, P. (2016). Electron microscopic observation of the early stages of *Cryptosporidium parvum* asexual multiplication and development in in vitro axenic culture. *European Journal of Protistology*, 52, pp.36-44.

Aldeyarbi, H. and Karanis, P. (2016). The Ultra-Structural Similarities between *Cryptosporidium parvum* and the Gregarines. *Journal of Eukaryotic Microbiology*, 63(1), pp.79-85.

Ali, S., Mumar, S., Kalam, K., Raja, K. and Baqi, S. (2014). Prevalence, clinical presentation and treatment outcome of cryptosporidiosis in immunocompetent adult patients presenting with acute diarrhoea. *Journal of Pakistan Medical Association*, 64(6), pp.613–8.

Allison, D., Hinterdorfer, P. and Han, W. (2002). Biomolecular force measurements and the atomic force microscope. *Current Opinion in Biotechnology*, 13(1), pp.47-51.

Allison, D., Sullivan, C., Mortensen, N., Retterer, S. and Doktycz, M. (2011). Bacterial Immobilization for Imaging by Atomic Force Microscopy. *Journal of Visualized Experiments*, (54).

Alvarez-Pellitero, P. and Sitja-Bobadilla, A. (2002). *Cryptosporidium molnari* n. sp. (Apicomplexa: Cryptosporidiidae) infecting two marine fish species, Sparus aurata L. and Dicentrarchus labrax L. International Journal of Parasitology 32, 1007–1021.

Amro, N., Kotra, L., Wadu-Mesthrige, K., Bulychev, A., Mobashery, S. and Liu, G. (2000). High-Resolution Atomic Force Microscopy Studies of the *Escherichia coli* Outer Membrane: Structural Basis for Permeability. *Langmuir*, 16(6), pp.2789-2796.

Anastassopoulou, J. and Theophanides, T. (2002). Magnesium–DNA interactions and the possible relation of magnesium to carcinogenesis. Irradiation and free radicals. *Critical Reviews in Oncology/Hematology*, 42(1), pp.79-91.

Angles, M., Chandy, J., Cox, P., Fisher, I. and Warnecke, M. (2007). Implications of biofilm-associated waterborne *Cryptosporidium* oocysts for the water industry. *Trends in Parasitology*, 23(8), pp.352-356

Anonymous (2010). Annual epidemiological report on communicable diseases in Europe, revised edition 2009. European Center for Disease Prevention and Control. http://ecdc.europa.eu/en/publications/Publications/ 0910_SUR_Annual_Epidemiological_Report_on_Communicable_Diseases_ in_Europe.pdf#page=101.

Arce, F., Carlson, R., Monds, J., Veeh, R., Hu, F., Stewart, P., Lal, R., Ehrlich, G. and Avci, R. (2009). Nanoscale structural and mechanical properties of non-typeable Haemophilus influenzae biofilms. *Journal of Bacteriology*, 191(8), pp.2512-2520.

Arrowood MJ. (1997). Diagnosis. *Cryptosporidium and Cryptosporidiosis*. 2nd ed. Boca Raton, FL, USA: CRC Press, pp. 43–64.

Arrowood, M., Sterling, C. and Healey, M. (1991). Immunofluorescent Microscopical Visualization of Trails Left by Gliding *Cryptosporidium parvum* Sporozoites. *The Journal of Parasitology*, 77(2), p.315.

Artieda, J., Basterrechea, M., Arriola, L., Yagüe, M., Albisua, E., Arostegui, N., Astigarraga, U., Botello, R. and Manterola, J. (2012). Outbreak of cryptosporidiosis in a child day-care centre in Gipuzkoa, Spain, October to December 2011. *Eurosurveillance*, 17(5).

Asano, Y., Karasudani, T., Okuyama, M., Takami, S., Oseto, M., Inouye, H., Yamamoto, K., Aokage, J., Saiki, N., Fujiwara, M., Shiraishi, M., Uchida, K., Saiki, H., Suzuki, M., Yamamoto, T., Udaka, M.,Kan,K.,Matsuura,S.andKimura,M. (2006). An outbreak of gastroenteritis associated with *Cryptosporidium meleagridis* among high school students of dormitory in Ehime, Japan. *Annual Report of Ehime Prefecture Institute of Public Health and Environmental Science*. 9 (1), pp. 21–25.

Barta, J. and Thompson, R. (2006). What is Cryptosporidium? Reappraising its biology and phylogenetic affinities. *Trends in Parasitology*, 22(10), pp.463-468.

Beckmann, M., Venkataraman, S., Doktycz, M., Nataro, J., Sullivan, C., Morrell-Falvey, J. and Allison, D. (2006). Measuring cell surface elasticity on enteroaggregative *Escherichia coli* wild type and dispersin mutant by AFM. *Ultramicroscopy*, 106(8-9), pp.695-702.

Beckmann, M., Venkataraman, S., Doktycz, M., Nataro, J., Sullivan, C., Morrell-Falvey, J. and Allison, D. (2006). Measuring cell surface elasticity on enteroaggregative *Escherichia coli* wild type and dispersin mutant by AFM. *Ultramicroscopy*, 106(8-9), pp.695-702.

Benoit, M., Gabriel, D., Gerisch, G. and Gaub, H. (2000). Discrete interactions in cell adhesion measured by single-molecule force spectroscopy. *Nature Cell Biology*, 2(6), pp.313-317.

Biolabs, N. (2018). *PCR Troubleshooting Guide | NEB*. [online] Neb.com. Available at: https://www.neb.com/tools-and-resources/troubleshooting-guides/pcr-troubleshooting-guide [Accessed 26 Aug. 2018].

Blackburn, B., Mazurek, J., Hlavsa, M., Park, J., Tillapaw, M., Parrish, M., Salehi, E., Franks, W., Koch, E., Smith, F., Xiao, L., Arrowood, M., Hill, V., da Silva, A., Johnston, S. and Jones, J. (2006). Cryptosporidiosis Associated with Ozonated Apple Cider. *Emerging Infectious Diseases*, 12(4), pp.684-686.

Blagburn, B. and Soave, R. (2007). Prophylaxis and chemotherapy. *Cryptosporidium and Cryptosporidiosis*. 2nd ed. Boca Raton: CRC Press, pp.111-128.

Boland, T. and Ratner, B. (1995). Direct measurement of hydrogen bonding in DNA nucleotide bases by atomic force microscopy. *Proceedings of the National Academy of Sciences*, 92(12), pp.5297-5301.

Bolshakova, A., Kiselyova, O. and Yaminsky, I. (2004). Microbial Surfaces Investigated Using Atomic Force Microscopy. *Biotechnology Progress*, 20(6), pp.1615-1622.

Bolshakova, A., Kiselyova, O., Filonov, A., Frolova, O., Lyubchenko, Y. and Yaminsky, I. (2001). Comparative studies of bacteria with an atomic force microscopy operating in different modes. *Ultramicroscopy*, 86(1-2), pp.121-128.

Bonnin, A., Dubremetz, J. and Camerlynck, P. (1991). Characterization and immunolocalization of an oocyst wall antigen of *Cryptosporidium parvum* (Protozoa: Apicomplexa). *Parasitology*, 103(02), p.171.

Borowski, H., Clode, P. and Thompson, R. (2008). Active invasion and/or encapsulation? A reappraisal of host-cell parasitism by *Cryptosporidium*. *Trends in Parasitology*, 24(11), pp.509-516.

Borowski, H., Clode, P. and Thompson, R. (2008). Active invasion and/or encapsulation? A reappraisal of host-cell parasitism by *Cryptosporidium*. *Trends in Parasitology*, 24(11), pp.509-516.

Borowski, H., Thompson, R., Armstrong, T. And Clode, P. (2009). Morphological characterization of *Cryptosporidium parvum* life-cycle stages in an in vitro model system. *Parasitology*, 137(01), p.13.

Borowski, H., Thompson, R., Armstrong, T. and Clode, P. (2010). Morphological characterization of *Cryptosporidium parvum* life-cycle stages in an in vitro model system. *Parasitology*, 137(01), p.13-26.

Bouchet, F. and Boulard, Y. (1991). Ultrastructural changes following treatment with a microwave pulse in the oocyst of Eimeria magna. *Parasitology Research*, 77(7), pp.585-589.

Bradley, P., Ward, C., Cheng, S., Alexander, D., Coller, S., Coombs, G., Dunn, J., Ferguson, D., Sanderson, S., Wastling, J. and Boothroyd, J. (2005). Proteomic Analysis of Rhoptry Organelles Reveals Many Novel Constituents for Host-Parasite Interactions in *Toxoplasma gondii*. *Journal of Biological Chemistry*, 280(40), pp.34245-34258.

Brantley, R., Williams, K., Silva, T., Sistrom, M., Thielman, N., Ward, H., Lima, A. and Guerrant, R. (2003). AIDS-associated diarrhoea and wasting in northeast Brazil is associated with subtherapeutic plasma levels of antiretroviral medications and with both bovine and human subtypes of *Cryptosporidium parvum*. *Brazilian Journal of Infectious Diseases*, 7(1).

Brunk, U., Collins, V. and Arro, E. (1981). The fixation, dehydration, drying and coating of cultured cells for SEM. *Journal of Microscopy*, 123(2), pp.121-131.

Budu-Amoako, E., Greenwood, S., Dixon, B., Barkema, H. and McClure, J. (2012). *Giardia* and *Cryptosporidium* on Dairy Farms and the Role these Farms May Play in Contaminating Water Sources in Prince Edward Island, Canada. *Journal of Veterinary Internal Medicine*, 26(3), pp.668-673.

Bull, S., Chalmers, R., Sturdee, A., Curry, A. and Kennaugh, J. (1998). Cross-reaction of an anti-*Cryptosporidium* monoclonal antibody with sporocysts of Monocystis species. *Veterinary Parasitology*, 77(2-3), pp.195-197.

Bushen, O., Kohli, A., Pinkerton, R., Dupnik, K., Newman, R., Sears, C., Fayer, R., Lima, A. and Guerrant, R. (2007). Heavy cryptosporidial infections in children in northeast Brazil: comparison of *Cryptosporidium hominis* and *Cryptosporidium parvum*. *Transactions of the Royal Society of Tropical Medicine and Hygiene*, 101(4), pp.378-384.

Cabada, M., White, A., Venugopalan, P. and Sureshbabu, J. (2015). Cryptosporidiosis Treatment & Management. *Medscape*. [online] Available at: https://emedicine.medscape.com/article/215490-treatment [Accessed 25 Jun. 2018].

Cama, V.A., Ross, J.M., Crawford, S., Kawai, V.,Chavez-Valdez, R., Vargas, D., Vivar, A., Ticona, E., Navincopa, M., Williamson, J., Ortega, Y., Gilman, R.H., Bern, C. and Xiao, L. (2007). Differences in clinical manifestations among *Cryptosporidium* species and subtypes in HIV-infected persons. Journal of Infectious Diseases 196, 684–691.

Cama, VA., Bern, C., Roberts, J., Cabrera, L., Sterling, CR., Ortega, Y., Gilman, RH., Xiao L. (2008). *Cryptosporidium* species and subtypes and clinical manifestation in children, Peru. *Emerging Infectious Diseases*, 14(10), pp.1567-1574.

Campbell, I., Tzipori, A., Hutchison, G. and Angus, K. (1982). Effect of disinfectants on survival of *Cryptosporidium* oocysts. *Veterinary Record*, 111(18), pp.414-415.

Canetta, E., Adya, A. and Walker, G. (2006). Atomic force microscopic study of the effects of ethanol on yeast cell surface morphology. *FEMS Microbiology Letters*, 255(2), pp.308-315.

Cappella, B. and Dietler, G. (1999). Force-distance curves by atomic force microscopy. *Surface Science Reports*, 34(1-3), pp.1-104.

Carreno, R., Matrin, D. and Barta, J. (1999). *Cryptosporidium* is more closely related to the gregarines than to coccidia as shown by phylogenetic analysis of apicomplexan parasites inferred using small-subunit ribosomal RNA gene sequences. *Parasitology Research*, 85(11), pp.899-904.

Cavalier-Smith, T. (2014). Gregarine site-heterogeneous 18S rDNA trees, revision of gregarine higher classification, and the evolutionary diversification of Sporozoa. *European Journal of Protistology*, 50(5), pp.472-495.

Centres for Disease Control (CDC) (1982). Cryptosporidiosis: assessment of chemotherapy of males with acquired immune deficiency syndrome (AIDS). *Morbidity and Mortality Weekly Report*, 31(44), pp.589-592.

Cerf, A., Cau, J., Vieu, C. and Dague, E. (2009). Nanomechanical Properties of Dead or Alive Single-Patterned Bacteria. *Langmuir*, 25(10), pp.5731-5736.

Chalmers, R., Robinson, G., Elwin, K., Hadfield, S., Xiao, L., Ryan, U., Modha, D. and Mallaghan, C. (2009). *Cryptosporidium* Rabbit Genotype, a Newly Identified Human Pathogen. *Emerging Infectious Diseases*, 15(5), pp.829-830.

Chalmers, R.M., Smith, R., Elwin, K., Clifton-Hadley, F.A. and Giles, M. (2011). Epidemiology of anthroponotic and zoonotic human cryptosporidiosis in England and Wales, 2004–2006. Epidemiology and Infection 139, 700–712.

Chandler, D. and Roberson, R. (2009). *Bioimaging*. Sudbury (Mass.): Jones and Bartlett.

Chappell, C.L. et al. (1996). *Cryptosporidium parvum*: intensity of infection and oocyst excretion patterns in healthy volunteers. The Journal of infectious diseases [Online] 173:232–6. Available at: http://www.ncbi.nlm.nih.gov/pubmed/8537664.

Chappell, C.L., Okhuysen, P.C., Langer-Curry, R., Widmer, G., Akiyoshi, D.E., Tanriverdi, S. and Tzipori, S. (2006). *Cryptosporidium hominis*: experimental challenge of healthy adults. *American Journal of Tropical Medicine and Hygiene*, 75 (5), 851–857.

Checkley, W., Gilman, R., Epstein, L., Suarez, M., Diaz, J., Cabrera, L., Black, R. and Sterling, C. (1997). Asymptomatic and Symptomatic Cryptosporidiosis: Their Acute Effect on Weight Gain in Peruvian Children. *American Journal of Epidemiology*, 145(2), pp.156-163.

Chen, X., O'Hara, S., Huang, B., Splinter, P., Nelson, J. and LaRusso, N. (2005). Localized glucose and water influx facilitates *Cryptosporidium parvum* cellular invasion by means of modulation of host-cell membrane protrusion. *Proceedings of the National Academy of Sciences*, 102(18), pp.6338-6343.

Clode, P., Koh, W. and Thompson, R. (2015). Life without a Host Cell: What is *Cryptosporidium*? *Trends in Parasitology*, 31(12), pp.614-624.

Considine, R., Dixon, D. and Drummond, C. (2002). Oocysts of *Cryptosporidium parvum* and model sand surfaces in aqueous solutions: an atomic force microscope (AFM) study. *Water Research*, 36(14), pp.3421-3428.

Considine, R., Dixon, D. and Drummond, C. (2002). Oocysts of *Cryptosporidium parvum* and model sand surfaces in aqueous solutions: an atomic force microscope (AFM) study. *Water Research*, 36(14), pp.3421-3428.

Corso PS, Kramer MH, Blair KA, Addiss DG, Davis JP, Haddix AC. (2003). Cost of illness in the 1993 waterborne *Cryptosporidium* outbreak, Milwaukee, Wisconsin. *Emerg Infect Dis*. 9(4):426-31

Current, W.L., Upton, S.J. and Haynes, T.B. (1986). The life cycle of *Cryptosporidium baileyi* n. sp. (Apicomplexa, Cryptosporidiidae) infecting chickens. Journal of Protozoology 33, 289–296.

DeSilva, M., Schafer, S., Kendall Scott, M., Robinson, B., Hills, A., Buser, G., Salis, K., Gargano, J., Yoder, J., Hill, V., Xiao, L., Roellig, D. and Hedberg, K. (2015). Communitywide cryptosporidiosis

outbreak associated with a surface water-supplied municipal water system – Baker City, Oregon, 2013. *Epidemiology and Infection*, 144(02), pp.274-284.

Dillingham, R., Lima, A. and Guerrant, R. (2002). Cryptosporidiosis: epidemiology and impact. *Microbes and Infection*, 4(10), pp.1059-1066.

Doktycz, M., Sullivan, C., Hoyt, P., Pelletier, D., Wu, S. and Allison, D. (2003). AFM imaging of bacteria in liquid media immobilized on gelatin coated mica surfaces. *Ultramicroscopy*, 97(1-4), pp.209-216.

Dorobantu, L., Bhattacharjee, S., Foght, J. and Gray, M. (2008). Atomic Force Microscopy Measurement of Heterogeneity in Bacterial Surface Hydrophobicity. *Langmuir*, 24(9), pp.4944-4951.

Drake, B. (1989). Imaging crystals, polymers, and processes in water with the atomic force microscope. *Deep Sea Research Part B. Oceanographic Literature Review*, 36(9), pp.818-825.

Dufrêne, Y., Ando, T., Garcia, R., Alsteens, D., Martinez-Martin, D., Engel, A., Gerber, C. and Müller, D. (2017). Imaging modes of atomic force microscopy for application in molecular and cell biology. *Nature Nanotechnology*, 12(4), pp.295-307.

Elwin, K., Hadfield, S.J., Robinson, G. and Chalmers, R.M. (2012a). The epidemiology of sporadic human infections with unusual cryptosporidia detected during routine typing in England and Wales, 2000–2008. Epidemiology and Infection 140, 673–683.

Elwin, K., Hadfield, S.J., Robinson, G., Crouch, N.D. and Chalmers, R.M. (2012b). *Cryptosporidium viatorum* n. sp. (Apicomplexa: Cryptosporidiidae) among travellers returning to Great Britain from the Indian subcontinent, 2007–2011. International Journal of Parasitology 42, 675–682.

Essid R, Mousli M, Aoun K, Abdelmalek R, Mellouli F, Kanoun F, et al. (2008). Identification of *Cryptosporidium* species infecting humans in Tunisia. *Am J Trop Med Hyg*. 79(5):702-5.

Farrell, L., Pepin, J., Kucharski, C., Lin, X., Xu, Z. and Uludag, H. (2007). A comparison of the effectiveness of cationic polymers poly-l-lysine (PLL) and polyethylenimine (PEI) for non-viral delivery of plasmid DNA to bone marrow stromal cells (BMSC). *European Journal of Pharmaceutics and Biopharmaceutics*, 65(3), pp.388-397.

Fayer, R. and Xiao, L. (2007). *Cryptosporidium and Cryptosporidiosis*. 2nd ed. Florida, USA: CRC Press, pp.1-28.

Fayer, R., Morgan, U. and Upton, S. (2000). Epidemiology of *Cryptosporidium*: transmission, detection and identification. *International Journal for Parasitology*, 30(12-13), pp.1305-1322.

Fayer, R., Santin, M. and Macarisin, D. (2010). *Cryptosporidium ubiquitum* n. sp. in animals and humans. Veterinary Parasitology 172, 23–32.

Fayer, R., Santin, M. and Trout, J.M. (2008). *Cryptosporidium ryanae* n. sp. (Apicomplex: Cryptosporidiidae) in cattle (*Bos taurus*). Veterinary Parasitology 156, 191–190.

Fayer, R., Speer, C. and Dubey, J. (1997). The general biology of *Cryptosporidium*. In *Cryptosporidium and Cryptosporidiosis*. 1st ed. Boca Raton: Taylor & Francis Ltd., pp.1-41.

Fayer, R., Trout, J.M. & Jenkins, M.C. (1998). Infectivity of *Cryptosporidium parvum* oocysts stored in water at environmental temperatures. J Parasitol 84, 1165–1169.

Fayer, R., Trout, J.M., Xiao, L., Morgan, U.M., Lal, A.A. and Dubey, J.P. (2001). *Cryptosporidium canis* n. sp. from domestic dogs. Journal of Parasitology 87, 1415–1422.

Feng, Y., Yang, W., Ryan, U., Zhang, L., Kvac, M., Koudela, B., Modry, D., Li, N., Fayer, R. and Xiao, L. (2011b). Development of a multilocus sequence tool for typing *Cryptosporidium muris* and *Cryptosporidium andersoni*. Journal of Clinical Microbiology 49, 34 –41.

Fischer, E., Hansen, B., Nair, V., Hoyt, F. and Dorward, D. (2012). S*canning Electron Microscopy.* In *Current Protocols in Microbiology*. 1st ed. USA: John Wiley & Sons Inc., pp.2B.2.1-2B.2.47.

Francius, G., Domenech, O., Mingeot-Leclercq, M. and Dufrene, Y. (2008). Direct Observation of *Staphylococcus aureus* Cell Wall Digestion by Lysostaphin. *Journal of Bacteriology*, 190(24), pp.7904-7909.

From the Centers for Disease Control and Prevention. Foodborne outbreak of diarrheal illness associated with *Cryptosporidium parvum*--Minnesota, 1995. (1996). *JAMA: The Journal of the American Medical Association*, 276(15), pp.1214-1214.

From the Centers for Disease Control and Prevention. Outbreak of cryptosporidiosis associated with a firefighting response — Indiana and Michigan, June 2011. (2012). *MMWR. Morbidity and Mortality Weekly Report*, 61(09), pp.153-6.

Gan, Y. (2009). Atomic and subnanometer resolution in ambient conditions by atomic force microscopy. *Surface Science Reports*, 64(3), pp.99-121.

Gatei, W., Wamae, C., Mbae, C., Waruru, A., Mulinge, E., Waithera, T., Gatika, S., Kamwati, S., Revathi, G. and Hart, C. (2006). Cryptosporidiosis: prevalence, genotype analysis, and symptoms associated with infections in children in Kenya. *Am J Trop Med Hyg.*, 75(1), pp.78-82.

Gentile, G., Venditti, M., Micozzi, A., Caprioli, A., Donelli, G., Caprioli, A., Donelli, G., Tirindelli, C., Meloni, G., Arcese, W. and Martino, P. (1991). Cryptosporidiosis in Patients with Hematologic Malignancies. *Clinical Infectious Diseases*, 13(5), pp.842-846.

Gerber, C. and Lang, H. (2006). How the doors to the nanoworld were opened. *Nature Nanotechnology*, 1(1), pp.3-5.

Gobet, P. (2001). Sensitive genotyping of *Cryptosporidium parvum* by PCR-RFLP analysis of the 70-kilodalton heat shock protein (HSP70) gene. *FEMS Microbiology Letters*, 200(1), pp.37-41.

Griffin, R. (1990). *Using the transmission electron microscope in the biological sciences*. 1st ed. New York: Ellis Horwood, pp.3-17.

Guéroult, M., Boittin, O., Mauffret, O., Etchebest, C. and Hartmann, B. (2012). Mg2+ in the Major Groove Modulates B-DNA Structure and Dynamics. *PLoS ONE*, 7(7), p.e41704.

Guerrant, D., Lima, A., Patrick, P., Schorling, J., Moore, S. and Guerrant, R. (1999). Association of early childhood diarrhoea and cryptosporidiosis with impaired physical fitness and cognitive function four-seven years later in a poor urban community in northeast Brazil. *The American Journal of Tropical Medicine and Hygiene*, 61(5), pp.707-713.

Harris, J. and Petry, F. (1999). *Cryptosporidium parvum*: Structural Components of the Oocyst Wall. *The Journal of Parasitology*, 85(5), p.839.

Harris, J., Adrian, M. and Petry, F. (2004). Amylopectin: a major component of the residual body in Cryptosporidium parvum oocysts. *Parasitology*, 128(3), pp.269-282.

Hawkes, P. (2012). *TSEM: A Review of Scanning Electron Microscopy in Transmission Mode and Its Applications. In Advances in Imaging and Electron Physics*. 1st ed. San Diego: Elsevier Science & Technology.

Hayes, E., Matte, T., O'Brien, T., McKinley, T., Logsdon, G., Rose, J., Ungar, B., Word, D., Wilson, M., Long, E., Hurwitz, E. and Juranek, D. (1989). Large Community Outbreak of Cryptosporidiosis Due to Contamination of a Filtered Public Water Supply. *New England Journal of Medicine*, 320(21), pp.1372-1376.

Helmy, Y.A., Krücken, J., Nöckler, K., von Samson Himmelstjerna, G. and Zessin, K.H. (2013). Molecular epidemiology of *Cryptosporidium* in livestock animals and humans in the Ismailia province of Egypt. Veterinary Parasitology 193, 15 –24.

Henderson, E., Haydon, P. and Sakaguchi, D. (1992). Actin filament dynamics in living glial cells imaged by atomic force microscopy. *Science*, 257(5078), pp.1944-1946.

Hijjawi, N., Meloni, B., Ng'anzo, M., Ryan, U., Olson, M., Cox, P., Monis, P. and Thompson, R. (2004). Complete development of *Cryptosporidium parvum* in host cell-free culture. *International Journal for Parasitology*, 34(7), pp.769-777.

Hinterdorfer, P., Baumgartner, W., Gruber, H., Schilcher, K. and Schindler, H. (1996). Detection and localization of individual antibody-antigen recognition events by atomic force microscopy. *Proceedings of the National Academy of Sciences*, 93(8), pp.3477-3481.

Hoh, J., Cleveland, J., Prater, C., Revel, J. and Hansma, P. (1992). Quantized adhesion detected with the atomic force microscope. *Journal of the American Chemical Society*, 114(12), pp.4917-4918.

Hong, D., Wong, C. and Gutierrez, K. (2007). Severe cryptosporidiosis in a seven-year-old renal transplant recipient - Case report and review of the literature. *Pediatric Transplantation*, 11(1), pp.94-100.

Insulander, M., Lebbad, M., Stenström, T. and Svenungsson, B. (2005). An outbreak of cryptosporidiosis associated with exposure to swimming pool water. *Scandinavian Journal of Infectious Diseases*, 37(5), pp.354-360.

Insulander, M., Silverlas, C., Lebbad, M., Karlsson, L., Mattsson, J.G. and Svenungsson, B. (2013). Molecular epidemiology and clinical manifestations of human cryptosporidiosis in Sweden. Epidemiology and Infection 141, 1009–1020.

Iseki, M. (1979). *Cryptosporidium felis* sp. n. (Protozoa: Eimeriorina) from the domestic cat. Japanese Journal of Parasitology 28, 285–307.

Jaggi N, Rajeshwari S, Mittal SK, Mathur MD, Baveja UK. (1994). Assessment of the immune and nutritional status of the host in childhood diarrhoea due to *Cryptosporidium*. *J Commun Dis.* 26(4):181-5.

Jellison, K., Distel, D., Hemond, H. and Schauer, D. (2004). Phylogenetic Analysis of the Hypervariable Region of the 18S rRNA Gene of *Cryptosporidium* Oocysts in Feces of Canada Geese (*Branta canadensis*): Evidence for Five Novel Genotypes. *Applied and Environmental Microbiology*, 70(1), pp.452-458.

Jenkins, M., Eaglesham, B., Anthony, L., Kachlany, S., Bowman, D. and Ghiorse, W. (2010). Significance of Wall Structure, Macromolecular Composition, and Surface Polymers to the Survival and Transport of *Cryptosporidium parvum* Oocysts. *Applied and Environmental Microbiology*, 76(6), pp.1926-1934.

Jirku, M., Valigurova, A., Koudela, B., Krzek, J., Modry, D. and Slapeta, J. (2008). New species of *Cryptosporidium* Tyzzer, 1907 (Apicomplexa) from amphibian host: morphology, biology, and phylogeny. Folia Parasitologica 55, 81 –94.

Jothikumar, N., da Silva, A., Moura, I., Qvarnstrom, Y. and Hill, V. (2008). Detection and differentiation of *Cryptosporidium hominis* and *Cryptosporidium parvum* by dual TaqMan assays. *Journal of Medical Microbiology*, 57(9), pp.1099-1105.

Kar, S., Daugschies, A., Cakmak, A., Yilmazer, N., Dittmar, K. and Bangoura, B. (2011). Cryptosporidium parvum oocyst viability and behaviour of the residual body during the excystation process. *Parasitology Research*, 109(6), pp.1719-1723.

Karanis, P., Kimura, A., Nagasawa, H., Igarashi, I. and Suzuki, N. (2008). Observations on *Cryptosporidium* Life Cycle Stages During Excystation. *Journal of Parasitology*, 94(1), pp.298-300.

Kelly, P., Makumbi, F., Carnaby, S., Simjee, A. and Farthing, M. (1998). Variable distribution of *Cryptosporidium parvum* in the intestine of AIDS patients revealed by polymerase chain reaction. *European Journal of Gastroenterology & Hepatology*, 10(10), pp.855-858.

Keyvani, A., Sadeghian, H., Tamer, M., Goosen, J. and van Keulen, F. (2017). Minimizing tip-sample forces and enhancing sensitivity in atomic force microscopy with dynamically compliant cantilevers. *Journal of Applied Physics*, 121(24), p.244505.

Khan, S.M., Debnath, C., Pramanik, A.K., Xiao, L., Nozaki, T. and Ganguly, S. (2010). Molecular characterization and assessment of zoonotic transmission of *Cryptosporidium* from dairy cattle in West Bengal, India. Veterinary Parasitology 171, 41 –47.

Kibbler CC, Smith A, Hamilton-Dutoit SJ, Milburn H, Pattinson JK, Prentice HG. (1987). Pulmonary cryprosporidiosis occurring in a bone marrow transplant patient. *Scandinavian Journal of Infectious Diseases*,19(5), pp. 581–584.

Koh, W., Clode, P., Monis, P. and Thompson, R. (2013). Multiplication of the waterborne pathogen Cryptosporidium parvum in an aquatic biofilm system. *Parasites & Vectors*, 6(1), p.270.

Koh, W., Thompson, A., Edwards, H., Monis, P. and Clode, P. (2014). Extracellular excystation and development of *Cryptosporidium*: tracing the fate of oocysts within Pseudomonas aquatic biofilm systems. *BMC Microbiology*, 14(1).

Koloren, Z. and Dinçer, S. (2008). Infectious Rates of HCT-8 Cells Infected with *Cryptosporidium Parvum* Sporozoites Obtained in In Vitro Different Excystation Conditions. *Biotechnology & Biotechnological Equipment*, 22(3), pp.856-858.

Korich, D., Mead, J., Madore, M., Sinclair, N. and Sterling, C. (1990). Effects of ozone, chlorine dioxide, chlorine, and monochloramine on *Cryptosporidium parvum* oocyst viability. *Applied and Environmental Microbiology*, 56(5), pp.1423–8.

Kotloff, K., Nataro, J., Blackwelder, W., Nasrin, D., Farag, T., Panchalingam, S., Wu, Y., Sow, S., Sur, D., Breiman, R., Faruque, A., Zaidi, A., Saha, D., Alonso, P., Tamboura, B., Sanogo, D., Onwuchekwa, U., Manna, B., Ramamurthy, T., Kanungo, S., Ochieng, J., Omore, R., Oundo, J., Hossain, A., Das, S., Ahmed, S., Qureshi, S., Quadri, F., Adegbola, R., Antonio, M., Hossain, M., Akinsola, A., Mandomando, I., Nhampossa, T., Acácio, S., Biswas, K., O'Reilly, C., Mintz, E., Berkeley, L., Muhsen, K., Sommerfelt, H., Robins-Browne, R. and Levine, M. (2013). Burden and aetiology of diarrhoeal disease in infants and young children in developing countries (the Global Enteric Multicenter Study, GEMS): a prospective, case-control study. *The Lancet*, 382(9888), pp.209-222.

Kuznar, Z. and Elimelech, M. (2005). Role of surface proteins in the deposition kinetics of *Cryptosporidium parvum* oocysts. *Langmuir*, 21(2), pp.710-716.

Kuznetsov, Y., Gershon, P. and McPherson, A. (2008). Atomic Force Microscopy Investigation of Vaccinia Virus Structure. *Journal of Virology*, 82(15), pp.7551-7566.

Kváč, M., Hanzlíková, D., Sak, B. and Kvetonová, D. (2009a). Prevalence and age-related infection of *Cryptosporidium suis, Cryptosporidium muris* and *Cryptosporidium* pig genotype II in pigs on a farm complex in the Czech Republic. Veterinary Parasitology 160, 319–322.

Kváč, M., Hofmannová, L., Hlásková, L., Květoňová, D., Vítovec, J., McEvoy, J. and Sak, B. (2014b). *Cryptosporidium erinacei* n. sp. (Apicomplexa: Cryptosporidiidae) in hedgehogs. Veterinary Parasitology 201,9 –17.

Kváč, M., Kestřánová, M., Pinková, M., Květoňová, D., Kalinová, J., Wagnerová, P., Kotková, M., Vítovec, J., Ditrich, O., McEvoy, J., Stenger, B. and Sak, B. (2013b). *Cryptosporidium scrofarum* n. sp. (Apicomplexa: Cryptosporidiidae) in domestic pigs (*Sus scrofa*). Veterinary Parasitology 191, 218–227.

Kváč, M., Kvetonová, D., Sak, B. and Ditrich, O. (2009b). *Cryptosporidium* pig genotype II in immunocompetent man. Emerging Infectious Diseases 15, 982–983.

Kvac, M., Sakova, K., Kvetonova, D., Kicia, M., Wesolowska, M., McEvoy, J. and Sak, B. (2013a). Gastroenteritis Caused by the Cryptosporidium Hedgehog Genotype in an Immunocompetent Man. *Journal of Clinical Microbiology*, 52(1), pp.347-349.

Kváč, M., Saková, K., Květoňová, D., Kicia, M., Wesołowska, M., McEvoy, J. and Sak, B. (2014a). Gastroenteritis caused by the *Cryptosporidium* hedgehog genotype in an immunocompetent man. Journal of Clinical Microbiology 52, 347–349.

Le Grimellec, C., Lesniewska, E., Giocondi, M., Finot, E., Vié, V. and Goudonnet, J. (1998). Imaging of the Surface of Living Cells by Low-Force Contact-Mode Atomic Force Microscopy. *Biophysical Journal*, 75(2), pp.695-703.

Leander, B. and Ramey, P. (2006). Cellular Identity of a Novel Small Subunit rDNA Sequence Clade of Apicomplexans: Description of the Marine Parasite *Rhytidocystis polygordiae* n. sp. (Host: Polygordius sp., Polychaeta). *The Journal of Eukaryotic Microbiology*, 53(4), pp.280-291.

Lee, G., Chrisey, L. and Colton, R. (1994). Direct measurement of the forces between complementary strands of DNA. *Science*, 266(5186), pp.771-773.

Leitch, G. and He, Q. (2012). Cryptosporidiosis-an overview. *Journal of Biomedical Research*, 25(1), pp.1-16.

Leoni, F., Amar, C., Nichols, G., Pedraza-Díaz, S. and McLauchlin, J. (2006). Genetic analysis of *Cryptosporidium* from 2414 humans with diarrhoea in England between 1985 and 2000. Journal of Medical Microbiology 55, 703–707.

Levine, N. (1988). *The Protozoan Phylum Apicomplexa*. Milton: CRC Press.
Levine, N.D. (1980). Some corrections of coccidian (Apicomplexa: Protozoa) nomenclature. Journal of Parasitology 66, 830–834.

Lindsay, D.S., Upton, S.J., Owens, D.S., Morgan, U.M., Mead, J.R. and Blagburn, B.L. (2000). *Cryptosporidium andersoni* n. sp. (Apicomplexa: Cryptosporidiidae) from cattle, *Bos taurus*. Journal of Eukaryotic Microbiology 47, 91 –85.

Liu, H., Shen, Y., Yin, J., Yuan, Z., Jiang, Y., Xu, Y., Pan, W., Hu, Y. and Cao, J. (2014). Prevalence and genetic characterization of *Cryptosporidium, Enterocytozoon, Giardia* and *Cyclospora* in diarrheal outpatients in China. BMC Infectious Diseases 14, 25.

Llorente, M., Clavel, A., Goñi, M., Varea, M., Seral, C., Becerril, R., Suarez, L. and Gómez-Lus, R. (2007). Genetic characterization of *Cryptosporidium* species from humans in Spain. *Parasitology International*, 56(3), pp.201-205.

López-Vélez, R., Tarazona, R., Camacho, A., Gomez-Mampaso, E., Guerrero, A., Moreira, V. and Villanueva, R. (1995). Intestinal and extraintestinal cryptosporidiosis in AIDS patients. *European Journal of Clinical Microbiology & Infectious Diseases*, 14(8), pp.677-681.

Lucio-Forster, A., Griffiths, J.K., Cama, V.A., Xiao, L. and Bowman, D.D. (2010). Minimal zoonotic risk of cryptosporidiosis from pet dogs and cats. Trends in Parasitology 26, 174–179.

Mac Kenzie, W., Hoxie, N., Proctor, M., Stephen, S., Blair, K., Peterson, D., Kazmierczak, J., Addiss, D., Fox, K., Rose, J. and Davis, J. (1994). A Massive Outbreak in Milwaukee of *Cryptosporidium* Infection Transmitted through the Public Water Supply. *New England Journal of Medicine*, 331(15), pp.1035-1035

Maggi, P., Larocca, A., Quarto, M., Serio, G., Brandonisio, O., Angarano, G. and Pastore, G. (2000). Effect of Antiretroviral Therapy on Cryptosporidiosis and Microsporidiosis in Patients Infected with Human Immunodeficiency Virus Type 1. *European Journal of Clinical Microbiology & Infectious Diseases*, 19(3), pp.213-217.

McGuigan, K., Mendez-Hermida, F., Castro-Hermida, J., Ares-Mazas, E., Kehoe, S., Boyle, M., Sichel, C., Fernandez-Ibanez, P., Meyer, B., Ramalingham, S. and Meyer, E. (2006). Batch solar disinfection inactivates oocysts of *Cryptosporidium parvum* and cysts of *Giardia muris* in drinking water. *Journal of Applied Microbiology*, 101(2), pp.453-463.

McKerr, C., Adak, G., Nichols, G., Gorton, R., Chalmers, R., Kafatos, G., Cosford, P., Charlett, A., Reacher, M., Pollock, K., Alexander, C. and Morton, S. (2015). An Outbreak of *Cryptosporidium parvum* across England & Scotland Associated with Consumption of Fresh Pre-Cut Salad Leaves, May 2012. *PLOS ONE*, 10(5), p.e0125955.

Mele, R., Gomez Morales, M., Tosini, F. and Pozio, E. (2004). *Cryptosporidium parvum* at Different Developmental Stages Modulates Host Cell Apoptosis In Vitro. *Infection and Immunity*, 72(10), pp.6061-6067.

Meynard, J., Meyohas, M., Binet, D., Frottiers, J. and Chouaid, C. (1996). Pulmonary cryptosporidiosis in the acquired immunodeficiency syndrome. *Infection*, 24(4), pp.328-331.

Micic, M., Hu, D., Suh, Y., Newton, G., Romine, M. and Lu, H. (2004). Correlated atomic force microscopy and fluorescence lifetime imaging of live bacterial cells. *Colloids and Surfaces B: Biointerfaces*, 34(4), pp.205-212.

Miller, C., Jossé, L., Brown, I., Blakeman, B., Povey, J., Yiangou, L., Price, M., Cinatl, J., Xue, W., Michaelis, M. and Tsaousis, A. (2018). A cell culture platform for *Cryptosporidium* that enables long-term cultivation and new tools for the systematic investigation of its biology. *International Journal for Parasitology*, 48(3-4), pp.197-201.

Molloy, S.F., Smith, H.V., Kirwan, P., Nichols, R.A., Asaolu, S.O., Connelly, L. and Holland, C.V. (2010). Identification of a high diversity of *Cryptosporidium* species genotypes and subtypes in a pediatric population in Nigeria. American Journal of Tropical Medicine and Hygiene 82, 608–613.

Morgan-Ryan, U.M., Fall, A., Ward, L.A., Hijjawi, N., Sulaiman, I., Fayer, R., Thompson, R.C.A., Olson, M., Lal, A.A. and Xiao, L. (2002). *Cryptosporidium hominis* n. sp. (Apicompolexa: Cryptosporidiidae) from Homo sapiens. Journal of Eukaryotic Microbiology 49, 433–440.

Moroni, M., Esposito, R., Cernuschi, M., Franzetti, F., Carosi, G. and Fiori, G. (1993). Treatment of AIDS-Related Refractory Diarrhoea with Octreotide. *Digestion*, 54(1), pp.30-32.

Morse, T.D., Nichols, R.A., Grimason, A.M., Campbell, B.M., Tembo, K.C. and Smith, H.V. (2007). Incidence of cryptosporidiosis species in paediatric patients in Malawi. Epidemiology and Infection 135, 1307–1315.

Mortensen, N., Fowlkes, J., Sullivan, C., Allison, D., Larsen, N., Molin, S. and Doktycz, M. (2009). Effects of Colistin on Surface Ultrastructure and Nanomechanics of *Pseudomonas aeruginosa* Cells. *Langmuir*, 25(6), pp.3728-3733.

Mosier, D. and Oberst, R. (2000). Cryptosporidiosis: A Global Challenge. *Annals of the New York Academy of Sciences*, 916(1), pp.102-111.

Müller, D. and Dufrêne, Y. (2008). Atomic force microscopy as a multifunctional molecular toolbox in nanobiotechnology. *Nature Nanotechnology*, 3(5), pp.261-269.

Müller, D. and Dufrêne, Y. (2011). Atomic force microscopy: a nanoscopic window on the cell surface. *Trends in Cell Biology*, 21(8), pp.461-469.

Müller, D., Amrein, M. and Engel, A. (1997). Adsorption of Biological Molecules to a Solid Support for Scanning Probe Microscopy. *Journal of Structural Biology*, 119(2), pp.172-188.

Muller, D., Baumeister, W. and Engel, A. (1999). Controlled unzipping of a bacterial surface layer with atomic force microscopy. *Proceedings of the National Academy of Sciences*, 96(23), pp.13170-13174.

Nair P, Mohamed JA, DuPont HL, et al. (2008). Epidemiology of cryptosporidiosis in north American travelers to Mexico. *American Journal of Tropical Medicine and Hygiene*. 79(2), pp.210–214.

Navin, T. and Juranek, D. (1984). Cryptosporidiosis: Clinical, Epidemiologic, and Parasitologic Review. *Clinical Infectious Diseases*, 6(3), pp.313-327.

Nazemalhosseini-Mojarad, E., Feng, Y. and Xiao, L. (2012). The importance of subtype analysis of *Cryptosporidium spp*. in epidemiological investigations of human cryptosporidiosis in Iran and other Mideast countries. *Gastroenterology and Hepatology from Bed to Bench*, 5(2):67-70.

Neill, M., Rice, S., Ahmad, N. and Flanigan, T. (1996). Cryptosporidiosis: An Unrecognized Cause of Diarrhea in Elderly Hospitalized Patients. *Clinical Infectious Diseases*, 22(1), pp.168-170.

Ng, J.S., Eastwood, K., Walker, B., Durrheim, D.N., Massey, P.D., Porigneaux, P., Kemp, R., McKinnon, B., Laurie, K., Miller, D., Bramley, E. and Ryan, U. (2012). Evidence of *Cryptosporidium* transmission

between cattle and humans in northern New South Wales. Experimental Parasitology 130, 437–441.

Nime, F., Burek, J., Page, D., Holscher, M. and Yardley, J. (1976). Acute Enterocolitis in a Human Being Infected with the Protozoan *Cryptosporidium*. *Gastroenterology*, 70(4), pp.592-598.

Nogales, E. (2016). The development of cryo-EM into a mainstream structural biology technique. *Nature Methods*, 13(1), pp.24-27

Novak, P., Li, C., Shevchuk, A., Stepanyan, R., Caldwell, M., Hughes, S. and Korchev, Y. (2009). Nanoscale live cell imaging using hopping probe ion conductance microscopy. *Nature Methods*, 6(4), pp.279–281.

O'Donoghue, P. (1995). *Cryptosporidium* and cryptosporidiosis in man and animals. *International Journal for Parasitology*, 25(2), pp.139-195.

O'Hara, S. and Chen, X. (2011). The cell biology of cryptosporidium infection. *Microbes and Infection*, 13(8-9), pp.721-730.

Okhuysen, P.C. et al. (1999). Virulence of Three Distinct *Cryptosporidium parvum* Isolates for Healthy Adults. The Journal of Infectious Diseases [Online] 180:1275–1281. Available at: https://academic.oup.com/jid/article-lookup/doi/10.1086/315033.

Ong, Y., Razatos, A., Georgiou, G. and Sharma, M. (1999). Adhesion Forces between *E. coli* Bacteria and Biomaterial Surfaces. *Langmuir*, 15(8), pp.2719-2725.

Panciera, R., Thomassen, R. and Garner, F. (1971). Cryptosporidial Infection in a Calf. *Veterinary Pathology*, 8(5-6), pp.479-484.

Pavlásek, I. (1999). Cryptosporidia: biology, diagnosis, host spectrum, specificity, and the environment. Remedia Klinicka Mikrobiologie 3, 290–301.

Pavlásek, I., Lávicková, M., Horák, P., Král, J. and Král, B. (1995). *Cryptosporidium varaniin* sp. (Apicomplexa: Cryptosporidiidae) in Emerald monitor (Varanus prasinus Schlegal, 1893) in captivity in Prague zoo. Gazella 22, 99 –108.

Pedraza-Diaz, S. (2001). Nested Polymerase Chain Reaction for Amplification of the *Cryptosporidium* Oocyst Wall Protein Gene. *Emerging Infectious Diseases*, 7(1), pp.49-56.

Petry, F. (2004). Structural Analysis of *Cryptosporidium parvum*. *Microscopy and Microanalysis*, 10(05), pp.586-601.

Pinckney, R., Lindsay, D., Toivio-Kinnucan, M. and Blagburn, B. (1993). Ultrastructure of *Isospora suis* during excystation and attempts to demonstrate extraintestinal stages in mice. *Veterinary Parasitology*, 47(3-4), pp.225-233.

Plomp, M., Leighton, T., Wheeler, K., Hill, H. and Malkin, A. (2007). In vitro high-resolution structural dynamics of single germinating bacterial spores. *Proceedings of the National Academy of Sciences*, 104(23), pp.9644-9649.

Plomp, M., McCaffery, J., Cheong, I., Huang, X., Bettegowda, C., Kinzler, K., Zhou, S., Vogelstein, B. and Malkin, A. (2007). Spore Coat Architecture of Clostridium novyi NT Spores. *Journal of Bacteriology*, 189(17), pp.6457-6468.

Power, M.L. and Ryan, U.M. (2008). A new species of *Cryptosporidium* (Apicomplexa: Cryptosporidiidae) from eastern grey kangaroos (Macropus giganteus). Journal of Parasitology 94, 1114–1117.

Preiser, G., Preiser, L. and Madeo, L. (2003). An Outbreak of Cryptosporidiosis Among Veterinary Science Students Who Work with Calves. *Journal of American College Health*, 51(5), pp.213-215.

Puleston, R., Mallaghan, C., Modha, D., Hunter, P., Nguyen-Van-Tam, J., Regan, C., Nichols, G. and Chalmers, R. (2014). The first recorded outbreak of cryptosporidiosis due to *Cryptosporidium cuniculus* (formerly rabbit genotype), following a water quality incident. *Journal of Water and Health*, 12(1), p.41.

Putignani, L. and Menichella, D. (2010). Global Distribution, Public Health and Clinical Impact of the Protozoan Pathogen *Cryptosporidium*. *Interdisciplinary Perspectives on Infectious Diseases*, 2010, pp.1-39.

Radmacher, M., Tillamnn, R., Fritz, M. and Gaub, H. (1992). From molecules to cells: imaging soft samples with the atomic force microscope. *Science*, 257(5078), pp.1900-1905.

Raskova, V., Kvetonova, D., Sak, B., McEvoy, J., Edwinson, A., Stenger, B. and Kvac, M. (2013). Human cryptosporidiosis caused by *Cryptosporidium tyzzeri* and *C. parvum* isolates presumably transmitted from wild mice. Journal of Clinical Microbiology 51, 360–362.

Razatos, A., Ong, Y., Sharma, M. and Georgiou, G. (1998). Molecular determinants of bacterial adhesion monitored by atomic force microscopy. *Proceedings of the National Academy of Sciences*, 95(19), pp.11059-11064.

Reduker, D., Speer, C. and Blixt, J. (1985). Ultrastructure of *Cryptosporidium parvum* Oocysts and Excysting Sporozoites as Revealed by High Resolution Scanning Electron Microscopy. *The Journal of Protozoology*, 32(4), pp.708-711.

Reduker, D., Speer, C. and Blixt, J. (1985a). Ultrastructural changes in the oocyst wall during excystation of *Cryptosporidium parvum* (Apicomplexa; Eucoccidiorida). *Canadian Journal of Zoology*, 63(8), pp.1892-1896.

Reduker, D., Speer, C. and Blixt, J. (1985b). Ultrastructure of *Cryptosporidium parvum* Oocysts and Excysting Sporozoites as Revealed by High Resolution Scanning Electron Microscopy. *The Journal of Protozoology*, 32(4), pp.708-711.

Reimer, L. and Kohl, H. (2010). *Transmission electron microscopy*. 1st ed. New York, NY: Springer.

Reinoso, R., Becares, E. and Smith, H. (2008). Effect of various environmental factors on the viability of *Cryptosporidium parvum* oocysts. *Journal of Applied Microbiology*, 104(4), pp.980-986.

Ren, X., Zhao, J., Zhang, L., Ning, C., Jian, F., Wang, R., Lv, C., Wang,Q., Arrowood, M.J. and Xiao, L. (2012). *Cryptosporidium tyzzeri* n. sp. (Apicomplexa: Cryptosporidiidae) in domestic mice (*Mus musculus*). Experimental Parasitology 130, 274–281.

Robichon, D., Girard, J., Cenatiempo, Y. and Cavellier, J. (1999). Atomic force microscopy imaging of dried or living bacteria. *Comptes Rendus de l'Académie des Sciences - Series III - Sciences de la Vie*, 322(8), pp.687-693.

Robinson, G., Wright, S., Elwin, K., Hadfield, S.J., Katzer, F., Bartley, P.M., Hunter, P.R., Nath, M., Innes, E.A. and Chalmers, R.M. (2010). Re-description of *Cryptosporidium cuniculus* in man and Takeuchi, 1979 (Apicomplexa: Cryptosporidiidae): morphology, biology and phylogeny. International Journal for Parasitology 40, 1539– 1548.

Rochelle, P., Fallar, D., Marshall, M., Montelone, B., Upton, S. and Woods, K. (2004). Irreversible UV Inactivation of *Cryptosporidium* spp. Despite the Presence of UV Repair Genes1. *The Journal of Eukaryotic Microbiology*, 51(5), pp.553-562.

Rode, S., Stark, R., Lübbe, J., Tröger, L., Schütte, J., Umeda, K., Kobayashi, K., Yamada, H. and Kühnle, A. (2011). Modification of a commercial atomic force microscopy for low-noise, high-resolution frequency-modulation imaging in liquid environment. *Review of Scientific Instruments*, 82(7), p.073703.

Rosales, M., Cordón, G., Moreno, M., Sánchez, C. and Mascaró., C. (2005). Extracellular like-gregarine stages of *Cryptosporidium parvum*. *Acta Tropica*, 95(1), pp.74-78.

Rossi, P., Rivasi, F., Codeluppi, M., Catania, A., Tamburrini, A., Righi, E. and Pozio, E. (1998). Gastric involvement in AIDS associated cryptosporidiosis. *Gut*, 43(4), pp.476-477.

Rossignol, J. (2010). Cryptosporidium and Giardia: Treatment options and prospects for new drugs. *Experimental Parasitology*, 124(1), pp.45-53.

Ryan, U., Fayer, R. and Xiao, L. (2014). Cryptosporidium species in humans and animals: current understanding and research needs. *Parasitology*, 141(13), pp.1667-1685.

Ryan, U.M., Monis, P., Enemark, H.L., Sulaiman, I., Samarasinge, B., Read, C., Buddle, R., Robertson, I., Zhou, L., Thompson, R.C.A. and Xiao, L. (2004). *Cryptosporidium suis* n. sp. (Apicomplexa: Cryptosporidiidae) in pigs (*Sus scrofa*). Journal of Parasitology 90, 769–773.

Ryan, U.M., Power, M. and Xiao, L.(2008). *Cryptosporidium fayeri* .sp. (Apicomplexa: Cryptosporidiidae) from the red kangaroo (*Macropus rufus*). Journal of Eukaryotic Microbiology 55, 22 –26.

Ryan, U.M., Xiao, L., Read, C., Sulaiman, I., Monis, P., Lal, A.A., Fayer, R. and Pavlasek, I. (2003c). A redescription of *Cryptosporidium galli* Pavlasek, 1999 (Apicomplexa: Cryptosporidiidae) from birds. Journal of Parasitology 89, 809–813.

Sahu, K., Bansal, H., Mukherjee, C., Sharma, M. and Gupta, P. (2009). Atomic force microscopic study on morphological alterations induced by photodynamic action of Toluidine Blue O in *Staphylococcus aureus* and *Escherichia coli*. *Journal of Photochemistry and Photobiology B: Biology*, 96(1), pp.9-16.

Scallan, E., Hoekstra, R., Angulo, F., Tauxe, R., Widdowson, M., Roy, S., Jones, J. and Griffin, P. (2011). Foodborne Illness Acquired in the United States—Major Pathogens. *Emerging Infectious Diseases*, 17(1), pp.7-15.

Schroder, D., Benton, J. and Rai-Choudhury, P. (1996). *Diagnostic Techniques for Semiconductor Materials Processing*. 1st ed. Pennington, New Jersey: The Electrochemical Sociely inc., pp.356-358.

Searcy, K., Packman, A., Atwill, E. and Harter, T. (2005). Association of *Cryptosporidium parvum* with Suspended Particles: Impact on Oocyst Sedimentation. *Applied and Environmental Microbiology*, 71(2), pp.1072-1078.

Searcy, K., Packman, A., Atwill, E. and Harter, T. (2006). Capture and Retention of *Cryptosporidium parvum* Oocysts by *Pseudomonas aeruginosa* Biofilms. *Applied and Environmental Microbiology*, 72(9), pp.6242-6247.

Shu, A., Wu, C., Chen, Y., Peng, H., Chang, H. and Yew, T. (2008). Evidence of DNA Transfer through F-pilus Channels during *Escherichia coli* Conjugation. *Langmuir*, 24(13), pp.6796-6802.

Sibley, L. (2004). Intracellular Parasite Invasion Strategies. *Science*, 304(5668), pp.248-253.

Sifuentes, L. and Di Giovanni, G. (2007). Aged HCT-8 Cell Monolayers Support *Cryptosporidium parvum* Infection. *Applied and Environmental Microbiology*, 73(23), pp.7548-7551.

Sischo, W., Atwill, E., Lanyon, L. and George, J. (2000). Cryptosporidia on dairy farms and the role these farms may have in contaminating surface water supplies in the northeastern United States. *Preventive Veterinary Medicine*, 43(4), pp.253-267.

Slavin, D. (1955). *Cryptosporidium meleagridis* (sp. nov.). Journal of Comparative Pathology 65, 262–270.

Smith, H., Cacciò, S., Cook, N., Nichols, R. and Tait, A. (2007). *Cryptosporidium* and *Giardia* as foodborne zoonoses. *Veterinary Parasitology*, 149(1-2), pp.29-40.

Smith HV, Nichols RAB, Grimason AM (2005). *Cryptosporidium* excystation and invasion: getting to the guts of the matter. Trends in Parasitology, 21, 133–42.

Sokolov, I., Firtel, M. and Henderson, G. (1996). In situ high-resolution atomic force microscope imaging of biological surfaces. *Journal of Vacuum Science & Technology A: Vacuum, Surfaces, and Films*, 14(3), pp.674-678.

Sparks, H., Nair, G., Castellanos-Gonzalez, A. and White, A. (2015). Treatment of *Cryptosporidium*: What We Know, Gaps, and the Way Forward. *Current Tropical Medicine Reports*, 2(3), pp.181-187.

Speer, C., Fayer, R. and Dubey, J. (2018). *Cryptosporidiosis of man and animals*. 1st ed. Boca Raton, FL: CRC Press.

Sponseller, J., Griffiths, J. and Tzipori, S. (2014). The Evolution of Respiratory Cryptosporidiosis: Evidence for Transmission by Inhalation. *Clinical Microbiology Reviews*, 27(3), pp.575-586.

Stokes, D. (2008). *Principles and practice of variable pressure/environmental scanning electron microscopy (VP-ESEM)*. 1st ed. [Oxford]: Chichester.

Strausbaugh, L. (2001). Emerging Health Care-Associated Infections in the Geriatric Population. *Emerging Infectious Diseases*, 7(2), pp.268-271.

Sullivan, C., Venkataraman, S., Retterer, S., Allison, D. and Doktycz, M. (2007). Comparison of the indentation and elasticity of *E. coli* and its spheroplasts by AFM. *Ultramicroscopy*, 107(10-11), pp.934-942.

Suo, Z., Avci, R., Yang, X. and Pascual, D. (2008). Efficient Immobilization and Patterning of Live Bacterial Cells. *Langmuir*, 24(8), pp.4161-4167.

Suzuki, E. (2002). High-resolution scanning electron microscopy of immunogold-labelled cells by the use of thin plasma coating of osmium. *Journal of Microscopy*, 208(3), pp.153-157.

Thompson, A., Koh, W. H., and Clode, P. L. (2016). Cryptosporidium — What is it? *Food and Waterborne Parasitology*, 4, pp.54-61.

Thompson, R. and Ash, A. (2016). Molecular epidemiology of *Giardia* and *Cryptosporidium* infections. *Infection, Genetics and Evolution*, 40, pp.315-323.

Thompson, R., Olson, M., Zhu, G., Enomoto, S., Abrahamsen, M. and Hijjawi, N. (2005). *Cryptosporidium* and cryptosporidiosis. *Advances in Parasitology*, 59, pp.77-158.

Tolboom, J. (1996). The Infectivity of *Cryptosporidium parvum* in Healthy Volunteers. *Journal of Pediatric Gastroenterology &amp Nutrition*, 23(2), p.201.

Touhami, A., Jericho, M. and Beveridge, T. (2004). Atomic Force Microscopy of Cell Growth and Division in *Staphylococcus aureus*. *Journal of Bacteriology*, 186(11), pp.3286-3295.

Tufenkji, N., Dixon, D., Considine, R. and Drummond, C. (2006). Multi-scale *Cryptosporidium*/sand interactions in water treatment. *Water Research*, 40(18), pp.3315-3331.

Tumwine JK, Kekitiinwa A, Nabukeera N, Akiyoshi DE, Rich SM, Widmer G, et al. (2003). *Cryptosporidium parvum* in children with diarrhoea in Mulago Hospital, Kampala, Uganda. *Am J Trop Med Hyg*. 68(6):710-5.

Tyzzer, E. (1907). A sporozoan found in the peptic glands of the common mouse. *Experimental Biology and Medicine*, 5(1), pp.12-13.

Tyzzer, E.E. (1910). An extracellular coccidium, *Cryptosporidium muris* (gen. et sp. nov) of the gastric glands of the common mouse. Journal of Medical Research 23, 487–511.

Tzipori, S. (1983). Cryptosporidiosis in Animals and Humans. *Microbiological Reviews*, 47(1), pp.84-96.

Uchihashi, T., Watanabe, H. and Kodera, N. (2018). 'Optimum Substrates for Imaging Biological Molecules with High-Speed Atomic Force Microscopy' in *Nanoscale imaging*. 1st ed. New York: Humana Press, pp.159-179.

Uga, S., Matsuo, J., Kono, E., Kimura, K., Inoue, M., Rai, S. and Ono, K. (2000). Prevalence of *Cryptosporidium parvum* infection and pattern of oocyst shedding in calves in Japan. *Veterinary Parasitology*, 94(1-2), pp.27-32.

Upton, S.J. and Current, W.L. (1985). The species of *Cryptosporidium* (Apicomplexa: Cryptosporidiidae) infecting mammals. Journal of Parasitology 74, 625–629.

Valigurová, A., Hofmannová, L., Koudela, B. and Vávra, J. (2007). An Ultrastructural Comparison of the Attachment Sites Between Gregarina steini and Cryptosporidium muris. *The Journal of Eukaryotic Microbiology*, 54, pp. 495-510.

Valigurová, A., Jirků, M., Koudela, B., Gelnar, M., Modrý, D. and Šlapeta, J. (2008). Cryptosporidia: Epicellular parasites embraced by the host cell membrane. *International Journal for Parasitology*, 38(8-9), pp.913-922.

Valigurová, A., Vaškovicová, N., Musilová, N. and Schrével, J. (2013). The enigma of eugregarine epicytic folds: where gliding motility originates?. *Frontiers in Zoology*, 10(1), p.57.

van der Mei, H., Busscher, H., Bos, R., de Vries, J., Boonaert, C. and Dufrêne, Y. (2000). Direct Probing by Atomic Force Microscopy of the Cell Surface Softness of a Fibrillated and Nonfibrillated Oral Streptococcal Strain. *Biophysical Journal*, 78(5), pp.2668-2674.

Venkataraman, S., Allison, D., Qi, H., Morrell-Falvey, J., Kallewaard, N., Crowe, J. and Doktycz, M. (2006). Automated image analysis of atomic force microscopy images of rotavirus particles. *Ultramicroscopy*, 106(8-9), pp.829-837.

Vetterling, J.M., Jervis, H.R., Merrill, T.G. and Sprinz, H. (1971). *Cryptosporidium wrairi* sp. n. from the guinea pig Cavia porcellus, with an amendation of the genus. Journal of Protozoology 18, 243–247.

Viljoen, G., Nel, L. and Crowther, J. (2005). *Molecular diagnostic PCR handbook*. Dordrecht: Springer.

Waldron, L.S., Cheung-Kwok-Sang, C. and Power, M.L. (2010). Wildlife-associated *Cryptosporidium fayeri* in humans, Australia. Emerging Infectious Disease 16, 2006–2007.

Waldron, L.S., Dimeski, B., Beggs, P.J., Ferrari, B.C. and Power, M.L. (2011). Molecular epidemiology, spatiotemporal analysis, and ecology of sporadic human cryptosporidiosis in Australia. Applied and Environmental Microbiology 77, 7757–7765.

Wang, L., Zhang, H.,Zhao,X.,Zhang,L.,Zhang,G.,Guo,M.,Liu,L., Feng, Y. and Xiao, L. (2013). Zoonotic *Cryptosporidium* species and *Enterocytozoon bieneusi* genotypes in HIV-positive patients on antiretroviral therapy. Journal of Clinical Microbiology 51, 557–63.

Wanyiri, J., Techasintana, P., O'Connor, R., Blackman, M., Kim, K. and Ward, H. (2009). Role of CpSUB1, a Subtilisin-Like Protease, in *Cryptosporidium parvum* Infection In Vitro. *Eukaryotic Cell*, 8(4), pp.470-477.

Widerström, M., Schönning, C., Lilja, M., Lebbad, M., Ljung, T., Allestam, G., Ferm, M., Björkholm, B., Hansen, A., Hiltula, J., Långmark, J., Löfdahl, M., Omberg, M., Reuterwall, C., Samuelsson, E., Widgren, K., Wallensten, A. and Lindh, J. (2014). Large Outbreak of *Cryptosporidium hominis* Infection Transmitted through the Public Water Supply, Sweden. *Emerging Infectious Diseases*, 20(4), pp.581-589.

Widmer, G., Klein, P. and Bonilla, R. (2007). Adaptation of *Cryptosporidium* oocysts to different excystation conditions. *Parasitology*, 134(11).

Wielinga, P., de Vries, A., van der Goot, T., Mank, T., Mars, M., Kortbeek, L. and van der Giessen, J. (2008). Molecular epidemiology of *Cryptosporidium* in humans and cattle in The Netherlands. *International Journal for Parasitology*, 38(7), pp.809-817.

Woodmansee, D. (1987). Studies of In Vitro Excystation of *Cryptosporidium parvum* from Calves. *The Journal of Eukaryotic Microbiology*, 34(4), pp.398-402.

Xiao, L. (2010). Molecular epidemiology of cryptosporidiosis: An update. *Experimental Parasitology*, 124(1), pp.80-89.

Xiao, L. and Feng, Y. (2008). Zoonotic cryptosporidiosis. *FEMS Immunology & Medical Microbiology*, 52(3), pp.309-323.

Xiao, L. and Ryan, U. (2004). Cryptosporidiosis: an update in molecular epidemiology. *Current Opinion in Infectious Diseases*, 17(5), pp.483-490.

Xiao, L., Bern, C., Arrowood, M., Sulaiman, I., Zhou, L., Kawai, V., Vivar, A., Lal, A.A. and Gilman, R.H. (2002a). Identification of the *Cryptosporidium* pig genotype in a human patient. Journal of Infectious Diseases 185, 1846–1848.

Xu, P., Widmer, G., Wang, Y., Ozaki, L., Alves, J., Serrano, M., Puiu, D., Manque, P., Akiyoshi, D., Mackey, A., Pearson, W., Dear, P., Bankier, A., Peterson, D., Abrahamsen, M., Kapur, V., Tzipori, S. and Buck, G. (2004). The genome of *Cryptosporidium hominis*. *Nature*, 431(7012), pp.1107-1112.

Yang, S., Healey, M., Du, C. and Zhang, J. (1996). Complete development of *Cryptosporidium parvum* in bovine fallopian tube epithelial cells. *Infection and Immunity*, 1996(64), pp.349–54.

Zardi, E., Picardi, A. and Afeltra, A. (2005). Treatment of Cryptosporidiosis in Immunocompromised Hosts. *Chemotherapy*, 51(4), pp.193-196.

Zhou, L., Singh, A., Jiang, J. and Xiao, L. (2004). Molecular Surveillance of *Cryptosporidium* spp. in Raw Wastewater in Milwaukee: Implications for Understanding Outbreak Occurrence and Transmission Dynamics. *Journal of Clinical Microbiology*, 42(4), pp.1859-1859.

Zintl, A., Proctor, A., Read, C., Dewaal, T., Shanaghy, N., Fanning, S. and Mulcahy, G. (2009). The prevalence of *Cryptosporidium* species and subtypes in human faecal samples in Ireland. *Epidemiology and Infection*, 137(02), p.270-277.

7.0 Appendix

7.1: Draft manuscript

Developing a novel imaging technique for AFM analysis of non-fixed *Cryptosporidium parvum* oocysts under physiological conditions

Tansy M. R Vallintine[1,2], Wei Feng Xue[2], Anastasios D. Tsaousis[1]

1. Laboratory of Molecular &Evolutionary Parasitology, RAPID group, School of Biosciences, University of Kent, Canterbury, UK
2. Kent Fungal Group, School of Biosciences, University of Kent, Canterbury, UK

Abstract:

Cryptosporidium is a waterborne apicomplexan parasite typically infecting the upper gastrointestinal tract of humans and animals. Infection in immunocompetent hosts can cause acute self-limiting diarrhoeal symptoms, although in infants and immunocompromised, infection can be life threatening. The infective stage of the parasite survives in the environment as a hardy cyst/spore or 'oocyst'. These oocysts have high resistance to disinfectants, enabling them to survive for long periods in various environments whilst remaining infective. The nature and characteristics of these "spores" remain elusive, and further research into oocyst composition is necessary to enable the development of effective water treatment methods and medical prophylaxis, for which options are currently limited. This project describes a novel method for live imaging and peak force quantitative nanomechanical property mapping of *Cryptosporidium* oocysts using atomic force microscopy (AFM). Employing this method, data on the surface topography and deformation

characteristics of *Cryptosporidium parvum* and oocysts has been acquired and analysed to identify physiological characteristics of live oocyst of the species *C. parvum*, both in air and in a near native liquid environment. Scanning electron microscopy (SEM), field emission scanning electron microscopy (FESEM), and fluorescence microscopy were used for comparison between imaging methods, and previous reports. This work will enable investigations into live *Cryptosporidium* oocyst structure, composition, and mechanical properties in unprecedented depth. In turn these capacities can be used to inform and advance our understanding of host specificity and excystation control, which could enable the development of new methods for treatment and eradication of the parasite, all areas of vital importance to progress research towards combating this significant disease.

Keywords: *Cryptosporidium parvum*, oocysts, AFM, SEM, fluorescence microscopy.

Introduction:

Cryptosporidium is a water borne apicomplexan parasite infecting the epithelial lining of the upper gastrointestinal (GI) and respiratory tracts of humans and other vertebrate species. Infection causes the disease cryptosporidiosis, a major international cause of diarrhoeal disease in humans and animals. In the immunocompetent, infection with *Cryptosporidium* causes mild to acute self-limiting diarrhoea and/or respiratory symptoms, however in infants and the immunocompromised, infection can be fatal. Cryptosporidiosis is primarily spread via the faecal-oral route, and can survive in the environment for prolonged periods as hardy cyst or 'oocysts'. Due to the mode of transition, the highest infection rates occur in developing countries where water sanitation systems can be inefficient. Cryptosporidiosis is a persistent and ubiquitous disease, with over 1000 accounts in humans occurring in 95 countries and on all continents except for Antarctica (Feyer et al., 1997; Ryan, Fayer and Xiao, 2014). Cryptosporidiosis is understood to be responsible for up to 20 % of reports of childhood diarrhoea in less economically developed countries (Mosier

and Oberst, 2000), with the proportion of affected individuals in a population ranging from 20-90% (subject to region) (Dillingham, Lima and Guerrant, 2002). It is responsible for 50.8 % of all parasite induced waterborne infections (Putignani and Menichella, 2010), and 8 – 19 % of diarrhoeal complaints in developing countries (Gatei et al., 2006). The pervasiveness of the *Cryptosporidium* parasite is the outcome of three factors; the substantial number of oocysts produced and excreted by the host, the environmentally hardy nature of the oocyst allowing long term survival of the parasite in the environment (several months in damp and temperate conditions), and the low dose of oocysts required for infection (Tolboom, 1996; Reinoso, Becares and Smith, 2008). The number of *C. parvum* oocysts required for infection in an otherwise healthy human host remains under debate, with research suggesting a median infective dose of between 132 oocysts (Chappell et al. 1996) to 82 oocysts (Okhuysen et al. 1999) with reports of infections occurring from doses of as low as 10 oocysts for both *C. parvum* and *C. hominis* (Okhuysen et al. 1999; Chappell et al. 2006). Of the 26-known species of *Cryptosporidium*, 20 species and genotypes have been reported to cause human infection, however the species accountable for the majority of outbreaks is *C. hominis*, closely followed by *C. parvum* (Xiao, 2010; Ryan, Fayer and Xiao, 2014).

The continued difficulty in tempering the widespread effects of cryptosporidiosis is partially rooted in the hardiness of *Cryptosporidium* oocysts, and the lack of effective medical treatments available. *Cryptosporidium* oocysts are impervious to many water purification treatments, including chlorination at concentrations suitable for reliable sterilisation of drinking water, and to surface disinfectants including ethanol and bleach (Campbell et al., 1982; Korich et al., 1990; Rochelle et al., 2004) There is currently no effective vaccine against cryptosporidiosis, and the only effective treatment is the broad spectrum antiparasitic drug nitazoxanide, which can only be used to treat otherwise healthy individuals (Ali et al., 2014; Sparks et al., 2015).

Due to the widespread significant effects of cryptosporidiosis combined with a lack of effective medications, there is a critical need to develop new techniques to advance research into these parasites and aid the development of new and effective prophylaxis and treatments.

Atomic force microscopy (AFM) is a powerful multifunctional imaging platform, which utilises a high-resolution scanning probe microscopy (SPM) technique to image and manipulate a range of biological samples, from arrays of living cells to single molecules (Dufrene et al., 2017). A three-dimensional topographical map is obtained through mechanical interaction between a probe and the sample surface. For liquid imaging of live cells, the method of immobilisation must be chosen with care to avoid compromising cell physiology whilst ensuring attachment is robust enough to withstand drag or detachment upon sample-probe contact. Commonly utilised techniques chemical immobilisation and physical entrapment (Razatos et al., 1998; Robichon et al., 1999; Doktycz et al., 2003; Beckmann et al., 2006; Bolshakova et al., 2001; Dorobantu et al., 2008; Cerf et al., 2009). A significant advantage of AFM imaging is that use of a fluid cell can enable imaging in fluid, with control over temperature, buffer composition and flow, allowing imaging of biological samples and live cells in a close to native environment (Drake, 1989; Radmacher et al., 1992). Using PeakForce QNM mode, it is also possible to map nano-mechanical measurements, including sample deformation, elasticity and dissipation (Hoh et al., 1992; Lee, Chrisey and Colton, 1994; Boland and Ratner, 1995; Hinterdorfer et al., 1996; Muller, Baumeister and Engel, 1999; Allison, Hinterdorfer and Han, 2002; Benoit et al., 2000; Doktycz et al., 2003). The ability of AFM to image, probe surfaces, and manipulate samples makes this one of the most versatile imaging techniques currently available. As research progressively moves into the fields of genomics and proteomics, there will be an increasing requirement for techniques capable of elucidating how and where gene products interact to establish regulatory and metabolic pathways. High powered and versatile imaging techniques capable of describing and/or localising molecular interactions within the live oocyst under a close to natural environment will enable functional delegation of gene products. The extremely streamlined genome of *C. parvum* (Abrahamsen et al., 2004), in combination with their clinical importance, renders this parasite a prime candidate for functional analysis by imaging. The techniques necessary for appropriate live imaging remain to be developed

Research aims:

Given the critical need for new techniques for use in research into *Cryptosporidium* species, we aimed to develop an AFM analysis technique capable of investigating the surface characteristics of infectious non-fixed *Cryptosporidium parvum* oocysts in a close to physiological environment.

For successful AFM analysis under fluid, sample ability to withstand probe contact requires a sufficient method of sample immobilisation to the substrate surface to prevent sample detachment and/or drift. To develop such a method, multiple oocyst immobilisation techniques were assessed, including differing substrate, immobilisation method and suspension buffer. For AFM analysis, oocyst samples were imaged using the Bruker Multimode 8 SPM in peak-force tapping ScanAssyst QNM in air and in liquid modes and analysed using NanoScope Analysis v1.40r1.

Methods:

Sample preparation:

C. parvum oocyst source and filter purification:

C. parvum oocyst stock (IOWA isolate) was obtained from Bunch Grass Farm, Deary, Idaho and stored at 4 °C. To ensure maximum sample purity, oocyst stock suspension was filter sterilised prior to slide deposition. 500 ul/slide of 2 x 10^7 oocysts/ml stock solution (approximately 1 x 10^7 oocysts/slide) stock was filtered using a syringe filter with 0.45 µm pore size (Sartorius Minisart® syringe filter) and rinsed through with 50 ml HPLC water. For oocyst retrieval from the filter membrane, fluid flow was reversed for a volume of 15 ml and deposited into a fresh 15 ml falcon tube. The filtered oocysts were pelleted by centrifugation at 200 x g for 18 minutes, the supernatant removed, and the pellet re-suspended in 50 µl/slide HPLC water.

Glass slide preparation and oocyst filter sterilisation:

15 mm spherical glass coverslips (Agar Scientific) were pre-washed with 70 % EtOH and detergent to remove contaminants and fatty deposits and rinsed in HPLC water. Cover slips were then attached to metal AFM specimen discs using double sided adhesive, and 50 µl 0.01 % (imaging in air) or 0.05 % (imaging in liquid) poly-l-lysine solution (Sigma Aldrich) was applied to the centre of each coverslip. Slides were then placed in a warming oven at 60 °C for approximately 30 minutes until dry.

50 µl filter sterilised sample solution was deposited to the dried poly-l-lysine coated surface of each previously prepared slide and allowed to sediment in a humid environment at room temperature (r.t.) overnight. At no point were the samples allowed to dry. Following overnight sedimentation, slides were rinsed of excess oocysts using 2 ml HPLC water/slide and covered with a fluid droplet to ensure oocysts remained fully hydrated. For AFM imaging in air to ensure minimal sample dehydration whilst achieving sufficient dryness to allow imaging, samples were drained of the hydration droplet directly prior to imaging, air dried and subjected to a gentle nitrogen stream for four seconds.

Atomic force microscopy imaging:

AFM analysis was performed using the Bruker Multimode 8 SPM, and the resulting data was analysed using NanoScope Analysis v1.40r1. Images in air were attained using Bruker ScanAsyst-AIR probes, while ScanAsyst-FLUID or ScanAsyst-FLUID+ probes were used for imaging in liquid.

Oocysts were imaged using ScanAsyst® in air and liquid modes. Peak force quantitative nanomechanical mapping (PeakForce QNM®) mode in air and in liquid was used for mechanical property measurement. For optimal measurements using PeakForce QNM® mode, probe spring constant was calibrated prior to each session and on introduction of each new probe. For scanning

large areas in air to locate oocysts, parameters were set at a view window of 100 µm, with relatively high scan-rate of between 0.558 - 0.988 Hz, a low number of samples per line and lines per view (between 256 and 512), and a peak force setpoint of between 10 - 20 nN. For scanning of large areas in liquid, scan rate and peak force setpoint were decreased to between 0.1 and 0.2 Hz, and 1 and 5 nN respectively. For high-resolution imaging of smaller areas and individual oocysts, the number of samples per line and scan lines/view were increased to between 512 and 1024, and scan rate was decreased to 0.1 Hz.

In instances where deposition or drag were apparent during liquid imaging, scan rate and peak force setpoint can be decreased to between 1 - 5 nN. Whilst decreasing the peak force setpoint can result in softer, less defined images, it can enable imaging of less firmly immobilised samples that could otherwise become displaced upon tip-sample contact, and results in decrease noise. Difficulties arising during imaging in air, such as probe 'sticking' due to residual surface moisture, can be addressed by decreasing scan rate to the minimum (0.100 Hz) and/or additional nitrogen drying for a further 2 - 3 seconds, although oocysts hydration may be compromised.

Atomic force microscopy data analysis:

AFM images were analysed using NanoScope Analysis V. 1.5 particle analysis, slice and bearing analysis functions. Prior to analysis images were first order flattened and plane fit applied where applicable. For statistical analysis of oocyst measurements between imaging conditions mean values, sample variance, sample standard deviation and standard error were calculated for height, volume, area and diameter measurements. The significance of the difference between the measurement means for each condition was calculated using a 2-sample t-test assuming unequal variance.

Results:

In AFM imaging of *C. parvum* oocysts, both imaging conditions (imaging in air or liquid) and age of oocyst resulted in varying oocyst appearance and attachment characteristics. Initial AFM images of *C. parvum* oocysts under liquid were of oocysts shed three to five months prior to analysis. These images were compared to those of fresher oocyst stock, which was imaged within one month of shedding. In all cases, oocysts images under liquid maintained a hydrated appearance, with no collapse of the oocyst wall (Fig. 1). Older oocysts displayed increased attachment strength, decreased numbers, and more disperse attachment than exhibited by freshly produced oocysts, which exhibited comparatively closer packing with a lower overall attachment stability despite an increased substrate and oocyst-oocyst contact area (Fig. 2).

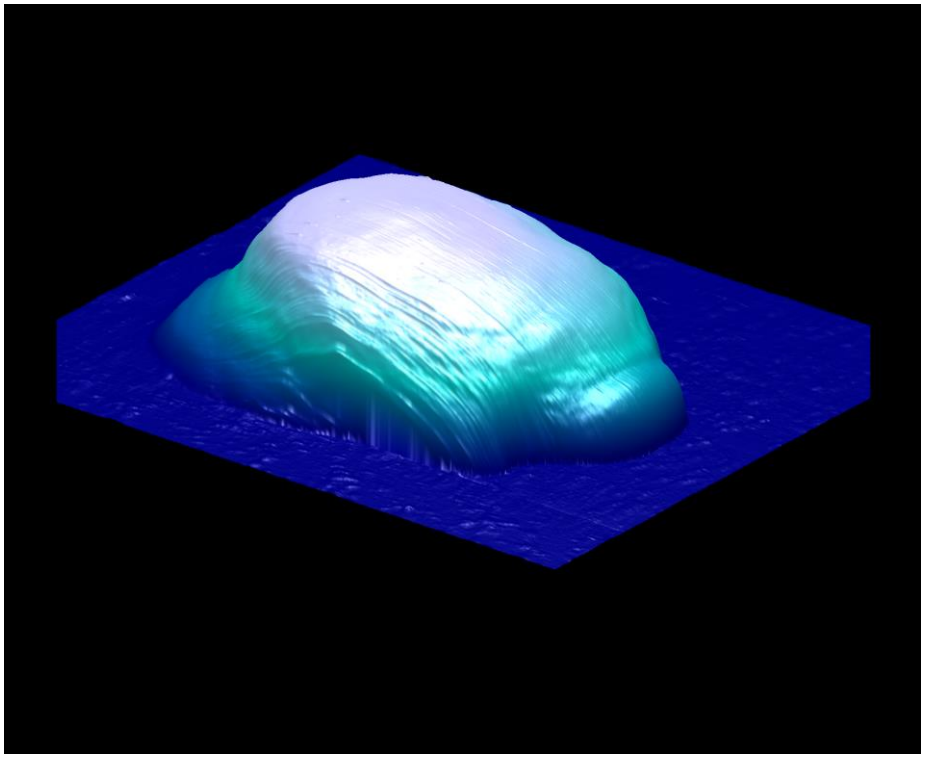

Fig. 1: Liquid AFM

Three-dimensional AFM image of a single oocyst imaged under fluid. Scan size: 6 µm.

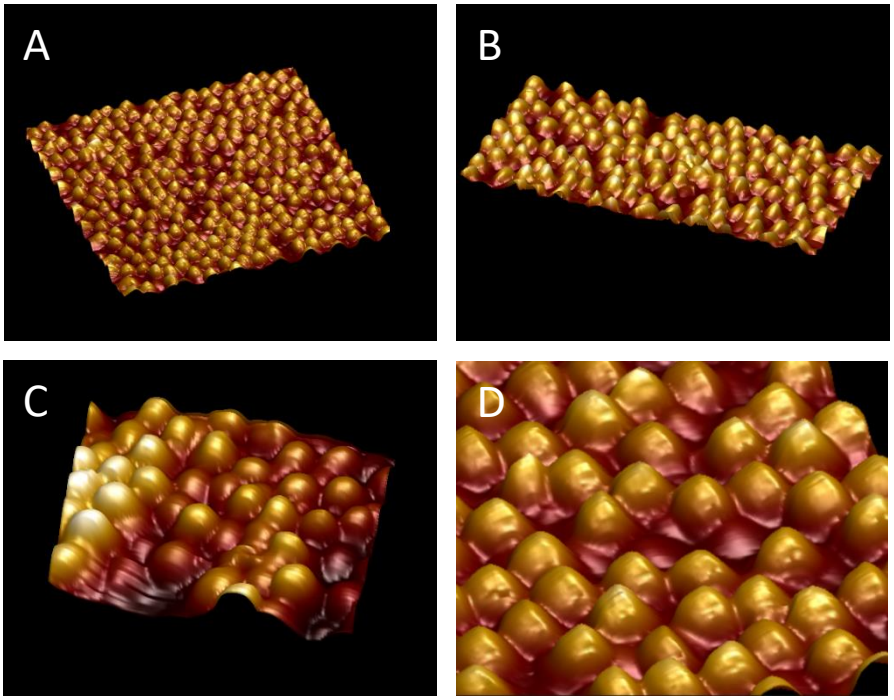

Figure 2: AFM images of C. parvum oocysts under liquid.
Oocysts imaged within 1 month of shedding exhibit confluent attachment with oocysts appearing roughly spherical at scan diameter 100 µm (A and B). Decreasing scan size to focus on individual oocysts (C – scan diameter 48.4 µm) results in the appearance of scan lines, whereas using the zoom function results in greater magnification with fewer scan artifacts (D – 6 µm).

Images under liquid show freshly produced oocysts (imaged within one month of shedding) to be roughly spherical with smooth surfaces lacking any ultrastructural features. In comparison, oocysts imaged three to five months post shedding displayed increasingly irregular, lumpy form (Fig. 3).

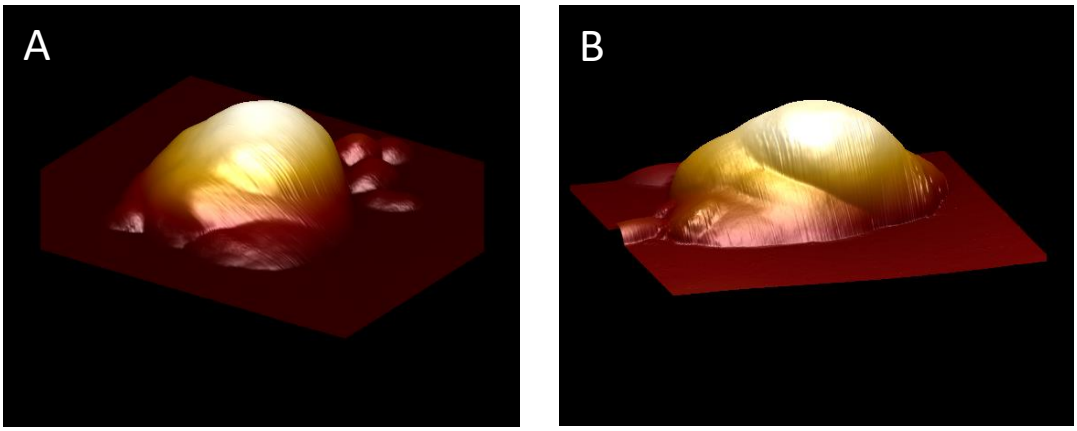

Fig 3: AFM images of oocysts imaged under liquid 4 months post shedding.

Three-dimensional topographical display reveals that oocysts stored for between three to five months prior to imaging develop an irregular 'bumpy' appearance. Scan size: 12.6 µm (A), 10 µm (B).

Both fresh and older oocysts imaged in air displayed higher attachment stability and numbers than seen in either liquid condition, with oocyst exhibiting cluster attachment patterning (Fig. 4). When imaged in air, oocyst appeared flattened, with some variation in collapse patterning. Individual oocysts displayed a tendency to fall flat, with the topographical profile of the oocyst contents visible (convex appearance in section) and folding and irregularity of the surface (Fig.5), while oocysts situated within clusters always displayed raised edges with a deflated central region (concave appearance in section), giving the appearance of a honeycomb like structure (Fig. 4).

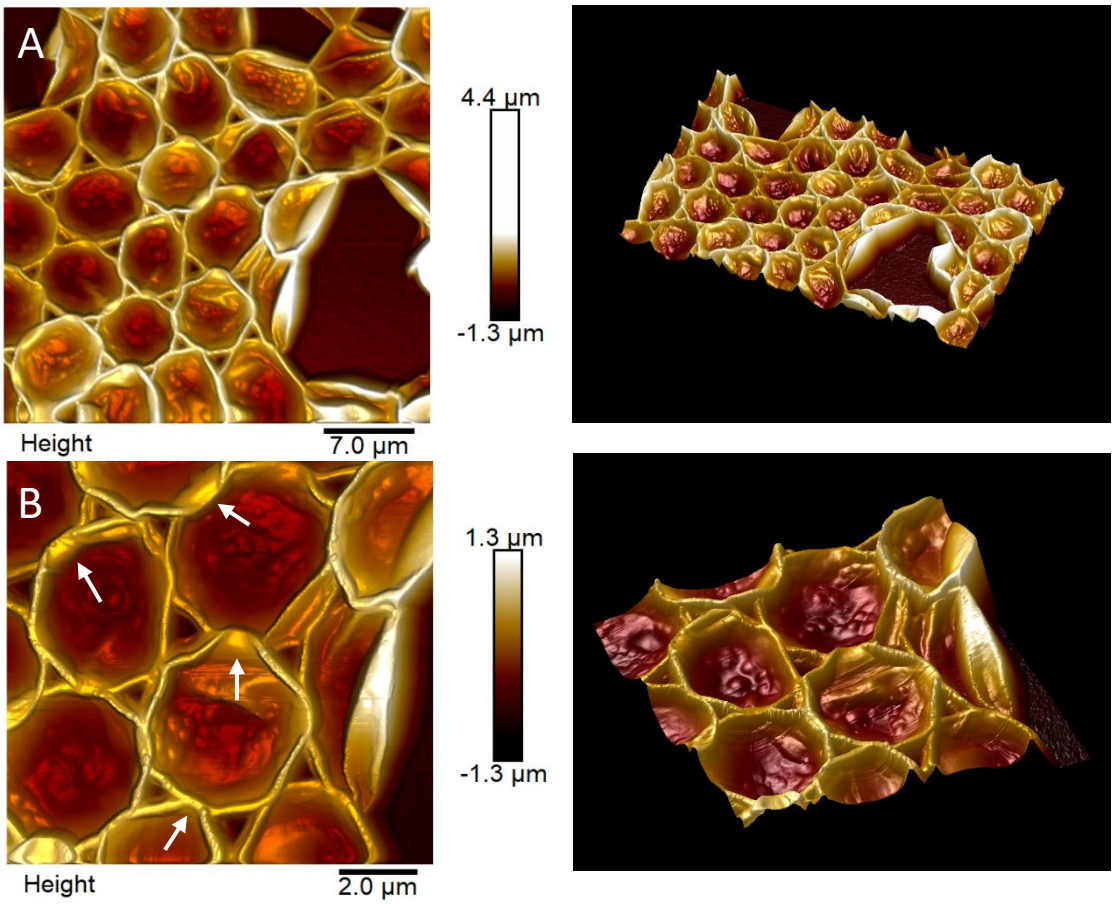

Fig. 4: AFM imaging of oocysts in air.

When imaging in air, confluent attachment resulted in concave dehydration patterning. Decreasing scan size from 33.2 µm (A) to 11 µm (B) revealed areas of adhesion at points of contact between oocyst walls (white arrows).

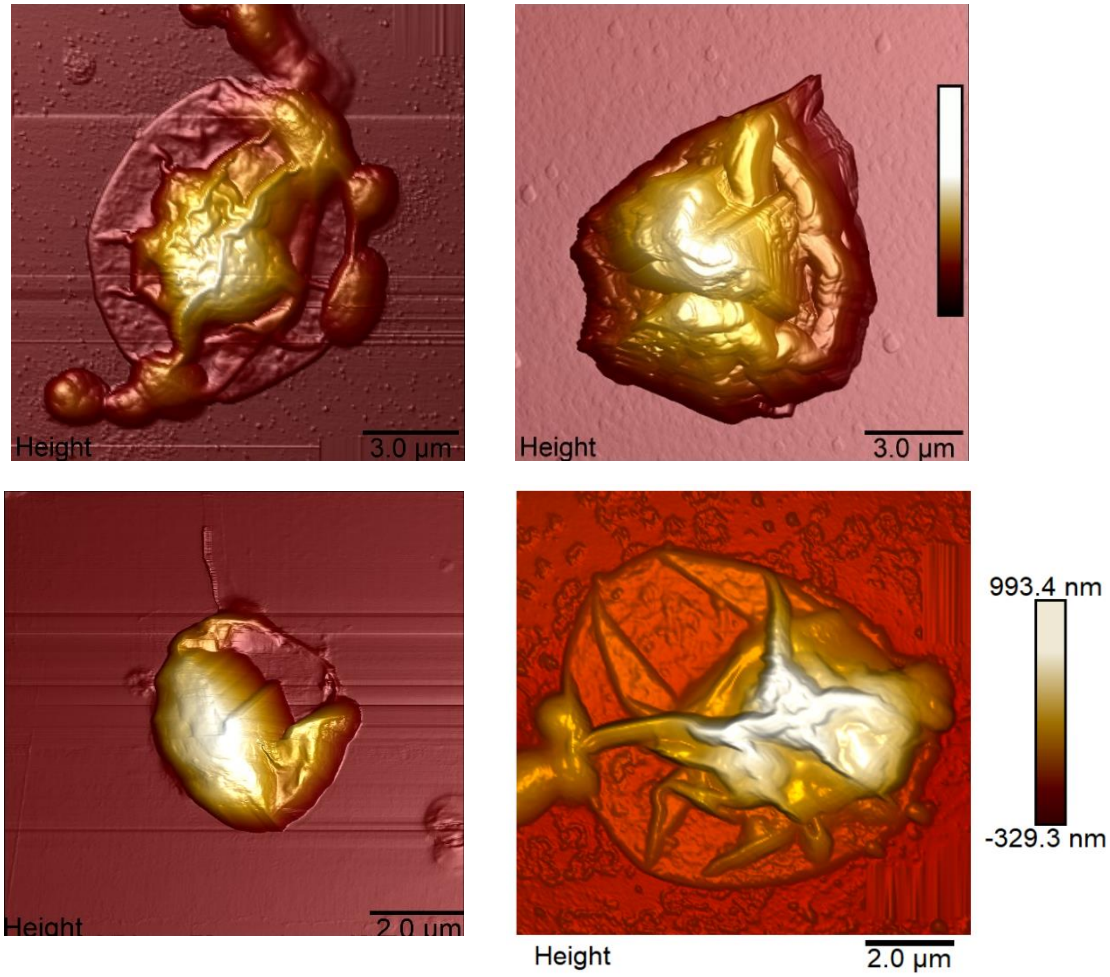

Fig. 5: High resolution AFM images of oocysts imaged in air

Single oocysts exhibiting stages of 'convex' dehydration form.

In all cases, imaging in air provided enhanced resolution of oocyst surfaces over oocysts imaged in liquid, enabling imaging of features such as the opened suture structure of an excysting oocyst (Fig. 6). In some instances, imaging in air revealed angular repetitive patterning resembling scoring of the oocyst surface, with parallel features running angles distinctive from the scanning angle. Further analysis found that the nature and direction of the patterning remained unchanged upon alteration of the scan angle, suggesting that these features are not scan line artifacts (fig. 6 and 7).

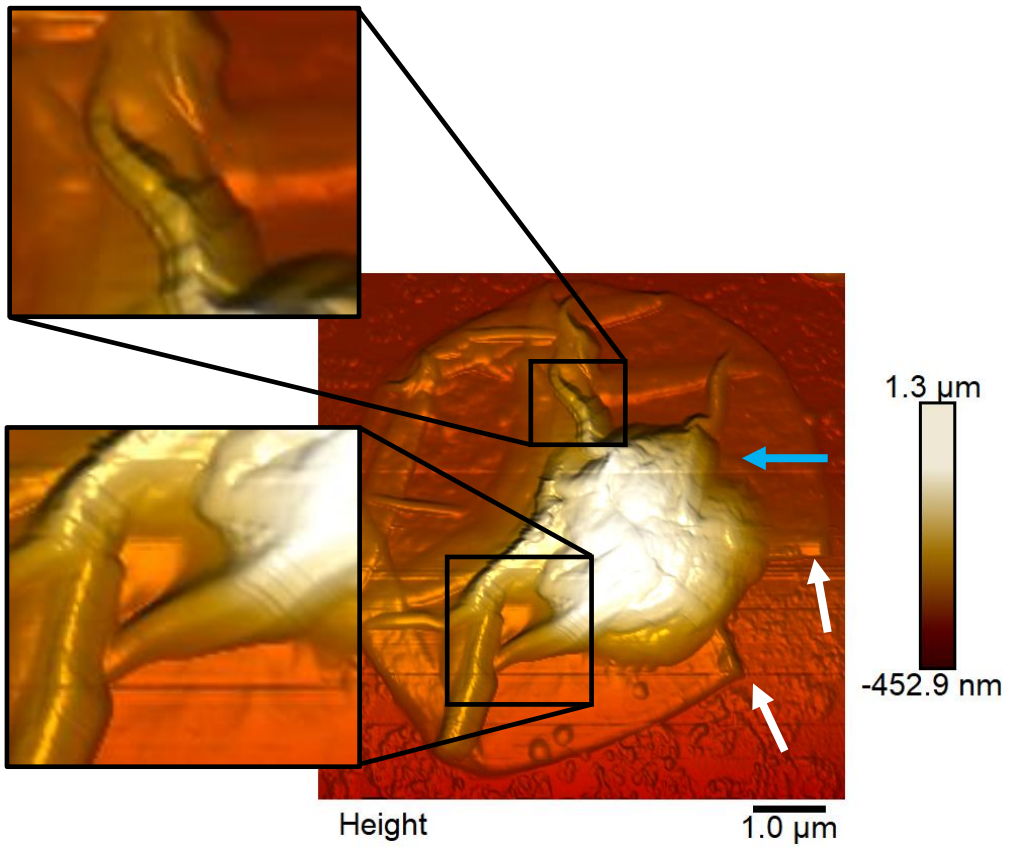

Fig. 6: AFM in air, identification of fine features.
A C. parvum oocyst imaged in air, showing an open suture structure (edges indicated with white arrows). Parallel repetitive angular features are visible (within black boxes). Scan line direction is indicated (blue arrow).

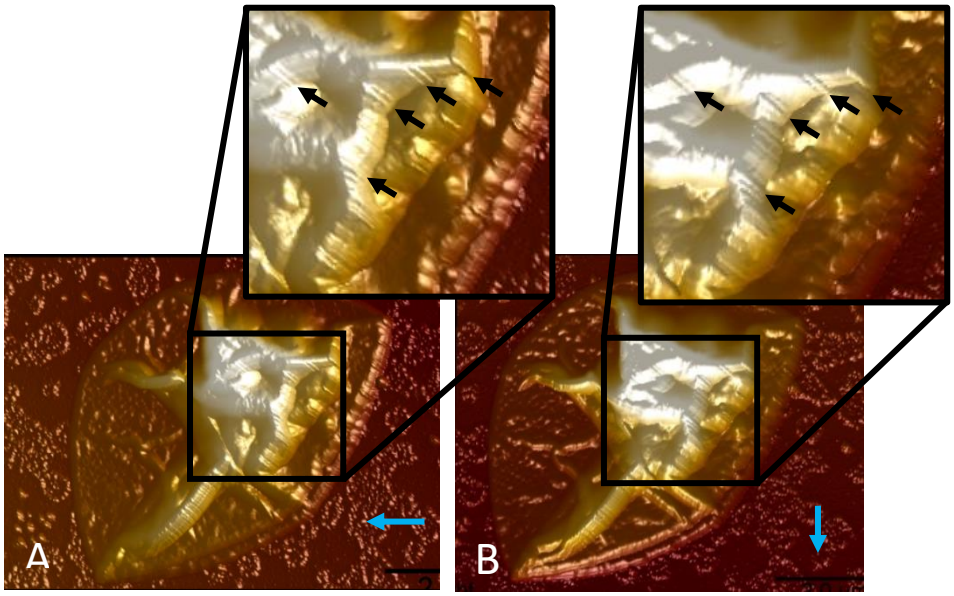

Fig. 7: Single oocysts imaged at different scan angles.
Parallel angular features remain unchanged when scan angle is altered from 0° (A), to 90° (B). Blue arrows indicate scan direction, black arrows indicate the location of prominent features. Scan size 8

Using the NanoScope Analysis 'slice' function, the mean height of oocysts imaged in liquid was founds to be 2.07 µm, where the mean height (measured at the highest point) of oocysts imaged in air was 1.51 µm. The 'particle analysis' function was used to determine both the area and diameter of individual oocysts. Oocysts imaged in liquid had a mean area and diameter of 24.82 μm^2 and 5.5 µm respectively, where oocysts images in air had a mean area of 22.8 μm^2 and a 5.17 µm mean diameter. The 'bearing analysis' function was used to determine oocyst volume, oocysts in liquid had a mean volume of 33.57 μm^3, where those imaged in air had a mean volume of 17.91 μm^3. Table 1 displays the complete set of statistical values calculated from oocyst measurements.

	Height		**Area**		**Volume**	
	Air	Fluid	Air	Fluid	Air	Fluid
Mean	1.509	2.064	22.788	24.815	17.907	33.565
Variance	0.397	0.457	111.707	116.838	2223.858	455.852
St. dev.	0.63	0.676	10.569	10.809	14.962	21.351
St. err.	0.168	0.195	2.93	3.12	3.999	6.163
n	14	12	13	12	14	12
t-value	0.042		0.641		0.046	

Table 1: The mean, variance, standard deviation, standard error t-value and n (sample number) for the height, area and volume of C. parvum oocysts imaged under AFM in both air and fluid.

To determine if there was a significant difference between the means of each measurement (height, area or volume) between each condition (images in air or in fluid) a two-sample t-test assuming unequal variance was performed for each measurement, where $p>0.05$ = not significant (ns), $p \leq 0.05$ = significant (*). Bar graphs displaying mean measurement under each condition with standard error and t-test significance results are displayed in figure 8.

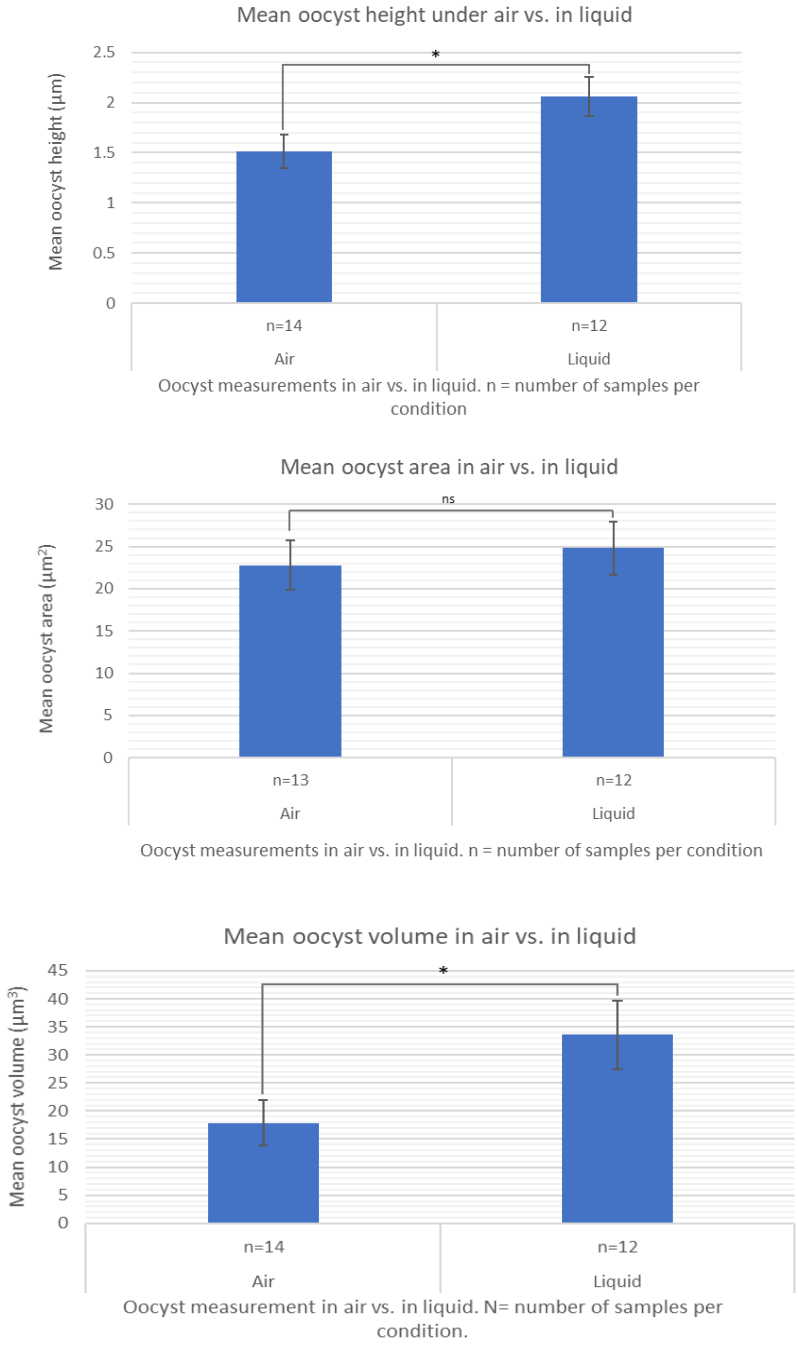

Fig 8: Bar graphs displaying the mean values for each measurement under the two imaging conditions.

Bars represent the mean values for each measurement. Asterisks and 'ns' annotation denote t-test significance results, where ns = not significant, * = significant. Error bars represent calculated standard error.

Statistical analysis revealed a significant difference between the mean values of volume and height of oocysts imaged in air and in fluid, with both height and volume of oocysts imaged in liquid being significantly greater than those imaged in air. There was no significant difference in oocyst area between the two conditions.

Discussion:

Until now, high resolution imaging of *C. parvum* has been limited to imaging of fixed (for AFM) and fixed and sputter coated (for FESEM) samples. Any information gathered by such studies has the potential to be flawed, as fixing involves killing samples and alteration of their protein structure and mechanical properties, for example by cross-linking between proteins (using formalin) or precipitation/denaturing (using methanol). FESEM analysis requires that biological samples are moved further from their natural state, as previously fixed samples must be critical point dried (which involved exposure to high pressure and temperature) (Chandler and Roberson, 2009), and coating of features in an ultrathin layer of conductive material (e.g. gold/palladium alloy) (Suzuki, 2002). The described AFM technique will allow researchers to reliably attain biologically accurate high-resolution imaging and nano-mechanical data of *C. parvum* oocysts for the first time.

Sample immobilisation:

Substrate optimisations revealed that glass surfaces were found to provide superior attachment numbers and strength to mica surfaces. Further, buffer optimisations revealed that application of phosphate buffered saline to sample slides using poly-l-lysine for sample immobilisation results in progressive oocyst detachment over time. Continued poly-l-lysine optimisations revealed that with increasing concentration of poly-l-lysine, the number of oocysts attaching to the substrate decreased, however the strength of the attachment formed increases. For oocysts shed within one

to two months of imaging, a glass substrate with poly-l-lysine concentration of between 0.07 and 0.08 % provided sufficient attachment strength for AFM imaging in liquid whilst maximising oocyst attachment numbers. For oocysts imaged between three and five months post shedding, a glass substrate with 0.05 % poly-l-lysine provided similar results.

Establishing a reliable sample-substrate attachment technique is an essential first step in any scanning-probe based imaging technique. For accurate measurement of many biological samples (including oocysts) it is desirable to avoid drying and to maintain biologically relevant conditions, necessitating sufficient immobilisation strength to withstand probe interaction forces under fluid.

Appearance:

AFM analysis in fluid revealed that *C. parvum* oocysts are roughly spherical and smooth in appearance, with irregularity and 'lumpiness' increasing as oocysts age. Imaging in air, however revealed varying sedimentation patterns between oocysts imaged in air and in liquid, in addition to different collapse patterning in air dependent upon oocyst-oocyst proximity with evidence of oocyst wall interaction at contact points. Imaging in air also revealed unusual surface topography in collapsed oocysts and provided increased resolution in comparison to liquid imaging. Data analysis revealed significant differences between the mean values of height and volume of oocysts between the two imaging conditions (imaged in air vs. in fluid).

For imaging in air, sample collapse was a result of dehydration as previously observed in FESEM. This partial dehydration was unavoidable, as imaging of humid samples resulted in 'sticking', a phenomenon caused by probe tip adhesion to minuscule water droplets on the substrate and sample surfaces (Schroder, Benton and Rai-Choudhury, 1996). The variation in dehydration profile observed between lone and confluent oocysts may be a result of the oocyst-oocyst wall interaction indicated in figure 4 resulting in adherence between adjacent oocyst walls. The uneven 'lumpy' appearance of oocysts imaged in air between three to five months post-shedding could be a result

of decreased oocyst wall integrity with corresponding changes in rigidity. The relatively smooth appearance of these oocysts compared to the collapsed flattened appearance with heightened resolution of those imaged in air is congruent with results of other investigations imaging other cell types, including bacterial cells (Doktycz et al., 2003). It is possible that the decreased image resolution of images obtained under fluid could be a result of increased frequency noise in fluid imaging (Rode et al., 2011), or due to interaction between the tip and oocyst surface structures (Amro et al., 2000; Bolshakova et al., 2001; Doktycz et al., 2003). Use of contact over non-contact mode can increase resolution, however in soft biological samples as in this study this method is not recommended as tip contact can alter the sample (Keyvani et al., 2017).

The difference in poly-l-lysine concentration required for immobilisation of oocysts imaged within one month of shedding compared to those imaged after four to five months could be due to a decrease in oocyst wall rigidity (increased elasticity) with age leading to a decrease in force translated through the oocyst body, causing less stress to be applied to the poly-l-lysine-oocyst steric interaction upon probe contact. It is also possible that a decrease in surface proteins extending into solution over time could result in increased oocyst-poly-l-lysine contact. Data analysis revealed that there was no significant difference in oocyst area between the two imaging conditions, discluding increased surface area as a possible cause. Comparison of nano-mechanical measurements between oocysts of different ages could be used to investigate this theory further, although due to the decreased peak force required to image oocysts shed within one month of imaging resulting in inadequate nanomechanical feedback, a stronger immobilisation method may be required.

DATA analysis:

Data analysis of oocyst measurements acquired through AFM imaging revealed that oocysts imaged in fluid have significantly greater height and volume than those imaged in air. Volume measurements exhibited the greatest mean difference, as oocysts volume decreases as internal

fluid evaporates during desiccation. This effect is likely also responsible for the decrease in height observed. No significant difference was detected in the surface area covered by individual oocysts imaged in air and in fluid, as oocysts flatten upon dehydration whilst the oocyst wall surface area remains unchanged.

The accuracy of the estimated mean values for each measurement could be improved by increasing the number of samples (n) analysed. In this study relatively few samples (12-14 oocysts per condition) were analysed due to time constraints, scaling up to ≈50 high resolution oocyst images would provide more accurate estimated mean values.

Oocyst features:

As imaging at different scan angles did not alter the appearance of the repetitive groove-like features, these are not likely to be tip effects, and may be previously undocumented features only visible under certain conditions, and dependent upon partial oocyst dehydration. These features could be a collapse patterning caused by arrangement of structural components in the oocyst wall, such as the ordered linear protein matrix described by Harris and Petry (1999).

The small features observed on the surface of oocysts imaged after five months in storage were likely debris from excysted oocysts contents degrading in solution.

Future research:

An essential next step in this research will be to confirm that the developed AFM technique enables imaging of live infectious oocysts through cell culture infection using oocysts which have been imaged using the described technique, followed by detection of de-novo produced oocysts using fluorescence microscopy.

This study could be expanded to analyse and compare physiology of oocysts of different *Cryptosporidium* species. Further, as previously discussed relating to phylogenetic classification of *Cryptosporidium*, the enhanced capacities of this method could be used to review and compare the morphology of *Cryptosporidium* oocysts to cysts of other parasitic genera such as *Giardia*. In this instance modification of immobilisation method may be required due to differing cyst surface chemistry. Similarly, this technique may be used to compare topographical and nano-mechanical measurements between oocysts shed from animal infections and thick and thin-walled oocysts produced through cell line infection.

Future research could utilise the described method of AFM imaging in air for three-dimensional and nano-mechanical analysis of non-fixed oocyst walls at a sub nm scale. This method has the potential to identify structures located to the oocyst wall and in combination with proteomic analysis shed light on oocyst host recognition and excystation initiation.

Conclusion:

In summary, a new technique has been developed for reliable AFM imaging and analysis of non-fixed *C. parvum* oocysts in fluid and in air where previously analysis of *Cryptosporidium spp*. oocysts using high-powered microscopy techniques have required a minimum of sample fixing prior to imaging. This will allow researchers to attain dependably biologically accurate imaging and mechanical data on *C. parvum* oocysts for the first time. With modification, this technique can be expanded to provide similar information on other cryptosporidium species, and cysts of other parasitic Genera. Research into the oocysts of these parasites is of vital importance, as this is the environmentally hardy, highly infectious stage which has allowed cryptosporidiosis to become a disease of such global significance. Due to the versatile nature of AFM analysis, the described method will enable imaging, measurement of nano-mechanical forces, and sample chemical and physiological manipulation of the oocyst surface down to individual proteins located to the oocyst

wall. These capabilities will open new avenues for research into oocyst proteomics in non-fixed samples. The information offered by such studies has the potential for use in the development of new treatments for eradication or de-activation of oocysts within the water supply, and the technique will add to the tools available for this vital research into the biology of the *Cryptosporidium* parasite.

Acknowledgements

I would like to thank the members of the Tsaousis lab for their assistance throughout this project, and Dr Anastasious Tsaousis and Dr Wei-Feng Xue for their supervision of this work and guidance in writing this paper. I would particularly like to thank Dr Ben Blakeman for providing training in the operation of the AFM in air.

Bibliography:

Abrahamsen, M. (2004). Complete Genome Sequence of the Apicomplexan, *Cryptosporidium parvum*. *Science*, 304(5669), pp.441-445.

Ali, S., Mumar, S., Kalam, K., Raja, K. and Baqi, S. (2014). Prevalence, clinical presentation and treatment outcome of cryptosporidiosis in immunocompetent adult patients presenting with acute diarrhoea. *Journal of Pakistan Medical Association*, 64(6), pp.613–8.

Allison, D., Hinterdorfer, P. and Han, W. (2002). Biomolecular force measurements and the atomic force microscope. *Current Opinion in Biotechnology*, 13(1), pp.47-51.

Amro, N., Kotra, L., Wadu-Mesthrige, K., Bulychev, A., Mobashery, S. and Liu, G. (2000). High-Resolution Atomic Force Microscopy Studies of the Escherichia coli Outer Membrane: Structural Basis for Permeability. *Langmuir*, 16(6), pp.2789-2796.

Beckmann, M., Venkataraman, S., Doktycz, M., Nataro, J., Sullivan, C., Morrell-Falvey, J. and Allison, D. (2006). Measuring cell surface elasticity on enteroaggregative Escherichia coli wild type and dispersin mutant by AFM. *Ultramicroscopy*, 106(8-9), pp.695-702.

Benoit, M., Gabriel, D., Gerisch, G. and Gaub, H. (2000). Discrete interactions in cell adhesion measured by single-molecule force spectroscopy. *Nature Cell Biology*, 2(6), pp.313-317.

Boland, T. and Ratner, B. (1995). Direct measurement of hydrogen bonding in DNA nucleotide bases by atomic force microscopy. *Proceedings of the National Academy of Sciences*, 92(12), pp.5297-5301.

Bolshakova, A., Kiselyova, O., Filonov, A., Frolova, O., Lyubchenko, Y. and Yaminsky, I. (2001). Comparative studies of bacteria with an atomic force microscopy operating in different modes. *Ultramicroscopy*, 86(1-2), pp.121-128.

Campbell, I., Tzipori, A., Hutchison, G. and Angus, K. (1982). Effect of disinfectants on survival of cryptosporidium oocysts. *Veterinary Record*, 111(18), pp.414-415.

Cappella, B. and Dietler, G. (1999). Force-distance curves by atomic force microscopy. *Surface Science Reports*, 34(1-3), pp.1-104.

Cerf, A., Cau, J., Vieu, C. and Dague, E. (2009). Nanomechanical Properties of Dead or Alive Single-Patterned Bacteria. *Langmuir*, 25(10), pp.5731-5736.

Chandler, D. and Roberson, R. (2009). *Bioimaging*. Sudbury (Mass.): Jones and Bartlett.

Chappell, C.L. et al. (1996). Cryptosporidium parvum: intensity of infection and oocyst excretion patterns in healthy volunteers. The Journal of infectious diseases [Online] 173:232–6. Available at: http://www.ncbi.nlm.nih.gov/pubmed/8537664.

Chappell, C.L., Okhuysen, P.C., Langer-Curry, R., Widmer, G., Akiyoshi, D.E., Tanriverdi, S. and Tzipori, S. (2006). Cryptosporidium hominis: experimental challenge of healthy adults. *American Journal of Tropical Medicine and Hygiene*, 75 (5), 851–857.

Considine, R., Dixon, D. and Drummond, C. (2002). Oocysts of Cryptosporidium parvum and model sand surfaces in aqueous solutions: an atomic force microscope (AFM) study. *Water Research*, 36(14), pp.3421-3428.

Dillingham, R., Lima, A. and Guerrant, R. (2002). Cryptosporidiosis: epidemiology and impact. *Microbes and Infection*, 4(10), pp.1059-1066.

Doktycz, M., Sullivan, C., Hoyt, P., Pelletier, D., Wu, S. and Allison, D. (2003). AFM imaging of bacteria in liquid media immobilized on gelatin coated mica surfaces. *Ultramicroscopy*, 97(1-4), pp.209-216.

Dorobantu, L., Bhattacharjee, S., Foght, J. and Gray, M. (2008). Atomic Force Microscopy Measurement of Heterogeneity in Bacterial Surface Hydrophobicity. *Langmuir*, 24(9), pp.4944-4951.

Drake, B. (1989). Imaging crystals, polymers, and processes in water with the atomic force microscope. *Deep Sea Research Part B. Oceanographic Literature Review*, 36(9), pp.818-825.

Dufrêne, Y., Ando, T., Garcia, R., Alsteens, D., Martinez-Martin, D., Engel, A., Gerber, C. and Müller, D. (2017). Imaging modes of atomic force microscopy for application in molecular and cell biology. *Nature Nanotechnology*, 12(4), pp.295-307.

Fayer, R. and Xiao, L. (2007). *Cryptosporidium and Cryptosporidiosis*. 2nd ed. Florida, USA: CRC Press, pp.1-28.

Fayer, R., Speer, C. and Dubey, J. (1997). The general biology of cryptosporidium. In *Cryptosporidium and Cryptosporidiosis*. 1st ed. Boca Raton: Taylor & Francis Ltd., pp.1-41.

Gatei, W., Wamae, C., Mbae, C., Waruru, A., Mulinge, E., Waithera, T., Gatika, S., Kamwati, S., Revathi, G. and Hart, C. (2006). Cryptosporidiosis: prevalence, genotype analysis, and symptoms associated with infections in children in Kenya. *Am J Trop Med Hyg.*, 75(1), pp.78-82.

Gerber, C. and Lang, H. (2006). How the doors to the nanoworld were opened. *Nature Nanotechnology*, 1(1), pp.3-5.

Harris, J. and Petry, F. (1999). Cryptosporidium parvum: Structural Components of the Oocyst Wall. *The Journal of Parasitology*, 85(5), p.839.

Henderson, E., Haydon, P. and Sakaguchi, D. (1992). Actin filament dynamics in living glial cells imaged by atomic force microscopy. *Science*, 257(5078), pp.1944-1946.

Hinterdorfer, P., Baumgartner, W., Gruber, H., Schilcher, K. and Schindler, H. (1996). Detection and localization of individual antibody-antigen recognition events by atomic force microscopy. *Proceedings of the National Academy of Sciences*, 93(8), pp.3477-3481.

Hoh, J., Cleveland, J., Prater, C., Revel, J. and Hansma, P. (1992). Quantized adhesion detected with the atomic force microscope. *Journal of the American Chemical Society*, 114(12), pp.4917-4918.

Keyvani, A., Sadeghian, H., Tamer, M., Goosen, J. and van Keulen, F. (2017). Minimizing tip-sample forces and enhancing sensitivity in atomic force microscopy with dynamically compliant cantilevers. *Journal of Applied Physics*, 121(24), p.244505.

Korich, D., Mead, J., Madore, M., Sinclair, N. and Sterling, C. (1990). Effects of ozone, chlorine dioxide, chlorine, and monochloramine on Cryptosporidium parvum oocyst viability. *Applied and Environmental Microbiology*, 56(5), pp.1423–8.

Le Grimellec, C., Lesniewska, E., Giocondi, M., Finot, E., Vié, V. and Goudonnet, J. (1998). Imaging of the Surface of Living Cells by Low-Force Contact-Mode Atomic Force Microscopy. *Biophysical Journal*, 75(2), pp.695-703.

Lee, G., Chrisey, L. and Colton, R. (1994). Direct measurement of the forces between complementary strands of DNA. *Science*, 266(5186), pp.771-773.

Mosier, D. and Oberst, R. (2000). Cryptosporidiosis: A Global Challenge. *Annals of the New York Academy of Sciences*, 916(1), pp.102-111.

Müller, D. and Dufrêne, Y. (2008). Atomic force microscopy as a multifunctional molecular toolbox in nanobiotechnology. *Nature Nanotechnology*, 3(5), pp.261-269.

Muller, D., Baumeister, W. and Engel, A. (1999). Controlled unzipping of a bacterial surface layer with atomic force microscopy. *Proceedings of the National Academy of Sciences*, 96(23), pp.13170-13174.

Novak, P., Li, C., Shevchuk, A., Stepanyan, R., Caldwell, M., Hughes, S. and Korchev, Y. (2009). Nanoscale live cell imaging using hopping probe ion conductance microscopy. *Nature Methods*, 6(4), pp.279–281.

Okhuysen, P.C. et al. (1999). Virulence of Three Distinct Cryptosporidium parvum Isolates for Healthy Adults. The Journal of Infectious Diseases [Online] 180:1275–1281. Available at: https://academic.oup.com/jid/article-lookup/doi/10.1086/315033.

Ong, Y., Razatos, A., Georgiou, G. and Sharma, M. (1999). Adhesion Forces betweenE.coliBacteria and Biomaterial Surfaces. *Langmuir*, 15(8), pp.2719-2725.

Putignani, L. and Menichella, D. (2010). Global Distribution, Public Health and Clinical Impact of the Protozoan PathogenCryptosporidium. *Interdisciplinary Perspectives on Infectious Diseases*, 2010, pp.1-39.

Radmacher, M., Tillamnn, R., Fritz, M. and Gaub, H. (1992). From molecules to cells: imaging soft samples with the atomic force microscope. *Science*, 257(5078), pp.1900-1905.

Razatos, A., Ong, Y., Sharma, M. and Georgiou, G. (1998). Molecular determinants of bacterial adhesion monitored by atomic force microscopy. *Proceedings of the National Academy of Sciences*, 95(19), pp.11059-11064.

Reinoso, R., Becares, E. and Smith, H. (2008). Effect of various environmental factors on the viability of Cryptosporidium parvum oocysts. *Journal of Applied Microbiology*, 104(4), pp.980-986.

Robichon, D., Girard, J., Cenatiempo, Y. and Cavellier, J. (1999). Atomic force microscopy imaging of dried or living bacteria. *Comptes Rendus de l'Académie des Sciences - Series III - Sciences de la Vie*, 322(8), pp.687-693.

Rochelle, P., Fallar, D., Marshall, M., Montelone, B., Upton, S. and Woods, K. (2004). Irreversible UV Inactivation of Cryptosporidium spp. Despite the Presence of UV Repair Genes1. *The Journal of Eukaryotic Microbiology*, 51(5), pp.553-562.

Rode, S., Stark, R., Lübbe, J., Tröger, L., Schütte, J., Umeda, K., Kobayashi, K., Yamada, H. and Kühnle, A. (2011). Modification of a commercial atomic force microscopy for low-noise, high-resolution frequency-modulation imaging in liquid environment. *Review of Scientific Instruments*, 82(7), p.073703.

Ryan, U., Fayer, R. and Xiao, L. (2014). Cryptosporidium species in humans and animals: current understanding and research needs. *Parasitology*, 141(13), pp.1667-1685.

Schroder, D., Benton, J. and Rai-Choudhury, P. (1996). *Diagnostic Techniques for Semiconductor Materials Processing*. 1st ed. Pennington, New Jersey: The Electrochemical Sociely inc., pp.356-358.

Searcy, K., Packman, A., Atwill, E. and Harter, T. (2005). Association of Cryptosporidium parvum with Suspended Particles: Impact on Oocyst Sedimentation. *Applied and Environmental Microbiology*, 71(2), pp.1072-1078.

Sokolov, I., Firtel, M. and Henderson, G. (1996). In situ high-resolution atomic force microscope imaging of biological surfaces. *Journal of Vacuum Science & Technology A: Vacuum, Surfaces, and Films*, 14(3), pp.674-678.

Sparks, H., Nair, G., Castellanos-Gonzalez, A. and White, A. (2015). Treatment of Cryptosporidium: What We Know, Gaps, and the Way Forward. *Current Tropical Medicine Reports*, 2(3), pp.181-187.

Suzuki, E. (2002). High-resolution scanning electron microscopy of immunogold-labelled cells by the use of thin plasma coating of osmium. *Journal of Microscopy*, 208(3), pp.153-157.

Tolboom, J. (1996). The Infectivity of Cryptosporidium parvum in Healthy Volunteers. *Journal of Pediatric Gastroenterology &amp Nutrition*, 23(2), p.201.

Tufenkji, N., Dixon, D., Considine, R. and Drummond, C. (2006). Multi-scale Cryptosporidium/sand interactions in water treatment. *Water Research*, 40(18), pp.3315-3331.

Xiao, L. (2010). Molecular epidemiology of cryptosporidiosis: An update. *Experimental Parasitology*, 124(1), pp.80-89.